AN ABSTRACT OF THE THESIS OF

John S. Kimball for the degree of Doctor of Philosophy in Bioresource Engineering presented on January 20, 1995. Title: Temporal Scale, Cover Type and Climate Effects on Surface Energy and Mass Exchange.

Abstract approved: Redacted for Privacy

Richard H. Cuenca

Understanding the effects of climate variation on surface-atmosphere energy and mass exchange is critical to assessing the impact of global change on ecosystems and water resources. The purpose of this research was to examine the effect of cover type, climate and temporal scale on surface energy and mass exchange calculations in order to provide a framework for the application of micro-climatological models in point to regional scale hydrologic studies. Aerodynamic turbulent transfer, Penman-Monteith and Priestley-Taylor methods were used to predict latent energy exchange over an irrigated grass cover in Oregon and an alpine snowcover in the Sierra Nevada mountains of California. The models produced similar results on a daily basis when wind speeds were low and available energy was large and positive. Turbulent transfer results deviated from other models at hourly time-scales, especially on clear days. Model differences were attributed to experimental assumptions of surface saturation, minimal surface resistances and an observed time lag between the diurnal progressions of net radiation and the estimated surface-

atmosphere humidity gradient. When wind velocities were large and available radiant energy was near zero, the turbulent transfer and Penman-Monteith methods produced similar results while the Priestley-Taylor method was unreliable. Model estimates of surface energy exchange were relatively unaffected by data temporal resolution when the diurnal range in meteorological conditions was small. Accounting for the diurnal variability in meteorological data was found to be important, however, when the diurnal range in climate conditions was large. A 2-layer energy balance snowmelt model was used to evaluate the sensitivity of snowmelt processes to conditions which occur during rain-on-snow events. Rainfall accounted for the majority of runoff due to rapid snowcover liquid water saturation during rain-on-snow events. The advective energy from rainfall had a minimal effect on estimated snowmelt except under extreme events. Wind velocity had the greatest influence on snowmelt through the regulation of sensible and latent energy exchange. Rapid snowmelt in cleared mountainous areas was found to be more likely the result of increased turbulence that accompanies a rainfall event rather than the magnitude and intensity of precipitation. Overall, this research showed that different micro-climatological methods are sensitive to different data parameters, cover and climate conditions and can produce unreliable results when model assumptions and data requirements are not met.

Temporal Scale, Cover Type and Climate Effects on Surface Energy and Mass Exchange

by

John S. Kimball

A THESIS

submitted to

Oregon State University

in partial fulfillment of
the requirements for the degree of

Doctor of Philosophy

Completed January 20, 1995
Commencement June, 1995

Doctor of Philosophy thesis of John S. Kimball presented on January 20, 1995

APPROVED:

Redacted for Privacy

Major Professor, representing Bioresource Engineering

Redacted for Privacy

Chair of Department of Bioresource Engineering

Redacted for Privacy

Dean of Graduate School

I understand that my thesis will become part of the permanent collection of Oregon State University libraries. My signature below authorizes release of my thesis to any reader upon request.

Redacted for Privacy

John S. Kimball, Author

ACKNOWLEDGMENTS

This work was funded by National Aeronautics and Space Administration grants NAG-955496 and NAG 5-2301. Additional funding came from a U.S. Environmental Protection Agency inter-agency agreement DW-14936911 with the U.S. Geological Survey and U.S. Department of Agriculture Forest Service cooperative agreement PNW 94-0623. Facilities and support were provided by the U.S. Environmental Protection Agency's Environmental Research Laboratory in Corvallis, Oregon. Many thanks are extended to fellow researchers, faculty, friends and family who provided valuable insight, equipment, friendship and support that made the completion of this project possible. I would like to thank Dr. Richard Cuenca, Dr. Danny Marks, Dr. Dennis Lettenmaier and Dr. Michael Unsworth for their generous support, friendship and guidance over the course of this project. I would also like to thank the rest of my committee members for their time and excellent suggestions: Dr. Bill Braunworth, Dr. Marshall English and Dr. Hermann Gucinski. My sincere gratitude and respect is extended to Samuel Farias-Ortega, a fellow graduate student and researcher who provided valuable friendship, support and advice. Finally my most sincere thanks and appreciation is extended to my wife Shannon and our family. Their support, love and encouragement have been a great blessing and strength in my life.

TABLE OF CONTENTS

TABLE OF CONTENTS (Continued)

TABLE OF CONTENTS (Continued)

LIST OF FIGURES

LIST OF FIGURES (Continued)

LIST OF TABLES

LIST OF TABLES (Continued)

Temporal Scale, Cover Type and Climate Effects on Surface Energy and Mass Exchange

1 INTRODUCTION

Concern over global climate change has focused increased attention on climate-land surface interactions. In regions where much of the annual water balance is controlled by seasonal snowcover, the degree to which climate conditions affect runoff, soil moisture and evapotranspiration are uncertain, largely because the relationships between climate, terrain and regional snow accumulation and melt processes are not well established (Dozier, 1987). Thus the potential impacts of changing climate on socioeconomic activities such as forestry, agriculture, municipal and industrial water supply, fisheries and recreation remain indeterminate.

Much of the research in snow hydrology in the past fifteen years has resulted in an improved understanding of the physical properties of snow deposition and atmosphere-snowcover interactions (Davis and Marks, 1980; Marks et al., 1986; Dozier, 1987; Elder et al., 1991; Jordan, 1991). Most of this research has focused on detailed simulations of hydrologic processes over small, well instrumented study sites which are seldom greater than 2 km^2 in area. Detailed watershed-scale models have not yet been extended to more regional scales (i.e. 10^2-10^6 km^2) due to uncertainties involving the interactions between climate, energy and mass exchange over variable surface cover and complex topography

and a general lack of data sets at spatial and temporal resolutions required for model input and validation.

Surface fluxes of heat and moisture are the major mechanisms of land surface-atmosphere interaction. The magnitude and nature of these fluxes regulate the partition of energy and moisture between the surface and atmosphere and influence, both directly and indirectly, key hydrologic processes such as snow metamorphism, runoff and available moisture. Hydrologic models provide a useful mechanism for evaluating the interactions between climate and water resources. A wide variety of hydrologic models have been developed which account for surface fluxes of heat and moisture using methods ranging in complexity from simple statistical parameterizations of surface fluxes to process oriented approaches requiring detailed measurements of temperature, humidity, wind and radiation. Process oriented, hydrologic models are increasingly being applied at greater spatial scales, over a variety of surface cover types and variable temporal scales in order to address regional to global scale problems (Neilson, 1993; Running and Coughlan, 1988; Sellers et al., 1986). It is not clear what the differences are between model sensitivities to climate and surface cover characteristics and the appropriate temporal scales over which they can be applied.

The purpose of this research is to examine the effect of cover type, climate and temporal scale on surface energy and mass exchange calculations. This study addresses three general questions: 1) What is an appropriate method for determining latent energy exchange and evaporation over variable cover and climate conditions, 2) what are the temporal scale effects of input data on surface energy and mass exchange calculations and 3) what are the

important parameters governing surface energy and mass exchange for a snowpack within a transitional rain-on-snow zone. The specific objectives of this study are to compare and contrast three different methods of estimating latent energy and mass exchange over different surfaces and to evaluate the effect of temporally averaged climate data on estimates of sensible and latent energy exchange in order to provide a framework for the application of temporally averaged data in hydrologic studies. These concepts are then used within the framework of an energy balance-snowmelt model to evaluate the sensitivity of a snowcover energy and mass balance to conditions which occur during rain-on-snow events.

2 BACKGROUND

2.1 The water balance of terrestrial systems

The distribution and nature of water in all its phases plays a central role in the regulation of climate and the maintenance and quality of life on Earth. The hydrologic cycle describes the movement of water in all of its phases through the various reservoirs of the climate system, namely, the oceans, ice masses and snow deposits, terrestrial lakes and streams, ground water, atmosphere and biosphere. The relative amount of water for a terrestrial surface can be described using a continuity or water balance approach:

$$P - R - E - T = \Delta S \tag{1}$$

where P, R, E, T, and ΔS are the precipitation, surface runoff, evaporation, transpiration and storage terms, respectively. Precipitation includes both rainfall and snow and represents the primary input of water from the atmosphere to the surface. The runoff term represents the loss of water from the system by surface water flow or deep percolation. The ΔS term accounts for the temporary storage of water in the terrestrial system in the form of soil moisture, snow and ice, water bodies or vegetation. Evaporation is the process by which water moves from a liquid at the surface to a gaseous phase in the atmosphere. E is expressed in Equation (1) as a general term encompassing both evaporation and sublimation whereby water moves from a solid to gaseous phase.

2.2 Definitions of surface evaporation

Evaporation generally represents the movement of water from water bodies, the surface of wet leaves or bare soil to the atmosphere while transpiration (T) defines the movement of water from the soil, through plants to the atmosphere. Evaporation and transpiration are difficult to separate in natural systems and are frequently described using the single term evapotranspiration (ET) which encompasses the evaporation from free water, soil, vegetation and other surfaces.

Potential evapotranspiration was a term first used by Thornthwaite (1948). This term has generally come to refer to the maximum rate of evapotranspiration from a large area covered by a uniform, sufficiently moist, actively growing vegetated cover (Brutsaert, 1982). Potential evapotranspiration is considered approximately equal to evapotranspiration when available moisture is non-limiting such as over water, and moist, vegetated surfaces. Evapotranspiration under these conditions is regulated by external factors such as wind speed, vapor pressure deficit and the amount of available radiant energy at the surface (Penman, 1948). A snowcover represents a frozen, free water surface where ice is converted directly to the vapor state and back again by sublimation and condensation. Ice can also melt and evaporate, but this process is generally considered negligible when the snow surface layer temperature is less than 0.0 °C (Langham, 1981; Marks and Dozier, 1992).

As a soil or vegetated surface dries and moisture becomes limiting, plant and soil mechanisms increasingly restrict the amount of water loss to the atmosphere and the evapotranspiration rate is reduced. Plants respond to stress by closing small pores on the

leaves called stomata in order to reduce the rate of transpiration to the atmosphere (Jarvis and Mansfield, 1981). These stresses can be induced by a variety of external factors such as temperature, soil moisture, light intensity, CO_2 concentrations, humidity and wind speed (Aylor et al., 1973; Cowen, 1977; Hall and Schulze, 1980). As a soil surface layer dries, soil resistances restrict the rate at which water moves toward the surface from lower soil layers, effectively reducing the uptake of soil water by plants and direct losses of soil moisture to the atmosphere (Philip, 1957).

The current definition of potential evapotranspiration is generally not considered all inclusive because transpiration rates are strongly influenced by vegetation characteristics even under saturated soil moisture conditions (i.e. potential conditions). Potential evapotranspiration has been defined as the atmospheric demand for water under prevailing meteorological conditions (Penman, 1948; Priestley and Taylor, 1972; Rind et al., 1990). This definition, however, only approximates evaporation over short vegetation. Evapotranspiration rates under potential conditions, over a forest canopy, for example, have been found to be much less than evaporation over a free water surface under the same meteorological conditions (McNaughton and Black, 1973; Stewart, 1977). This definition has led to further confusion since potential evapotranspiration is often calculated from meteorological data observed under non-potential conditions or extrapolated from station data under potential conditions to regional scales where plant, soil and moisture characteristics are different. The resulting rates of evapotranspiration are clearly different than would be expected over a moist, uniform, vegetated cover since surface moisture levels and plant

characteristics influence available energy, temperature, humidity, wind speed and plant and soil resistances.

A more inclusive term has been used to describe evapotranspiration under potential conditions. Potential evaporation represents the evaporation from any large, uniform surface which is sufficiently wet or moist so that the air in contact with it is near saturation (Brutsaert, 1982). Another term which avoids the ambiguities inherent in the potential evapotranspiration term is reference evapotranspiration which can be defined as the rate of evapotranspiration from an extensive, uniform, well watered, actively growing, green grass covered surface, 8 - 15 cm in height (Burman et al., 1983).

2.3 The energy balance of terrestrial systems

The energy balance of most land surfaces can be defined as:

$$\Delta Q = R_n + M + L_vE + H + G \qquad (2)$$

where R_n, M, L_vE, H, and G represent the net radiative, advective, latent, sensible and conductive energy fluxes, respectively. For bare soil and short vegetation canopy surfaces the energy storage term, ΔQ, is negligible and the sum of all the other terms in Equation (2) is assumed to be approximately zero. For a snowpack, ΔQ represents the amount of energy stored within the snowcover. If the snowpack is in thermal equilibrium, the net change in snowpack energy is zero. If the snowcover is not in thermal equilibrium, a negative ΔQ

term denotes a net decrease in snowpack energy indicating a cooling snowcover while a positive ΔQ denotes a net energy transfer to the snowpack. If the snowpack is at a temperature less than 0.0 °C, a positive ΔQ will warm the snowcover until the entire snowpack is approximately isothermal at 0.0 °C. At this point any additional energy transferred to the snowcover will result in snow melt.

In most terrestrial environments, G and M are relatively small while turbulent energy and mass fluxes represented by sensible and latent energy are second only to net radiation in importance in the surface energy balance (Budyko, 1974; Baumgartner and Reichel, 1975; Korzun et al., 1978). The latent energy term in Equation (2) is equivalent to the mass flux of water vapor by evaporation and sublimation processes and represents the linkage between the hydrologic and energy balances of terrestrial systems. The partitioning of net radiant energy at the surface into sensible and latent energy is primarily controlled by the amount of available radiant energy, wind velocity and temperature and humidity gradients between the surface and atmosphere. These factors, in turn, are controlled by physical characteristics of the surface such as albedo, available moisture, vegetation, surface roughness, albedo, slope and aspect.

2.4 Methods for characterizing latent energy exchange

Numerous micrometeorological approaches have been used for estimating latent energy exchange and evapotranspiration. Historically, the majority of these methods were developed for use over well-watered agricultural crops to estimate evapotranspiration but have

since been applied over a variety of surface cover types at varying spatial and temporal scales (Penman, 1948; Monteith, 1965; Priestley and Taylor, 1972; McNaughton and Black, 1973; Stewart and Thom, 1973; Brutsaert,1982; Shuttleworth and Wallace, 1985). Most of these methods utilize hydrological, meteorological and plant physiological concepts to varying degrees to derive estimates of evaporation (Brutsaert, 1982; Sharma, 1985; Kanemasu, 1989; Monteith and Unsworth, 1990). Generally, however, these methods utilize one or a combination of two approaches, namely, the measurement or estimation of components of the energy budget to derive latent energy exchange indirectly or a mass transfer approach where L_vE is estimated from wind and humidity gradient information (Brutsaert, 1982). Several methods have been used to obtain estimates of latent energy fluxes and evaporation under historic and current climate conditions as well as projected future vegetation and climate scenarios over local to regional scales (Dickinson, 1984; Running and Coughlan, 1988; Rind et al., 1990; Neilson, 1993). These methods range in complexity from simple statistical parameterizations of surface fluxes to process-oriented approaches requiring detailed measurements of air temperature, humidity, wind and net radiation.

The purpose of this investigation is not to conduct an exhaustive review of all of the methods currently available to estimate latent energy exchange and evaporation. Several papers and texts are currently available that serve this purpose (Brutsaert, 1982; Sharma, 1985; Kanemasu, 1989; Monteith and Unsworth, 1990). This investigation focuses on three of the more commonly used methods that utilize fairly distinct approaches to derive

latent energy exchange; namely, the Priestley-Taylor, Penman-Monteith and aerodynamic turbulent transfer models.

2.4.1 Penman-Monteith model

Combination methods utilize both energy balance and aerodynamic approaches to estimate latent energy exchange. If the net radiation, R_n, and conductive energy fluxes, G, can be measured or estimated, sensible energy can be measured by aerodynamic methods and latent energy can be derived as a residual in the energy balance (Brutsaert, 1982; Kanemasu, 1989; Monteith and Unsworth, 1990). Penman (1948) presented a combination approach for the calculation of latent energy and evaporation for uniform, well watered, freely evaporating surfaces with minimal advection. Monteith (1965) modified Penman's approach by incorporating a canopy resistance term to approximate the physiological constraints imposed by vegetation and soil factors on surface evapotranspiration under moisture limiting conditions (Stewart, 1984):

$$L_vE = [s\,(R_n - G) + (\rho C_p\,(q_{sat} - q_a) / r_a)] / (s + \gamma\,(1 + r_c / r_a)) \qquad (3)$$

where q_a and q_{sat} are the measured and saturated vapor pressure terms, s is a linear approximation of the slope of the saturation vapor pressure-air temperature curve, γ is the psychrometric constant ($\cong$ 66 Pa K^{-1}), r_c is the surface resistance, and ρ and C_p are the density and specific heat of dry air, respectively.

The aerodynamic resistance term, r_a, can be estimated using an approach described by Monteith (1965) and Stewart (1984) which has been modified to account for non-neutral atmospheric conditions (Mahrt and Ek, 1984):

$$r_a = (\log((z - d_0) / z_0))^2 / k^2 u \quad (4)$$

where u is the horizontal wind speed at height z, k is the von Karman's constant, and d_0 and z_0 are the zero-plane displacement and aerodynamic surface roughness heights, respectively. The aerodynamic resistance term quantifies the atmospheric boundary layer resistance to evaporation. r_a is dependent on the aerodynamic roughness of the surface, wind speed and atmospheric stability. Over aerodynamically smooth surfaces such as snow or short, uniform vegetation, r_a is large and evaporation is strongly influenced by the amount of available energy (Priestley and Taylor, 1972; Stewart, 1984). Over aerodynamically rough surfaces such as forests, r_a is greatly reduced and evaporation is primarily controlled by the vapor pressure deficit of the air and the canopy resistance term (McNaughton and Black, 1973; Stewart and Thom, 1973; Shuttleworth and Calder, 1979).

The canopy resistance parameter, r_c, incorporates bulk stomatal and soil resistances to evaporation. For uniform, vegetated surfaces, r_c is related to leaf area and the degree of stomatal closure. For a bare soil surface, r_c is a function of the length of the diffusion pathway of water vapor in the soil. The canopy resistance term is dependent on numerous biological and external factors such as plant type, condition and morphology, available moisture, temperature, humidity, CO_2 concentration and the amount of net radiation. r_c can

be determined by measuring or estimating R_n, G, H, r_a and L_vE independently and solving for r_c in Equation (3). Other methods for deriving r_c range from simple statistical approximations to detailed plant and soil moisture modeling schemes (Jarvis et al., 1981; Sellers et al., 1986). Over aerodynamically rough surfaces under potential conditions L_vE is primarily dependent on the vapor pressure deficit of the air and r_c, which has been shown to vary significantly throughout the day (McNaughton and Black, 1973; Stewart and Thom, 1973; Lemeur and Zhang, 1990). Over aerodynamically smooth surfaces such as grass or agricultural crop surfaces, L_vE is primarily dependent on the amount of net radiation and r_c can be assumed to be approximately constant under sufficiently moist surface conditions (Priestley and Taylor, 1972; Davies and Allen, 1973; Stewart and Rouse, 1977; Jensen et al., 1990; Flint and Childs, 1991).

Surface roughness terms for momentum, z_m, heat, z_h, and moisture, z_v, can be defined as the zero velocity intercepts of the straight lines of semi-logarithmic plots of mean wind velocity, potential temperature and moisture versus elevation within the lowest 10% of the boundary layer (Brutsaert, 1982; Beljaars and Holtslag, 1991). z_m, z_h and z_v are semi-empirical coefficients that relate, in part, to the theoretical point above the surface where momentum, heat and moisture gradients are effectively zero. The surface roughness elements are a function of the height, density and structure of the surface elements and wind speed. Monin-Obukhov similarity theory is a generally accepted framework for describing the transport of momentum, heat and moisture within the boundary layer (Monin and Obukhov, 1954; Brutsaert, 1982). This theory assumes that for flat, uniform terrain, under neutral atmospheric conditions, the transport of momentum heat and moisture between the

surface and atmosphere are the same and $K_m = K_h = K_v$, where K_m, K_h, and K_v are the transfer coefficients for momentum, heat and vapor, respectively (Brutsaert, 1982). Under these conditions z_m, z_h, and z_v can be assumed to be approximately equal and defined using a single roughness term, z_0 (Monteith, 1965; Brutsaert, 1982; Marks and Dozier, 1992). Paeschke (1937) found that for rough snow, various grassy and crop surfaces, the ratio of the height of the roughness obstacles, h_0, to the roughness length, z_0, is approximately 7.35. Kondo (1971) found that the zero plane displacement, d_0, is approximately two-thirds the height of the roughness obstacles for a variety of surfaces. The assumption of equality between z_m, z_h and z_v generally holds for extensive, aerodynamically smooth surfaces such as water, snow and closely cropped grass. Over rough surfaces and non-homogeneous terrain, however, z_m has been found to be 2 to 6400 times greater than z_h and z_v (Garratt and Hicks, 1973; Garratt, 1978; Brutsaert, 1982; Beljaars and Holtslag, 1991).

The Penman-Monteith approach has been widely used for estimating latent energy exchange over extensive, uniform surfaces such as bare soil and closed canopies of vegetation (McNaughton and Black, 1973; McNaughton and Jarvis, 1984; Stewart, 1984; Running et al., 1989; Parlange and Katul, 1992; Stannard, 1993). The method assumes that advection is negligible and the sources of sensible and latent energy are at the same height and temperature. This assumption is generally satisfied by extensive surfaces of water, snow, bare soils or closed canopies with adequate wind fetch but is not met by sparse or partially open canopy conditions. Shuttleworth and Wallace (1985) modified the Penman-Monteith method for sparse canopies by accounting for the evaporation from both vegetation and soil. The Penman-Monteith equation generally requires net radiation, surface

conductive energy flux, air temperature, specific humidity and horizontal wind speed measurements at a single level as well as a measurement or estimation of r_c and r_a.

2.4.2 Priestley-Taylor model

Priestley and Taylor (1972) suggested that air moving over an extensive, wet, uniform surface should come into equilibrium with that surface when the saturation vapor pressure deficit of the air is in equilibrium with the surface. The evaporation rate under these conditions is termed the equilibrium evaporation rate and is controlled by the amount of available energy, R_n-G. Priestley and Taylor found, however, that the actual rate of evaporation from water or saturated surfaces exceeded the equilibrium evaporation rate by an approximate factor of 1.26 and that the evaporation rate for an extensive, saturated land or water surface with minimal advection could be described as:

$$L_vE = \alpha (s / (s + \gamma)) (R_n - G) \quad (5)$$

The Priestley-Taylor equation represents a simplification of the Penman-Monteith approach whereby bulk stomatal, soil and aerodynamic resistances are represented by a single, unitless coefficient, α. Priestley and Taylor found that approximately 80% of the evaporation rate was controlled by the available energy term while advection accounted for 21-22% of evaporation (i.e. $\alpha \cong 1.26 - 1.28$) for both saturated land and water surfaces. The variation in α has generally been attributed to variations in large scale advection, but

the observation that α is approximately 1.26 has been substantiated by other investigators for a variety of surface cover types (Davies and Allen, 1973; McNaughton and Black, 1973; Jury and Tanner, 1975; Kanemasu et al., 1976; Bailey and Davies, 1981; Parlange and Katul, 1992; Pereira and Nova, 1992; Stannard, 1993). At hourly time scales, however, α has been found to vary significantly throughout the day (Priestley and Taylor, 1972; Pereira and Nova, 1992). Priestley and Taylor (1972) found that for saturated surfaces, α can be described as:

$$\alpha = (L_v * \Delta q) / (((s / (s + \gamma)) * (L_v * \Delta q + C_p * \Delta T)) \quad (6)$$

where Δq and ΔT are the near surface-atmosphere humidity and air temperature gradients, respectively, and L_v is the latent heat of vaporization ($\cong 2.5 \times 10^6$ J kg^{-1}). For unsaturated surfaces, α is reduced and has generally been described using empirical approaches based on the degree of soil wetness (Priestley and Taylor, 1972; Davies and Allen, 1973; Flint and Childs, 1991; Stannard, 1993). The Priestley-Taylor method assumes that evaporation is primarily a function of available energy and the available energy and moisture deficit terms in Equation (5) are well correlated. These assumptions generally hold for moist, aerodynamically smooth surfaces with minimal advection. A large degree of error can occur over non-homogeneous terrain or rough surfaces such as forested canopies where r_a is greatly reduced and evaporation is primarily controlled by vapor pressure deficit and canopy resistance parameters (Priestley and Taylor, 1972; McNaughton and Black, 1973; Stewart and Rouse, 1977).

2.4.3 Aerodynamic turbulent transfer method

The turbulent transfer method attempts to describe the aerodynamics of flow near a surface so that the transport of momentum, water vapor, and heat can be estimated. This approach relies on the existence of strong relationships between vertical fluxes of momentum, energy and mass and gradients of wind, temperature and humidity. The aerodynamic approach generally requires wind and humidity information at two or more levels above the surface in order to describe the vertical fluxes of energy and mass between the surface and atmosphere. This approach has been used to describe energy exchange and mass transfer over a variety of surfaces including snow (Businger, 1973; Stewart, 1982; Andreas et al., 1984), barley (Neuwirth, 1974), and pine forests (Stewart and Thom, 1973; Thom et al., 1975). If the surface is wet and the surface temperature and roughness is known then latent and sensible energy fluxes can be determined from air temperature, humidity and wind speed information at a single measurement height (Brutsaert and Yu, 1968; Stewart, 1982; Brutsaert, 1982; Marks and Dozier, 1992). The method used in this investigation is an aerodynamic turbulent transfer model adapted from Brutsaert (1982) and later modified by Marks (1988). The following equations are solved iteratively to obtain estimates of latent energy and mass fluxes at a point:

Obukhov stability length:

$$L = (u^{*3}\ p\ ) / [k\ g\ (H / (T_a\ C_p) + 0.61\ E)] \qquad (7)$$

Friction velocity:

$$u^* = (u\ k) / \ln [((z_u - d_0) / z_0) - (\psi_{sm}\ (z_u / L))] \quad (8)$$

Sensible energy flux:

$$H = ((\Theta_a - \Theta_s)\ a_H\ k\ u^*\ p\ C_p) / \ln [\ ((z_T - d_0) / z_0) - (\psi_{sh}\ (z_T / L))] \quad (9)$$

Mass flux:

$$E = L_v\ ((q - q_s)\ a_E\ k\ u^*\ p) / \ln [\ ((z_q - d_0) / z_0) - (\psi_{sv}\ (z_q / L))] \quad (10)$$

Air and surface temperatures, T_a, T_s, air and surface humidities, q, q_s and wind speed, u, are obtained from measurement data. The friction velocity, u*, is solved iteratively in Equations (7)-(10). The stability functions, ψ_{sm}, ψ_{sv} and ψ_{sh} are calculated as follows:

For stable conditions, $\zeta = (z/L) > 0$):

$$\psi_{sm}(\zeta) = \psi_{sv}(\zeta) = \psi_{sh}(\zeta) = -\beta_s,\ 0 < \zeta \leq 1,\ \beta_s = 5 \quad (11)$$

$$\psi_{sm}(\zeta) = \psi_{sv}(\zeta) = \psi_{sh}(\zeta) = -\beta_s,\ \zeta > 1,\ \beta_s = 5 \quad (12)$$

For unstable conditions ($\zeta = (z/L) < 0$):

$$X = (1 - \beta_u\ \zeta)^{1/4},\ \beta_u = 16 \quad (13)$$

$$\psi_{sm} = 2\ln[(1+X)/2] + \ln[(1+X^2)/2] - 2\arctan X + \pi/2 \quad (14)$$

$$\psi_{sh}(\zeta) = \psi_{sv}(\zeta) = 2\ln[(1+X^2)/2] \quad (15)$$

The three most critical terms in Equations (7)-(10) are wind speed, and the vapor pressure gradient between the air and surface. Air and surface temperatures only indirectly effect estimates of E through the calculation of surface humidity and stability.

2.5 Importance of scale

The latent energy component described in Equation (1) represents the interface between the hydrologic and energy balances over most surfaces and is an important component of hydrologic studies at local to regional scales. Energy balance and aerodynamic methods are increasingly being used at more regional scales, over complex topography and surface cover conditions at varying temporal scales in order to address local to regional scale hydrologic problems. Remotely sensed data have been used with ground-based meteorological data to estimate evapotranspiration at local to regional scales (Price, 1982; Jackson et al., 1983; Gurney and Camillo, 1984; Jackson, 1985; Running, 1989). General Circulation Models (GCM's) use a simplified aerodynamic approach to estimate the evaporation demand under historic, current and projected future climate conditions (Dickinson, 1984; Rind et al., 1990). The BATS (biosphere-atmosphere transfer scheme) and SiB (simple biospheric model) ecotype simulation models use generalized forms of the Penman-Monteith method to derive regional to continental scale estimates of evapotranspiration

(Dickinson, 1984; Sellers et al., 1986). Both models incorporate bulk aerodynamic and canopy resistance parameters that are based on gross plant morphological characteristics and generalized surface roughness parameters. Neilson's MAPSS (Mapped-Atmosphere-Plant-Soil System) ecotype simulation model uses an aerodynamic turbulent transfer approach to derive potential evaporation over continental scale plant communities (Neilson, 1993). This model also incorporates a surface roughness parameter based on general plant community morphology and surface characteristics.

Energy balance and aerodynamic methods have generally been developed for use within fairly narrow ranges of surface cover, temporal scale and climate conditions. These methods are based on similarity theory (i.e. $K_m = K_h = K_v$) in which fluxes of momentum, heat and water vapor are assumed constant with height (Brutsaert, 1982; Monteith and Unsworth, 1990). These methods are also based on the assumption of spatially consistent surface roughness and minimal advection. These assumptions are generally satisfied over level terrain with extensive, uniform cover. Over non-uniform topography or variable surface cover the similarity assumptions may not hold and roughness parameters for momentum, heat and water may not be consistent (Garratt, 1984; Beljaars and Holtslag, 1991). Surface resistances may also vary depending on vegetation type, morphology and condition. Estimates of latent energy exchange and evaporation are rarely desired at less than daily temporal scales for regional scale studies due to the scarcity of meteorological data and enormous data storage and processing requirements. It is often tempting to use meteorological data that have been averaged over long time periods to determine evaporation from aerodynamic or energy balance methods. Evidence suggests that this may

result in large estimation errors when the diurnal variability in meteorological parameters is large (Jobson, 1972; Brutsaert, 1982; Monteith and Unsworth, 1990).

Currently there are few guidelines for the application of detailed energy balance and aerodynamic models over coarse temporal and spatial scales and complex surfaces. Coupled climate and radiation data are not readily available at the spatial and temporal resolutions necessary to adequately evaluate energy balance based models or verify model results (Dickinson, 1984; Mintz et al., 1986; Sato et al., 1989).

3 COMPARISON OF METHODS FOR ESTIMATING LATENT ENERGY EXCHANGE UNDER VARIABLE COVER AND CLIMATE CONDITIONS

3.1 Abstract

Understanding the effects of climate variation on surface-atmosphere energy and mass exchange is critical to assessing the impact of global change on ecosystems and water resources. Aerodynamic turbulent transfer, Penman-Monteith, and Priestley-Taylor methods were used to predict potential evaporation and sublimation over a stand of Alta fescue grass in Oregon, and an alpine snowcover in the Sierra Nevada. The models were compared using integrated hourly meteorological and radiation data collected under variable climate conditions. The turbulent transfer method was most sensitive to wind speed and surface-atmosphere humidity gradients while the Penman-Monteith method was sensitive to both radiation and turbulence. The Priestley-Taylor method was primarily sensitive to changes in net radiant energy.

The three models produced similar results at the grass site on a daily basis where the turbulent fluxes were small and available energy was large and positive. At hourly time scales, the three models compared favorably with Bowen ratio results on cloudy days. On clear days differences between Bowen ratio and turbulent transfer results were large and were attributed to experimental assumptions of surface saturation, zero canopy resistances and an observed time lag between the diurnal progressions of surface heating and cooling and net radiation. At the alpine site, where wind speeds were high and net radiation was frequently near zero, the hourly progressions in estimated latent energy exchange between

the turbulent transfer and Penman-Monteith methods were in general agreement, though marked differences in the magnitudes of estimated sublimation between the two methods were attributed to differences between the saturation vapor pressure deficit and vapor pressure gradient terms used to drive the models. The Priestley-Taylor method produced similar results to the other methods over the grass site despite its relatively simplistic design. At the snow site, however, the Priestley-Taylor method produced much lower latent energy flux estimates than the other models and sublimation estimates that were much less than snowpack measurements indicated. In general, the accuracy of the Priestley-Taylor method appears to be limited to low wind conditions where net radiation dominates the surface energy balance and is well correlated with turbulent fluxes.

3.2 Introduction

Projected changes in global climate driven by increases in atmospheric CO_2 indicate significant alterations may occur in climatic conditions over the next 50 to 100 years (Keeling, 1973; Ramanathan et al., 1985; Dickinson and Cicerone, 1986; Broecker, 1987; Hansen et al., 1988). This would affect the terrestrial biosphere through changes in the regional energy balance which, in turn, could have a profound effect on the regional water cycle (Dickinson, 1985; Warrilow and Buckeley, 1989; Rind et al., 1990; Marks, 1993). Evapotranspiration (ET) represents the combined evaporation from the surface and transpiration from vegetation. This component of the hydrologic cycle is the connecting link between surface-atmosphere energy and mass exchange processes and represents a major loss from land surface hydrologic systems. Potential evaporation (E_p) can be defined as the

atmospheric demand for water and represents the upward limit of the evapotranspiration rate over a sufficiently moist surface under prevailing meteorologic conditions (Brutsaert, 1982). E_p is an important indicator of the upper limit of the evapotranspiration rate over most surfaces and is a widely used approximation of ET over moist surfaces when the aerodynamic surface roughness is not large (Priestley and Taylor, 1972; McNaughton and Black, 1973; Dickinson, 1984; Sharma, 1984). The potential evaporation component in regional climate and general circulation models (GCMs) has been demonstrated to play a major role in determining the likelihood of droughts (Rind et al., 1990), regional vegetation types and distributions (Neilson, 1993), the increased vigor of the hydrologic cycle and the diurnal range of surface temperatures over deserts (Warrilow and Buckley, 1989).

E_p is considered approximately equal to ET when available moisture is non-limiting such as over water, snow and moist, vegetated surfaces. Surface energy and mass exchange under these conditions is regulated by external factors such as wind speed, humidity and the amount of available radiant energy at the surface (Penman, 1948). A snowcover represents a frozen, free water surface where ice is converted directly to the vapor state by sublimation. Ice can also melt and evaporate, but this process is generally negligible compared to sublimation when the temperature of the snowcover is less than 0.0 °C (Langham, 1981; Marks and Dozier, 1992). As a soil or vegetated surface dries and moisture becomes limiting, plant and soil mechanisms increasingly restrict the amount of water lost to the atmosphere and the evapotranspiration rate is reduced. Plants respond to stress by closing small pores on leaf surfaces called stomata in order to reduce the amount of moisture loss to the atmosphere (Jarvis and Mansfield, 1981). These stresses can be induced by a variety

of forcings such as temperature, soil moisture, light intensity, CO_2 concentrations, humidity and wind speed (Aylor et al., 1973; Cowen, 1977; Hall and Schulze, 1980). As a soil surface dries, soil water resistances restrict the rate at which water moves upward toward the surface from lower soil layers, effectively reducing soil moisture losses to the atmosphere (Philip, 1957).

The energy balance of most land surfaces can be defined as follows:

$$R_n \cong M + L_vE + H + G \tag{1}$$

where R_n, H, G, and M are the net radiative, sensible, conductive and advective energy fluxes, respectively, and L_vE is the latent heat flux where L_v is the latent heat of vaporization or sublimation for water or ice, respectively, and E is the mass flux. In most terrestrial environments, G and M are relatively small while turbulent energy and mass flux represented by sensible and latent energy is second only to radiation in importance in the surface energy balance (Budyko, 1974; Baumgartner and Reichel, 1975; Korzun et al., 1978). The energy balance over a snowpack is similar to that described by Equation (1) except for an additional snowcover energy term, Q, which is equal to the sum of R_n, L_vE, H, G and M. In temperature equilibrium, Q is equal to zero. A negative energy balance (negative Q term) will tend to cool the snowcover while a positive energy balance (positive Q term) will warm the snowpack, redistributing energy predominantly by mass transfer to lower snow layers. If the snowcover energy term remains positive the snowcover will continue to warm until the entire snowpack is approximately isothermal at 0.0 °C. At this point any

additional transfer of energy to the snowpack will result in snowmelt (Langham, 1981). The partitioning of net radiation at the surface into sensible and latent energy is primarily controlled by the amount of available radiant energy, wind velocity, and temperature and humidity gradients between the surface and atmosphere. These factors, in turn, are controlled by climate conditions and physical characteristics of the surface such as available moisture, vegetation, surface roughness, albedo, slope and aspect.

Numerous micrometeorological approaches have been used for estimating latent energy exchange and evapotranspiration. Historically, the majority of these methods were developed for use over well-watered, agricultural crops but have since been applied over a variety of surface cover types at varying spatial and temporal scales (Kanemasu, 1989; Brutsaert, 1982; Sharma, 1985; Monteith and Unsworth, 1990). Most of these methods utilize hydrologic, meteorologic and plant physiological concepts to varying degrees to derive estimates of energy and mass exchange. Generally, however, these methods utilize one or some combination of two approaches, namely, the measurement or estimation of components of the energy budget to derive latent energy exchange indirectly or a mass transfer approach where L_vE is estimated from wind and humidity gradient information (Brutsaert, 1982). Several methods have been used to obtain surface E_p under historic and current climate conditions as well as projected future vegetation and climate conditions at local to regional scales (Priestley and Taylor, 1972; Dickinson, 1984; Running and Coughlan, 1988; Rind et al., 1990; Neilson, 1993). These methods range in complexity from simple statistical parameterizations of surface fluxes to process-oriented approaches requiring detailed measurements of air temperature, humidity, wind and net radiation.

The latent energy component described in Equation (1) represents the interface between the hydrologic and energy balances over most surfaces and is an important component of hydrologic studies at local to regional scales. Energy balance and aerodynamic methods of estimating latent energy and mass exchange that have generally been developed for use within a fairly narrow range of surface cover, temporal scale and climate conditions are increasingly being used at more regional scales, over complex topography and surface cover conditions at varying temporal scales. The purpose of this investigation is to establish a framework for the application of some commonly used approaches for estimating latent energy and mass exchange in regional hydrologic and energy balance studies. The specific objectives of this study are to compare and contrast three distinct combination energy balance and aerodynamic approaches for estimating latent energy exchange under varied surface cover and climate conditions. Specifically, a Penman-Monteith approach, two configurations of the Priestley-Taylor model and an aerodynamic turbulent transfer model are evaluated with respect to different meteorological conditions over grass and snow surfaces.

3.3 Site descriptions and data collection

The Oregon Evapotranspiration Investigation Plot (ETIP) was located at the Oregon State University Schmidt Farm, approximately 15 km north of Corvallis, OR. The ETIP site was 2.11 ha (136 m x 155 m) in area and was covered by a uniform, well established stand of Alta fescue (Festuca elator) grass maintained at a height of 8-20 cm. The soils found at the site are classified as Amity and Woodburn silt loams. These soils are deep and

moderately to well drained through most of the profile. The ETIP site had manual and automatic meteorological stations, Bowen ratio and radiation stations. The stations were located in the center of the field site to maximize wind fetch. Vapor pressure, air temperature and horizontal wind speed were measured at 0.4 and1.4 m heights by a dewpoint hygrometer (DEW-10), a chromel-constant thermocouple and a three cup anemometer-photochopper, respectively. Surface temperature was measured by an Everest interscience temperature transducer with a 45° field-of-view and a resolution of 0.5 °C. Surface conditions were maintained at or near saturation (soil moisture >= 85 % of field capacity). Net all-wave radiation was measured using a REBS net radiometer. Soil conductive energy fluxes were estimated using soil heat flux plates (REBS model HFT-1) at a soil depth of 0.08 m and thermocouples (model TCAU) at soil depths of 0.02 and 0.06 m. All measurements were obtained at 5 second intervals and averaged over 20 minute time periods. These data were then integrated over hourly time periods. A total of 10 days were used in this study representing both clear (i.e. cloud cover <= 1 % of a 90° overhead field-of view) and cloudy sky conditions. The days selected were May 22-31, 1992 (DOY 142-151).

The Emerald Lake watershed (EML) is a remote, high elevation alpine cirque located in Sequoia National Park in the Southern Sierra Nevada mountains of California. The site is 125 ha in area and is composed of bare, granite rock and talus with scattered patches of thin organic soil and alpine vegetation. Detailed meteorologic measurements were collected over a period of approximately 22 days from April 14 - May 6, 1986 (DOY 104-126) at an exposed ridge site located approximately 300 m above a small tarn lake. This site remained snow covered over the entire period of data collection.

Temperature, wind speed, humidity and radiation measurements were obtained approximately every 30 seconds and integrated over 15 minute intervals. The 15 minute data were then integrated over hourly time periods. Data collection at the site was extremely problematic due to its remote location and extreme weather conditions. Climate and radiation data were therefore obtained both by direct measurement and indirect estimation techniques. A detailed description of site characteristics, meteorologic and radiation instrumentation, measurements and monitoring within the Emerald Lake Watershed is presented by Marks, Dozier and Davis (1992) and Marks and Dozier (1992).

3.4 Methods

3.4.1 Priestley-Taylor model

Priestley and Taylor (1972) found that evapotranspiration for a saturated land or water surface with minimal advection could be described using radiation data and a unitless coefficient, α, as follows:

$$L_vE = \alpha \ (s / (s + \gamma)) (R_n - G) \qquad (2)$$

Priestley and Taylor found that on average for both saturated land and water surfaces α was approximately 1.26. This observation has been substantiated by other investigators for a variety of surface cover types (Davies and Allen, 1973; McNaughton and Black, 1973;

Jury and Tanner, 1975; Kanemasu et al., 1976; Bailey and Davies, 1981; Parlange and Katul, 1992; Pereira and Nova, 1992; Stannard, 1993). At hourly time scales, however, α has been found to vary significantly throughout the day (Priestley and Taylor, 1972; Pereira and Nova, 1992). For saturated surfaces, α has theoretical significance and can be described as:

$$\alpha = (L_v * \Delta q) / (((s / (s + \gamma)) * (L_v * \Delta q + C_p * \Delta T)) \quad (3)$$

where Δq and ΔT represent the mean surface humidity and temperature gradients, respectively. For unsaturated surfaces, α is reduced and has generally been described using empirical approaches based on the degree of soil wetness (Priestley and Taylor, 1972; Davies and Allen, 1973; Flint and Childs, 1991; Stannard, 1993). For this investigation, surface conditions were assumed to be at saturation and α was determined at an hourly time step from Equation (3). The Priestley-Taylor parameter was also maintained at a constant value determined from the average of the calculated hourly parameter values.

The slope of the saturation vapor pressure-temperature curve, s, was approximated using a method outlined by Running (1988):

$$s = (q_{s1} - q_{s2}) / 100 \quad (4)$$

where q_{s1} and q_{s2} are the saturation vapor pressures (P_a) at T_a + 0.5 °C and T_a - 0.5 °C respectively.

Equations (2)-(4) require inputs of net radiation, surface conductive energy flux, air and surface temperatures and humidities. Surface temperature and humidity parameters are used in Equation (3) to derive the Priestley-Taylor parameter and are not required if a constant α is used.

3.4.2 Penman-Monteith model

Combination methods for estimating latent energy exchange utilize the premise that if the net radiation and conductive energy flux can be measured or estimated and sensible energy can be measured by aerodynamic methods, the latent energy flux can be derived as a residual in the energy balance (Brutsaert, 1982; Kanemasu, 1989; Monteith and Unsworth, 1990). Penman (1948) presented a combination approach for the calculation of the latent energy flux for uniform, well watered, freely evaporating surfaces with minimal advection. Monteith (1965) modified Penman's approach by incorporating a canopy resistance term to approximate the physiological constraints imposed by vegetation and soil factors on surface evapotranspiration under moisture limiting conditions. The Penman-Monteith equation has been widely used for estimating the latent energy exchange over uniform surfaces, such as bare soil and closed canopy conditions, at varying spatial scales (McNaughton and Jarvis, 1984; Stewart, 1984; Running et al., 1989; Parlange and Katul, 1992). The method is based on the assumption that advection is minimal and the sources

of sensible and latent energy are at the same height and temperature (i.e. big leaf assumption). The big leaf assumption is generally satisfied by water, snow, bare soils or closed canopies with adequate wind fetch but is not met by sparse or partially open canopy conditions. Shuttleworth and Wallace (1985) modified the Penman-Monteith method for sparse canopies by accounting for the evaporation from both vegetation and soil.

The latent energy flux was estimated using the Penman-Monteith approach described by Stewart (1984):

$$L_vE = s\,(R_n - G) + (\rho C_p\,(q_{sat} - q_a) / r_a) / (s + \gamma\,(1 + r_c / r_a)) \quad (5)$$

The slope of the saturation vapor pressure-temperature curve was estimated from Equation (4) while air density, ρ, was calculated using a linear fit of air density to temperature (Running and Coughlan, 1988):

$$\rho = (1.292 - 0.00428 * T_a) \quad (6)$$

The aerodynamic resistance term, r_a, was estimated using an approach described by Stewart (1984) and modified to correct for stability (Mahrt and Ek, 1984):

$$r_a = [(\log((z - d_0) / z_0))^2 / k^2 u] * F^{-1} \quad (7)$$

The stability function, F, can be expressed for stable and unstable atmospheric conditions as follows:

For $R_{iB} > 0$:

$$F = e^{RiB} \tag{8}$$

For $R_{iB} < 0$:

$$F = 1 - 15 * R_{iB} / 1 + 75 * (k^2 / (\ln (z - d_0) / z_0)^2 * (-R_{iB} * (z - d_0) / z_0)^{0.5} \tag{9}$$

The bulk Richardson number, R_{iB}, represents the ratio of the production of energy by buoyancy forces to the dissipation of energy by mechanical turbulence at the surface. This term can be expressed as:

$$R_{iB} = g * (T_a - T_s) * z / T_{avg} * u^2 \tag{10}$$

The Penman-Monteith model requires radiation, air temperature, humidity and horizontal wind speed measurements at a single level. Zero plane displacement, d_0, and surface roughness, z_0, were estimated from canopy and surface obstacle heights, h_0, as follows (Paeschke, 1937; Kondo, 1971; Brutsaert, 1982):

$$d_0 = h_0 * (2/3) \tag{11}$$

$$h_0 = 7.35 * z_0 \tag{12}$$

Surface roughness heights were set to constant values of 1 cm and 0.75 cm for the grass and snow surfaces, respectively. Representative values for z_0 were selected based upon site observations and representative values in the literature for the general cover types (Oke, 1978; Brutsaert, 1982). At the grass site the canopy resistance term, r_c, was set to a constant value of 40 s m^{-1} to approximate the grass canopy resistance under near saturated conditions (Jensen et al., 1990). At the snow site, the snowpack was assumed to represent a frozen free water surface and the canopy resistance term was set equal to zero.

3.4.3 Aerodynamic turbulent transfer method

The turbulent transfer method attempts to describe the aerodynamics of flow near a surface so that the transport of momentum, water vapor, and heat can be estimated. The aerodynamic approach generally requires wind and humidity information at two or more levels above the surface in order to describe the fluxes of energy and mass at the surface. If the surface is wet and the surface temperature and roughness are known then latent and sensible energy fluxes can be determined from air temperature, humidity and wind speed information at a single measurement height (Brutsaert, 1982; Marks and Dozier, 1992). The method used for this experiment is an aerodynamic turbulent transfer model adapted from Brutsaert (1982) and later modified by Marks (1988).

The following equations are solved iteratively to obtain estimates of the latent energy flux at a point:

Obukhov stability length:

$$L = (u^{*3}\ p)/ [k\ g\ (H / (T_a C_p) + 0.61\ E)] \quad (13)$$

Friction velocity:

$$u^* = (u\ k) / \ln [((z_u - d_0) / z_0) - (\psi_{sm}\ (z_u / L))] \quad (14)$$

Sensible heat flux:

$$H = ((\Theta_a - \Theta_s)\ a_H\ k\ u^*\ p\ C_p) / \ln [\ ((z_T - d_0) / z_0) - (\psi_{sh}\ (z_T / L))] \quad (15)$$

Mass flux:

$$E = ((q - q_s)\ a_E\ k\ u^*\ p) / \ln [\ ((z_q - d_0) / z_0) - (\psi_{sv}\ (z_q / L))] \quad (16)$$

For this experiment, a_H and a_E were assumed approximately equal to 1.0 (Brutsaert, 1982), k, z_0 and d_0 were set to the constant values discussed previously. Measurement heights, z_u, z_T and z_q were 1.4 m and 1.0 m at the grass and snow sites, respectively. Station elevations, z, were 70 m and 3087 m at the grass and snow sites, respectively. Temperature, humidity and wind speed were obtained from station measurement data. The friction velocity, u*, was solved iteratively in Equations (13)-(16). The stability functions for momentum, ψ_{sm}, water vapor, ψ_{sv}, and heat, ψ_{sh}, were calculated as follows:

For stable conditions, $\zeta = (z/L) > 0$):

$$\psi_{sm}(\zeta) = \psi_{sv}(\zeta) = \psi_{sh}(\zeta) = -\beta_s,\ 0 < \zeta \leq 1,\ \beta_s = 5 \quad (17)$$

$$\psi_{sm}(\zeta) = \psi_{sv}(\zeta) = \psi_{sh}(\zeta) = -\beta_s,\ \zeta > 1,\ \beta_s = 5 \quad (18)$$

For unstable conditions ($\zeta = (z/L) < 0$):

$$X = (1 - \beta_u \zeta)^{1/4},\ \beta_u = 16 \quad (19)$$

$$\psi_{sm} = 2\ln[(1+X)/2] + \ln[(1+X^2)/2] - 2\arctan X + \pi/2 \quad (20)$$

$$\psi_{sh}(\zeta) = \psi_{sv}(\zeta) = 2\ln[(1+X^2)/2] \quad (21)$$

3.5 Climate and radiation

The three most critical terms in the calculation of latent energy exchange using the turbulent transfer method are wind speed, and the humidity difference between the air and surface. Air and surface temperatures only affect the estimated latent energy exchange indirectly through the calculation of surface humidity and stability. Available radiant energy at the surface, wind speed and the humidity deficit of the air are the most critical terms in the Penman-Monteith equations while the Priestley-Taylor model is primarily dependent on the available radiant energy term. The relative importance of wind, humidity, temperature and radiation in the determination of latent energy exchange using these methods is dependent on the relative magnitudes of the input parameters and can be expected to vary depending on temporal and site conditions.

One of the objectives of this investigation is to evaluate the applicability of the Penman-Monteith, Priestley-Taylor and turbulent transfer models over variable surface cover and climate conditions that might be expected when applying these models at more regional scales. One of the fundamental factors governing the use of aerodynamic and combination energy balance models is the availability of detailed meteorological and radiation data required for model inputs. Detailed temperature, humidity, wind and radiation data are rarely available from meteorological stations at more than a single measurement height. These limitations generally require some simplification of model inputs. Continuous, hourly records of climate and radiation data were obtained at the snow and grass sites for the study periods discussed previously. Model inputs were derived from measurements of surface temperature and radiation, wind, humidity and air temperature at a single height. Additional model input requirements were derived from assumptions of surface conditions. At the snow site, the surface was assumed to be at saturation and surface vapor pressures were approximated as the saturation vapor pressures at the measured surface temperatures. At the grass site the surface was maintained near saturated conditions and the saturation vapor pressure at the measured surface temperature was used as a surrogate for a surface vapor pressure measurement. Horizontal wind speeds at the surface were also assumed to be zero.

3.5.1 Wind

The Emerald Lake site was situated on an exposed, high elevation ridge top and had much larger wind velocity daily means, maxima, minima and diurnal amplitudes than the

grass site. Daily winds over the snow surface were fairly strong and steady, averaging approximately 13 m s^{-1} over the entire study period. On several occasions winds attained velocities in excess of 25 m s^{-1} and only rarely dropped below 4 m s^{-1}. The grass site was characterized by fairly calm conditions with generally light winds which averaged only 14 % of wind velocities at the alpine site. Hourly winds at the grass site exhibited a mean diurnal range of 2.9 m s^{-1} with average daily velocities of less than 2 m s^{-1} over the 10 day study period. Wind data from both sites showed strong diurnal patterns which were fairly consistent on a daily basis.

3.5.2 Temperature

The Emerald Lake site remained snow covered during the entire period of data collection. Surface temperatures at the site were thus constrained to be ≤ 0.0 °C throughout the entire data collection period. Air temperatures over the snow surface were generally cool ($\cong$ 3.1 °C; Std. Dev. = 7.9 °C) and exhibited a moderate diurnal amplitude of approximately 14 °C ranging between early afternoon maxima and pre-dawn minima. Estimated surface temperatures closely tracked the diurnal progression of air temperatures and ranged from daily maxima of 0.0 °C in the early afternoon periods to pre-dawn minima of approximately -10 °C. Hourly temperature gradients between the snow surface and overlying air were predominantly negative, averaging approximately -7 °C (i.e. Std. Dev. = 4.93) over the entire study period. These results indicated a net daily transfer of sensible energy to the snow surface. On a daily basis, the temperature gradient over the snow surface ranged from a maximum of approximately -15 °C during early afternoon to -3 °C at

night, resulting in a diurnal range of approximately 12 °C. Near zero or positive temperature gradients at night were mainly the result of radiant cooling of the air near the surface.

Mean surface and air temperatures at the grass site were much warmer than temperatures observed at the alpine site. Mean hourly surface temperatures were 17.6 °C (i.e. Std. Dev. = 8.1 °C) but sometimes ranged as high as 30 °C at mid-day. Air temperatures followed a similar diurnal pattern but had slightly lower daily mean, maximum and minimum values than the surface. Air and surface temperatures at the grass site exhibited large diurnal amplitudes of approximately 14 °C and 23 °C, respectively, with a mean surface temperature amplitude approximately 60 % larger than the air temperature amplitude. The mean hourly temperature gradient between the surface and the air ranged from a positive 8.7 °C during the day when surface temperatures were warmer than the overlying air to a negative -2.1 °C at night in response to radiant cooling of the surface. On a daily basis this pattern resulted in a positive though fairly small mean hourly temperature gradient of 0.65 °C (i.e. Std. Dev. = 4.0 °C).

3.5.3 Humidity

The grass site was characterized by much larger average daily humidities than the snow site. These conditions were generally attributed to much warmer surface and air temperatures. Humidities at both sites exhibited distinct diurnal patterns corresponding to daily temperature progressions that were generally consistent over the data sampling periods. The magnitude and diurnal range of air and estimated surface humidities and the

estimated vapor pressure gradient between the surface and air were fairly large over the grass surface. These conditions are mainly attributed to the extreme daily range in surface heating and cooling observed at the site. The maximum estimated hourly humidity gradient was a strongly positive 29.2 mb during the day but decreased to a slightly negative -2.1 mb at night due to radiative cooling and saturation of the air near the surface. Over a 24 hour period the mean hourly estimated humidity gradient was approximately 8.5 mb (i.e. Std. Dev. = 11.1 mb).

The mean hourly vapor pressure deficit of the air over the grass surface was 6.3 mb (i.e. Std. Dev. = 6.6 mb) and ranged from a maximum of approximately 16 mb during the early afternoon to a minimum of -0.04 mb at night. On a daily basis the vapor pressure deficit was relatively large but was only 74 % of the magnitude of the estimated humidity gradient between the surface and the air due to the much larger range in estimated daily surface vapor pressures relative to the air.

Because snow is composed of a mixture of ice, water and air, it was assumed that the air fraction is always saturated and that the snow surface vapor pressure is the saturation vapor pressure at the estimated snow surface temperature (Marks and Dozier, 1992). Estimated snow surface vapor pressures were therefore constrained to be less than or equal to 6.1 mb which is the saturation vapor pressure at a temperature of 0.0 °C. Mean hourly estimated snow surface vapor pressures were approximately 4.5 mb (i.e. Std. Dev. = 1.3 mb) and represented only 20 % of the magnitute of surface vapor pressures at the warmer grass site. Mean hourly air vapor pressures were also low ($\cong$ 1.7 mb; Std. Dev. = 0.24 mb) and exhibited a maximum diurnal amplitude of 0.6 mb which was only 11 % of the maximum

diurnal amplitude in vapor pressure at the grass site. The magnitude and diurnal range of the humidity gradient between the snow surface and air was also small due to the fairly cold surface and air temperatures observed at the snow site. The mean hourly humidity gradient was approximately 3 mb (i.e. Std. Dev. = 1.3 mb) which represented only 33 % of the magnitude of the humidity gradient at the grass site. Over a 24 hour period the estimated humidity gradient at the snow site was always positive, ranging from a maximum of 4.6 mb during the early afternoon to a minimum of 4.1 mb at night. Air conditions over the snow surface were generally dry over the entire study period resulting in a mean hourly vapor pressure deficit of 7.1 mb (i.e. Std. Dev. = 5.4 mb) that was approximately 2.5 times greater than the surface-atmosphere vapor pressure gradient. The vapor pressure deficit of the air exhibited a fairly large maximum diurnal amplitude of approximately 13 mb which ranged from 15.9 mb during early afternoon to 2.8 mb at night.

3.5.4 Available energy

The amount of available radiant energy used to drive sensible and latent energy exchange at the grass site was calculated as the difference between mean hourly net radiative and conductive energy fluxes (i.e. R_n and G). On an hourly basis R_n averaged approximately 147 W m^{-2} (i.e. Std. Dev. = 213 W m^{-2}). Weather conditions at the grass site were predominantly clear over the entire study period; thus at hourly time scales R_n followed a regular diurnal progression ranging from a minimum of -48.6 W m^{-2} at night to a maximum of 520.3 W m^{-2} during early afternoon. The amount of energy transferred by conduction followed a similar pattern but represented only 4.8 % of R_n due to the fairly low thermal

conductivity of the soil. The available radiant energy term was therefore predominantly influenced by R_n and ranged from a minimum of -10.8 W m^{-2} at night to a maximum of approximately 417.4 W m^{-2} during the mid-day periods. The mean hourly available energy flux was a positive 140 W m^{-2} (i.e. Std. Dev. = 163.0 W m^{-2}) which represented a fairly substantial amount of radiant energy available for evaporation.

The amount of available radiant energy over the snow surface was determined as the difference between R_n and the snowpack energy term, Q. The snowpack energy content was derived using snowpack measurement data and an energy balance-snowmelt model described by Marks (1988) and Marks and Dozier (1992).

The mean hourly net radiant energy flux at the snow site was approximately 9.5 W m^{-2} (i.e. Std. Dev. = 90.0 W m^{-2}) which represented only 6.4 % of mean hourly R_n at the grass site. The relatively low magnitude of R_n was due primarily to the high albedo of the snow surface. The magnitude of R_n followed a distinct diurnal pattern driven by temporal variations in the relative proportions of solar and thermal incidence and exidence. R_n ranged from a maximum daily value of 174.3 W m^{-2} during mid-day to -81.5 W m^{-2} at night.

The amount of energy attributed to Q also followed a distinct diurnal pattern. The snowpack generally experienced a warming trend in the morning in response to increasing R_n resulting in a positive Q which attained a maximum daily flux of approximately 283 W m^{-2} by early afternoon. The snowpack generally cooled rapidly following the peak in R_n, attaining minimum values of approximately -234 W m^{-2} by late evening. The mean hourly Q flux was approximately 13 W m^{-2} (i.e. Std. Dev. = 137.0 W m^{-2}) indicating a slight, net increase snowpack energy over the study period.

On average, Q was 37 % larger than R_n and represented a major component of the available radiant energy. The amount of available radiant energy was generally negative in the morning when the snow surface was warming. In the afternoon and evening periods the available energy term became positive in response to the cooling snowcover. At night, both R_n and Q were generally negative, resulting in a positive snowpack available energy term. Over the entire study period the mean available energy flux was only -3.4 W m^{-2} (i.e. Std. Dev. = 96.0 W m^{-2}) indicating that on average, little radiant energy was available to contribute to surface sublimation.

3.6 Results and discussion

The turbulent transfer, Penman-Monteith and Priestley-Taylor models were evaluated using hourly wind, temperature, humidity and radiation data collected over the snow and grass sites. Linear regression and error analyses were used to evaluate the agreement between estimates of hourly latent energy exchange and model sensitivities to climate and radiation parameters. Daily accumulations of estimated E_p and sublimation were also compared. Bowen ratio estimates of hourly ET were used to help validate model results at the grass site while estimates of the snowcover water balance derived from precipitation and snowcover properties measurements were used to help validate model results at the alpine site.

3.6.1 Model sensitivities to climate and radiation

Hourly data for each site were segregated into 3 data sets representing morning (0700-1200 hours), mid-day (1300-1700 hours) and night (1800-2400 hours) conditions in order to normalize the data relationships and evaluate model sensitivities to climate and radiation parameters. Correlation coefficients were computed and multiple linear regression analyses were performed between model estimates of E_p and the climate and radiation parameters used to calculate L_vE in each model. These results are summarized in Table 3.1. The models were generally most sensitive to the parameters that exhibited the largest magnitudes and diurnal amplitudes at each site. The grass site was characterized by large amounts of available energy during the day. A large degree of surface heating at the grass site produced substantial diurnal amplitudes in temperatures and humidities but light wind speeds tended to minimize turbulent fluxes at the surface. At the snow site, air conditions were fairly dry and wind velocities were quite large resulting in large saturation vapor pressure deficits and turbulent fluxes at the surface even though temperature and humidity gradients were relatively small.

Correlation and standardized partial regression coefficients indicate that the turbulent transfer model was most sensitive to the vapor pressure gradient at the grass site while wind speed generally controlled L_vE over the snow surface. Warm air temperatures and the large amount of R_n and relatively small G (i.e. 3-5 % of R_n) at the grass site resulted in a strong dependence of Penman-Monteith model results on available radiant energy and to a lesser extent, the vapor pressure deficit during the day. At night both terms exerted a fairly equal influence on E_p estimates. The light wind speeds at the grass site did not

Table 3.1. Correlation coefficients and multiple linear regression results between latent energy flux estimates and selected data parameters. Results are based on data collected under morning (0700-1200 Hrs., AM), afternoon (1300-1600 Hrs., PM) and night (1700-0 600 Hrs., N) conditions

TURBULENT TRANSFER MODEL						
	AM		PM		N	
GRASS SITE	qs-qa	u	qs-qa	u	qs-qa	u
Std. Regr. Coeff.	-0.91	-0.20	-0.94	-0.26	-0.70	-0.20
Prob.	0.0001	0.0001	0.0001	0.0001	0.0001	0.0001
Partial F	1126	57	1342	106	159	17
r-value	-0.96	-0.41	-0.95	-0.29	-0.84	-0.65
SNOW SITE	qs-qa	u	qs-qa	u	qs-qa	u
Std. Regr. Coeff.	0.002	-0.88	-0.14	-0.9	-0.17	-0.75
	0.9575	0.0001	0.0094	0.0001	0.0001	0.0001
Partial F	0.0029	366.7	6.9	316	16	317
r-value	0.36	-0.88	0.20	-0.86	0.03	-0.71

PENMAN-MONTEITH MODEL									
	AM			PM			N		
GRASS SITE	qsat-qa	u	Rn-G	qsat-qa	u	Rn-G	qsat-qa	u	Rn-G
Std. Regr. Coeff.	-0.34	0.02	-0.68	-0.43	-0.08	-0.68	-0.51	-0.14	-0.49
Prob.	0.0001	0.03	0.0001	0.0001	0.0001	0.0001	-0.51	-0.14	-0.49
Partial F	313	4.9	1166	1150	60	2790	32.6	11.0	33.3
r-value	-0.95	-0.34	-0.99	-0.80	-0.14	-0.93	-0.90	-0.62	-0.89
SNOW SITE	qsat-qa	u	Rn-Q	qsat-qa	u	Rn-Q	qsat-qa	u	Rn-Q
Std. Regr. Coeff.	-0.39	-1.0	-0.20	-0.40	-0.98	-0.22	-0.56	-0.80	-0.21
Prob.	0.0001	0.0001	0.0001	0.0001	0.0001	0.001	0.0001	0.0001	0.0001
Partial F	129	787	40	29	218	11	547	1096	77
r-value	0.13	-0.85	-0.47	0.42	-0.84	-0.51	-0.41	-0.69	-0.30

directly influence Penman-Monteith E_p estimates but created large aerodynamic resistances that strongly moderated vapor pressure deficit effects on E_p. Large wind velocities, dry air conditions and low available radiant energy conditions at the snow site resulted in a

strong association between Penman-Monteith sublimation estimates and the wind speed and vapor pressure deficit of the air, respectively.

The calculated Priestley-Taylor parameter values (α) exhibited little variation at both hourly and daily time steps. Averaged hourly α values were 1.74 (i.e. Std. Dev. = 0.3) and 1.24 (i.e. Std. Dev. = 0.18) for the snow and grass sites, respectively. The differences between the parameters are attributed to large differences in temperature and surface conditions between both sites. Over both sites, Priestley-Taylor model results were controlled by the available radiant energy terms (i.e. R_n-G and R_n-Q). Temperature and humidity gradient information was used to calculate α but did not exert a major influence on L_vE estimates.

3.6.2 Model comparisons of hourly E_p and sublimation

Plots of hourly meteorological conditions and estimated L_vE for selected days are presented in Figures 3.1 and 3.2 for the grass site and Figures 3.3 and 3.4 for the alpine snow site. Linear regression and model results are summarized in Tables 3.2 and 3.3 and plots of model differences from Bowen ratio results are presented in Figure 3.5. The results for the grass site data show that the three models produced similar estimates of daily E_p but that the turbulent transfer model produced markedly different estimates of hourly L_vE. Model estimated L_vE fluxes generally followed the diurnal progressions of wind, available energy and humidity parameters, becoming maximized away from the surface (i.e. negative flux) in the early afternoon, when both available energy and turbulence were

maximized, and negligible at night when available energy and turbulence were generally at a minimum. At the grass site, mean differences in estimated E_p between the Bowen ratio method and Penman-Monteith, turbulent transfer and Priestley-Taylor models were 0.5 mm day^{-1} (i.e. Std. Dev. = 0.4 mm day^{-1}), 0.8 mm day^{-1} (i.e. Std. Dev. = 0.6 mm day^{-1}) and 0.9 mm day^{-1} (i.e. Std. Dev. = 0.35 mm day^{-1}), respectively. Overall, aerodynamic turbulent transfer, Penman-Monteith and Priestley-Taylor mean daily E_p estimates were within 1.0 mm day^{-1} of Bowen ratio results and maximum daily E_p differences were within 1.6 mm day^{-1} of Bowen ratio results.

At hourly temporal scales, mean differences between Bowen ratio and Penman-Monteith, turbulent transfer and Priestley-Taylor models were 15.3 W m^{-2} (i.e. Std. Dev. = 26.0 W m^{-2}), 22.1 W m^{-2} (i.e. Std. Dev. = 82.8 W m^{-2}) and 28.2 W m^{-2} (i.e. Std. Dev. = 41.3 W m^{-2}), respectively. The turbulent transfer model tended to under-predict L_vE relative to Bowen ratio method (i.e. L_vE difference < 68 W m^{-2}) in the morning hours between sunrise and 10:00 a.m. and to a greater extent in the evening between approximately 4:00 p.m. and sunset (i.e. L_vE difference < 268 W m^{-2}). During mid-day periods between approximately 10:00 a.m. and 3:00 p.m. the turbulent transfer model over predicted LvE relative to the Bowen ratio by up to 291 W m^{-2}. The degree to which turbulent transfer and Bowen ratio results differed was greatest on clear days when estimated surface humidities and estimated surface-atmosphere humidity gradients were highest and minimal on cloudy days.

Linear regression results for the grass site data showed that the Bowen ratio method accounted for approximately 84 % of the variability in turbulent transfer model estimates of hourly L_vE (i.e. Std. Error = 72.6 W m^{-2}). The slope of the regression indicated that

Table 3.2. Linear regression results between Bowen ratio (BR), turbulent transfer (TT), Penman-Monteith (PM) and calculated (PT1) and constant (PT2) α versions of the Priestley-Taylor model. Results are based on hourly latent energy flux estimates

GRASS SITE

X Y	R^2	Std. Err. (W m^-2)	Slope of Regr.
BR vs. TT	0.84	72.6	1.32
BR vs. PM	0.96	25.7	1.04
BR vs. PT1	0.96	30.5	1.22
BR vs. PT2	0.96	30.4	1.19
TT vs. PM	0.81	61.2	0.86
TT vs. PT1	0.89	47.6	0.91
TT vs. PT2	0.90	47.6	0.88
PM vs. PT1	0.96	34.0	1.02
PM vs. PT2	0.95	34.0	0.99
PT1 vs. PT2	0.99	6.8	0.97

SNOW SITE

TT vs. PM	0.97	31.5	1.37
TT vs. PT1	0.05	79.0	0.09
TT vs. PT2	0.04	79.0	0.08
PM vs. PT1	0.02	79.0	0.05
PM vs. PT2	0.02	79.0	0.04
PT1 vs. PT2	0.97	15.7	0.97

the turbulent transfer model tended to overpredict L_vE relative to the Bowen ratio by approximately 32 %. The Bowen ratio method accounted for a much larger 96 % of the variability in the Penman-Monteith and calculated and constant α versions of the Priestley-Taylor methods, with standard errors of 25.7, 30.5 and 30.4 W m^{-2}, respectively. The slopes of the regressions showed that the Penman-Monteith and calculated and constant α

versions of the Priestley-Taylor methods over-predicted L_vE relative to the Bowen ratio method by 4, 22 and 19 percent, respectively.

Table 3.3. Summary of estimated potential evaporation and sublimation. Results are based on daily and total length of study period time-scales

GRASS SITE					
	mean (mm day^-1)	max. (mm day^-1)	min. (mm day^-1)	Std. Dev. (mm day^-1)	Total (mm)
BR	-3.8	-5.0	-2.8	0.6	-38
TT	-4.6	-5.8	-3.2	0.9	-46
PM	-4.3	-5.3	-3.1	0.7	-43
PT1	-4.8	-5.4	-3.7	0.6	-48
PT2	-4.7	-5.4	-3.5	0.7	-47
SNOW SITE					
TT	-4.7	-9.0	-1.7	2.1	-109
PM	-6.7	-12.6	-2.3	2.8	-156
PT1	0.2	1.4	-1.2	0.7	3
PT2	0.2	1.6	-1.0	0.7	4

Overall, the three models tended to overpredict L_vE relative to Bowen ratio results. The Penman-Monteith method compared most favorably with Bowen ratio results at both hourly and daily time periods. The Priestley-Taylor methods also compared similarly with Bowen ratio results though to a lesser degree than the Penman-Monteith method. The turbulent transfer method produced similar estimates of daily E_p as the Bowen ratio method but on an hourly basis this method tended to over-estimate L_vE relative to the Bowen ratio method during mid-day periods and underestimate L_vE during morning and evening

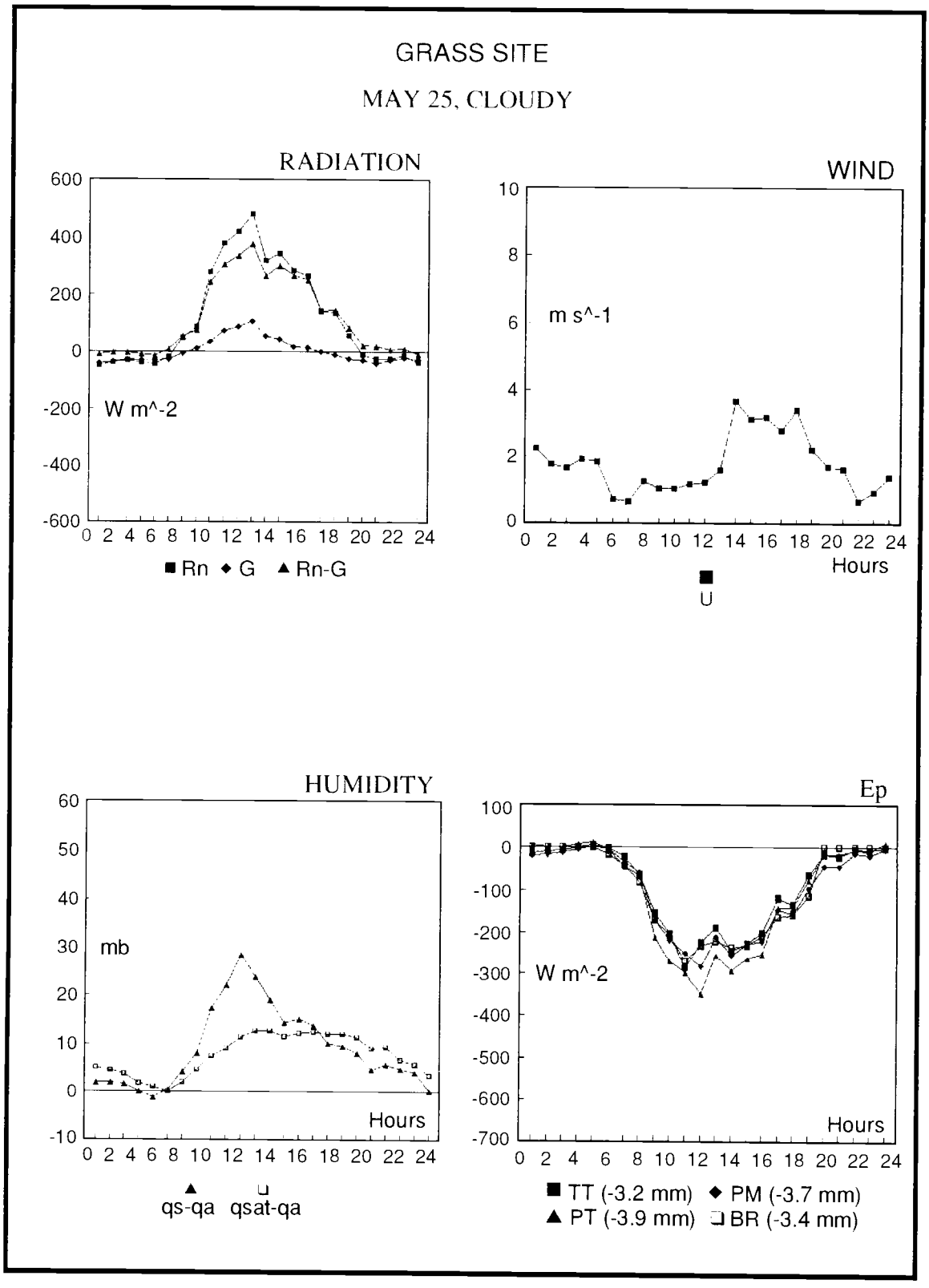

Figure 3.1. Plots of hourly climate, radiation and estimated latent energy exchange for a representative cloudy day at the grass site

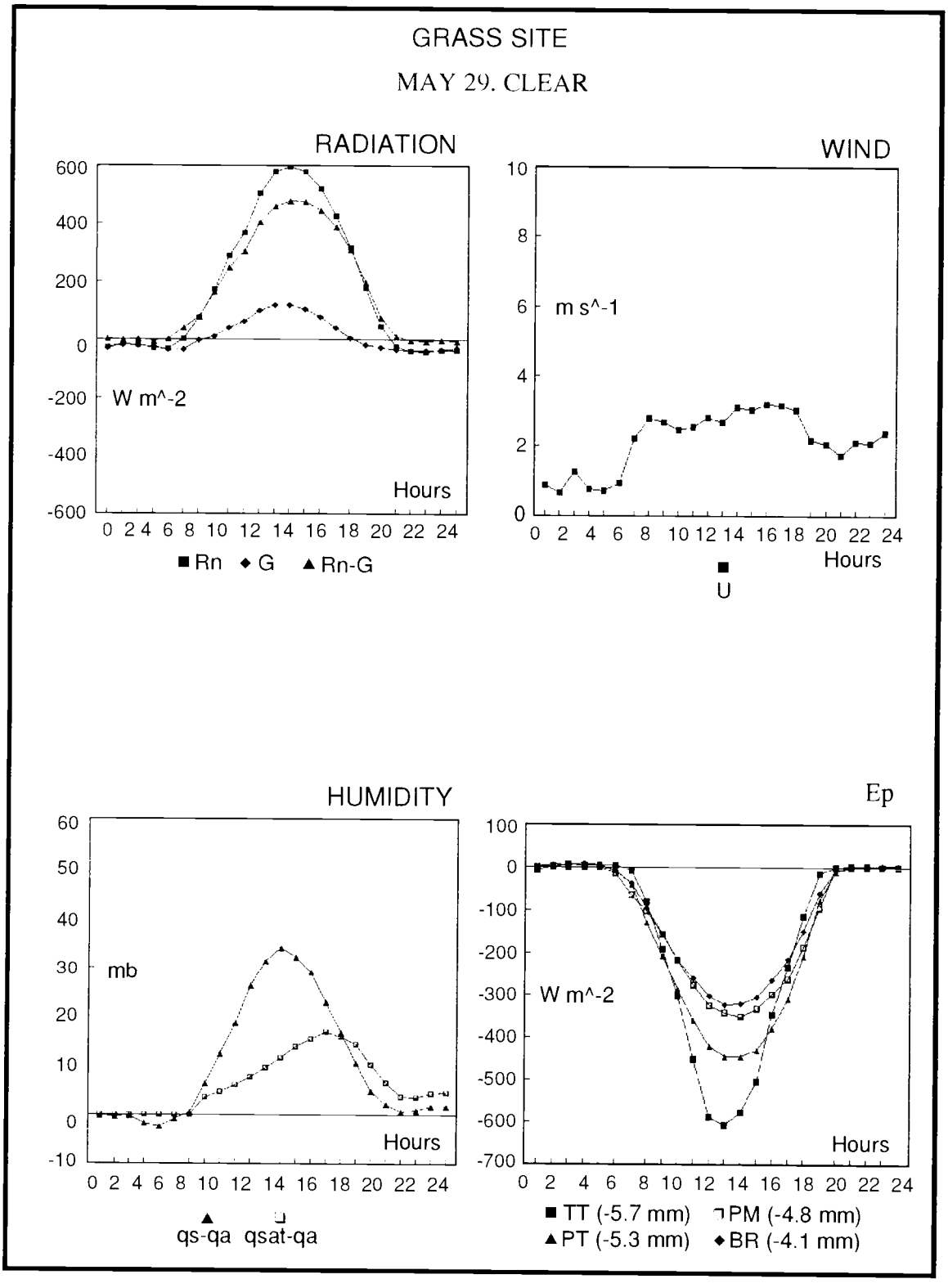

Figure 3.2. Plots of hourly climate, radiation and estimated latent energy exchange for a representative clear day at the grass site

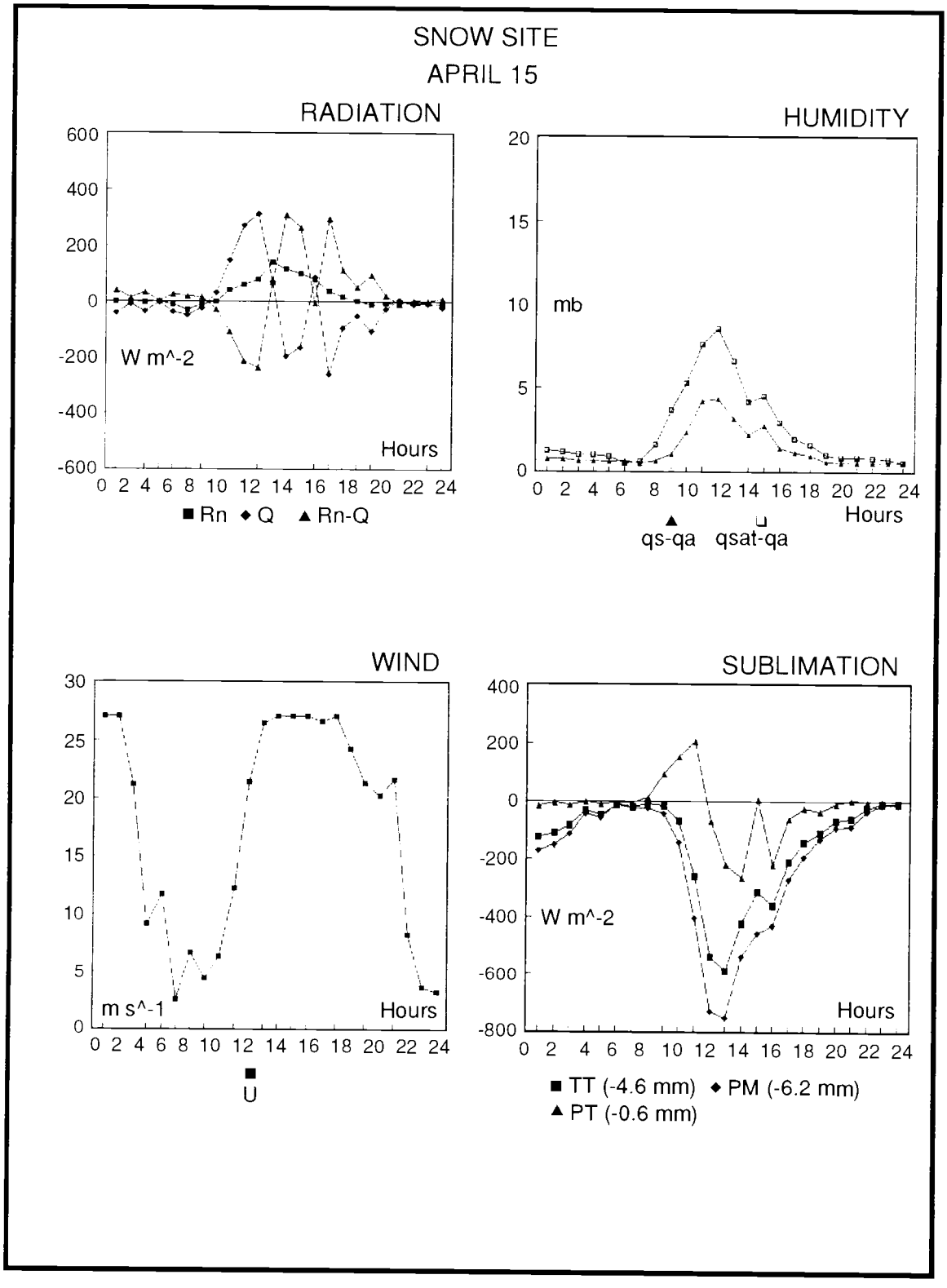

Figure 3.3. Plots of hourly climate, radiation and estimated latent energy exchange for April 15, 1986 at the snow site

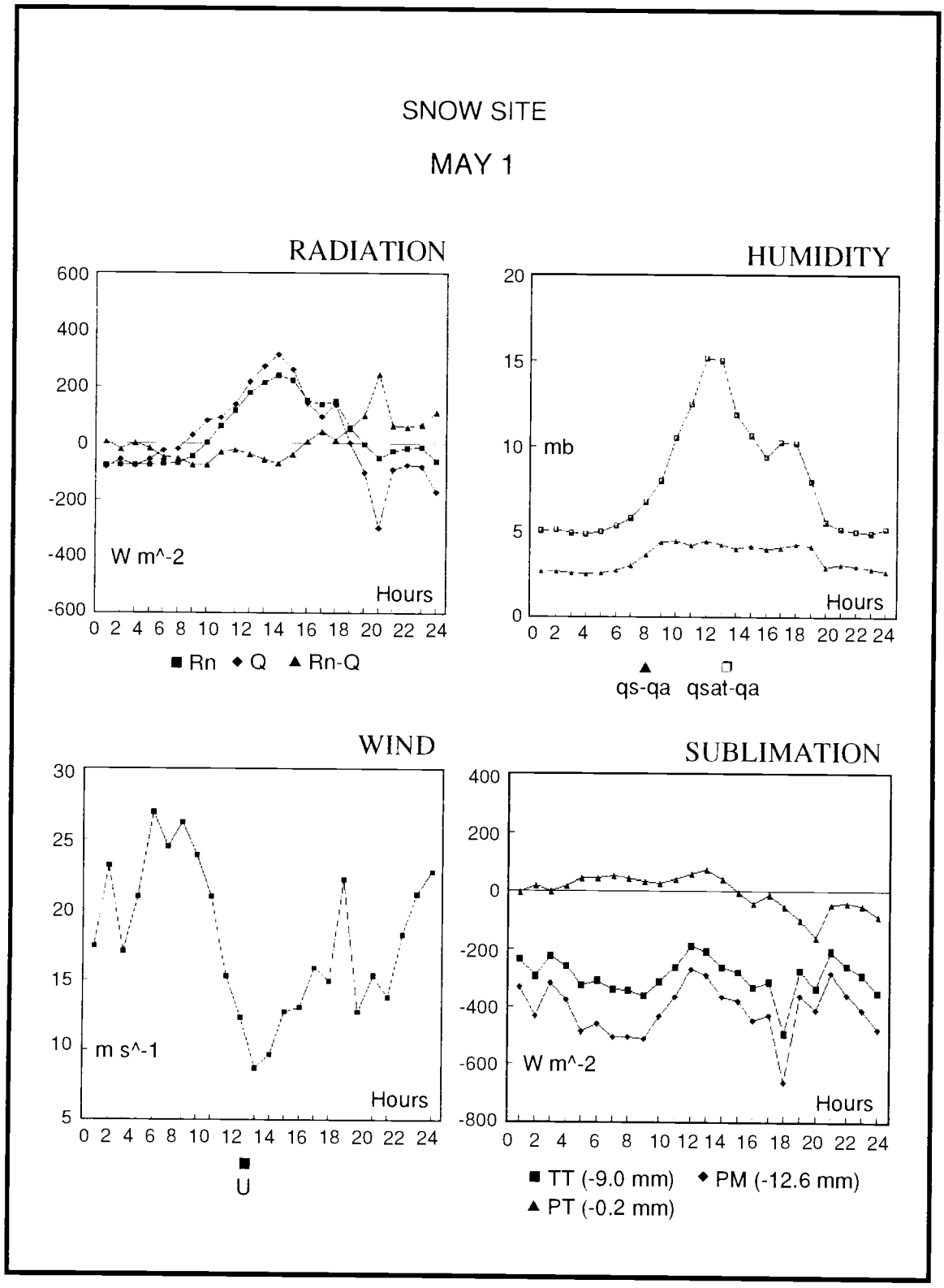

Figure 3.4. Plots of hourly climate, radiation and estimated latent energy exchange for May 1, 1986 at the snow site

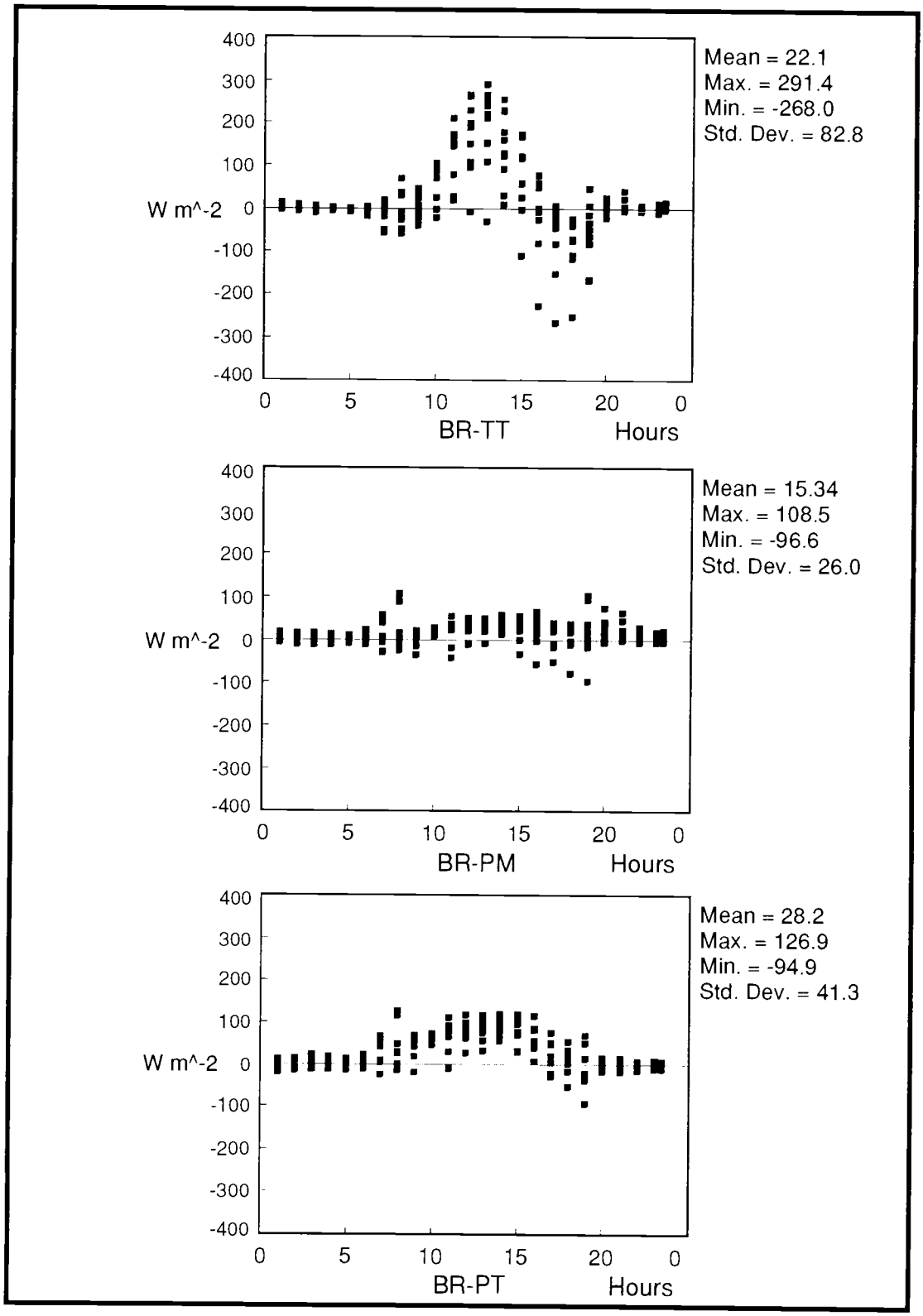

Figure 3.5. Plots of model differences in estimated hourly latent energy exchange from Bowen ratio results at the grass site over the 120 hour sample period

periods resulting in fairly substantial estimation differences of up to 290 W m^{-2}. The differences between Bowen ratio and model L_vE estimates were most likely due to experimental assumptions of saturated conditions. The Penman-Monteith and Priestley-Taylor models incorporated only minimal surface resistances. A primary experimental assumption of the turbulent transfer model was that q_s was the saturation value at T_s. The turbulent transfer model thus approximates conditions over a free water surface with no surface resistances to restrict the transport of water vapor. Surface saturation is also assumed in Equation (3) in order to derive α. Large surface temperatures during clear, mid-day periods, however, indicate that vegetation was probably under a certain degree of stress and the actual specific humidity was less than the saturated value at the surface temperature. Cloudy days had more moderate estimated surface humidities and lower wind speeds and more closely resembled potential conditions resulting in a higher correspondence between Bowen ratio, turbulent transfer and Priestley-Taylor L_vE estimates.

Regression results on the grass site data showed that Priestley-Taylor L_vE estimates derived using a calculated α accounted for approximately 98 % of the variance in Priestley-Taylor results derived using a constant α (i.e. Std. error = 6.8 W m^{-2}). The average difference in estimated L_vE between the two methods was only 3.4 W m^{-2} (i.e. Std. Dev. = 6.8 W m^{-2}) indicating that the results of the two Priestley-Taylor methods were virtually indistinguishable from one another.

Regression and error analyses showed general agreement between the three models at the grass site. The Penman-Moneith and Priestley-Taylor methods, however, were more closely associated with each other (i.e. R^2 = 0.96; Std. error = 34.0 W m^{-2}) than with the

turbulent transfer model (i.e. TT vs. PM: $R^2 = 0.81$, Std. error = 61.3 W m^{-2}; TT vs. PT: $R^2 = 0.85$, Std. error = 54.4 W m^{-2}) because they were primarily driven by available energy rather than turbulence and were less dependent on the assumption of surface saturation. The turbulent transfer model generally underestimated L_vE relative to the other methods in the morning and evening periods and overestimated the other methods during the mid-day periods between 10 a.m. and 3 p.m. These observed differences in the morning and evening periods may be attributed to a time lag between available energy, driven by R_n, and temperature and humidity gradients. The Bowen ratio, Penman-Montieth and Priestley-Taylor models respond directly to the amount of available radiant energy and predicted latent energy fluxes away from the surface when the available energy term was positive. Because G was fairly small at the grass site, the available energy term was usually positive at sunrise once R_n was sufficiently greater than G. The turbulent transfer model responds directly to wind speed and the surface-atmosphere humidity gradient and did not predict an evaporative flux until approximately 1-2 hours after sunrise when surface temperatures had warmed sufficiently to produce a positive humidity gradient. At mid-day, large surface-atmosphere humidity gradients driven by very warm surface temperatures resulted in generally greater turbulent transfer evaporative flux estimates than the other methods. During evening the grass surface generally cooled rapidly resulting in a larger rate of decrease in turbulent transfer L_vE estimates than Penman-Monteith and Priestley-Taylor model results.

At the snow site, Penman-Monteith and turbulent transfer model evaporative flux estimates were primarily negative (i.e. away from the surface) due to a high degree of

turbulence driven by high winds and cold, dry conditions over the entire study period. Sublimation estimates were large, averaging approximately 3.4 and 2.5 mm day^{-1} for the Penman-Monteith and turbulent transfer models, respectively. The models tracked each other closely at the hourly time step. This observation is supported by regression results which indicated a strong relationship (i.e. $R^2 = 0.97$; Std. error = 31.5 W m^{-2}) between the models. Although the models were highly correlated, the slope of the regression was positive ($\cong 1.37$) indicating that on average, the Penman-Monteith model overestimated hourly sublimation by 37 % relative to the turbulent transfer model. This offset ranged from a mid-day maximum of approximately 236 W m^{-2} to a minimum of 79 W m^{-2} at night. Differences between Penman-Monteith and turbulent transfer results were largely due to the magnitude of the differences between the humidity deficit (q_{sat}-q_a) and gradient (q_s-q_a) terms used to calculate L_vE in the Penman-Monteith and turbulent transfer models, respectively. Plots of the diurnal progressions of these terms (e.g. Figures 3.3 - 3.4) show that the average hourly, vapor pressure deficit term was 2.5 times larger than the estimated vapor pressure gradient term, resulting in Penman-Monteith L_vE estimates that were approximately 1.4 times larger than turbulent transfer model results.

Regression analyses showed that both versions of the Priestley-Taylor model were virtually identical at the snow site (i.e. $R^2 = 0.97$; Std. error = 7.9 W m^{-2}) with model differences within 79 W m^{-2} (Avg. = 0.8 W m^{-2}; Std. Dev. = 16 W m^{-2}), indicating that model results were consistent regardless of whether a calculated or constant α term was used. Priestley-Taylor model L_vE estimates ranged from slightly negative during the day to positive at night in response to daily progressions of available radiant energy. This

pattern resulted in an average daily condensation of 0.2 mm day^{-1} (Std. Dev. = 0.7 mm day^{-1}) and a cumulative net gain to the snowpack of 3.5 mm for the 22 day study period .

Measured snowpack losses and gains from sublimation and condensation were calculated as residuals from cumulative precipitation and net snowpack water loss measurements for the 22 day study period and were used to verify model results. These results are summarized in Table 3.4. Snowpack sublimation was estimated using a mass difference method from snow depth and profile density measurements taken from snow pits at the beginning and end of the 22 day study period. Initial and final snow depth measurements were 6 m and 5.9 m, respectively. Measured snow densities were approximately 548 kg m^{-3} with a range of measurement error of 25 kg m^{-3}. Snowpack sublimation estimated from the snow measurements was approximately -155 mm but due to the extreme depth of snowcover and measurement accuracies, values from -57 mm to -171 mm are considered to be within the noise of the measurement methods.

Cumulative snowpack water losses from sublimation for the 22 day study period were approximately 109 and 156 mm for the turbulent transfer and Penman-Monteith models, respectively. The Penman-Monteith model compared well with snowpack measurements, predicting within 99 % of measured sublimation losses. The turbulent transfer method also compared favorably with measured results considering the range of sublimation estimation accuracy of between -57 mm and -171 mm for the 22 day study period. The turbulent transfer method accounted for approximately 70 % of measured losses with an estimation error of approximately 30 %. The Priestley-Taylor methods predicted a total gain to the snowpack of approximately 3.5 mm resulting in a large estimation error of approximately

102%. These results indicate that the Priestley-Taylor models did not adequately account for sublimation over the snow site.

Table 3.4. Comparison of model results with a snowcover mass balance. The snowcover mass balance was derived from precipitation, snow depth and density profile measurements

Estimated Params.	Model Params.	GAIN (mm)	LOSS (mm)	Sublimation Difference (Meas.-Est.) (mm)	Est. / Meas. Sublimation (%)
Precipitation		56			
Runoff			-2		
Sublimation*			-155		
Net Change in Snowpack			-101		
	TT		-109	46	70
	PM		-156	1	100
	PT	3.5		-158	-2.3
*Sublimation calculated from a mass difference method resulting in an estimated range from -57 mm to -171 mm					

Sublimation was the dominant process controlling snowpack mass losses over the 22 day study period, accounting for approximately 3 % of the 5.9 m snowpack depth. The estimation errors for the turbulent transfer, Penman-Monteith and Priestley-Taylor models represented approximately 0.8, 0.6 and 3 % of the total snowpack. Given the range of sublimation estimation error, these results indicate that the Penman-Monteith and turbulent transfer models are adequate estimators of snowpack latent energy exchange. The assumption of a correlation between R_n and L_vE inherent in the Priestley-Taylor method does

not appear to hold over snow when the turbulent flux is large and available radiant energy is minimal or negative. As a result, the Priestley-Taylor model appears to be an unreliable estimator of latent energy exchange over a snowpack.

3.7 Summary and conclusions

The turbulent transfer, Penman-Monteith and Priestley-Taylor models were generally found to be most sensitive to the climate or radiation parameters that exhibited the largest magnitudes and hourly variations at each site. At the grass site where air temperatures were relatively warm, wind speeds were low and the magnitudes and diurnal ranges in surface temperatures and net radiation were large, the turbulent transfer model was most sensitive to the surface-atmosphere humidity gradient while the Penman-Monteith model responded primarily to the available radiant energy term followed by the vapor pressure deficit. The snow site was characterized by cold, dry, stable conditions with high winds where available radiant energy was frequently near zero or negative. The turbulent transfer model was found to respond primarily to wind speed at this site while the Penman-Monteith model was most sensitive to wind speed followed by the vapor pressure deficit. The Priestley-Taylor model responded primarily to available energy over both snow and grass surfaces since temperatures and humidities were only used indirectly to calculate α.

On a daily basis the three models produced similar results over the grass site where the turbulent fluxes were small and available energy was large and positive. On an hourly basis the three models compared similarly with Bowen ratio results on cloudy days. On

clear days the Penman-Monteith method was most comparable to Bowen ratio results followed by the Priestley-Taylor models, but differences between Bowen ratio and turbulent transfer hourly L_vE estimates were generally much greater, especially during mid-day periods when surface temperatures were maximized. These differences were generally attributed to turbulent transfer model experimental assumptions of surface saturation and zero canopy resistances and an observed time lag between the diurnal progressions of surface heating and cooling and net radiation.

At the alpine site, available radiant energy was frequently near zero or negative and the turbulent flux was large. Under these conditions the turbulent transfer and Penman-Montieth model results were highly correlated at the hourly time step though the Penman-Monteith model predicted an evaporative flux which was approximately 3 times larger than the turbulent transfer model. The model differences were generally attributed to differences between the vapor pressure deficit and estimated humidity gradient terms.

The Priestley-Taylor model performed remarkably well over the vegetated surface considering its simplistic design relative to the other two methods though the method generally overestimated E_p due to assumptions of surface saturation. The Priestley-Taylor model performed similarly using either a calculated or constant α term at hourly time steps. Thus any additional information derived by calculating the α term appears to be unwarranted given the loss of model simplicity. The Priestley-Taylor model consistently underestimated sublimation compared to the Penman-Monteith and turbulent transfer models at the snow site under conditions where the available radiant energy was near zero or negative and turbulent fluxes were large. These results indicate that this method's use-

fulness may be limited to conditions where available radiant energy is well correlated with turbulent fluxes and dominates the evaporative process.

3.8 Terms

A = Advective energy flux (W m^{-2})
a_H, a_E = Ratio of eddy diffusivity and viscosity for heat and water vapor ($a_H = a_E \cong 1.0$)
C_p = Specific heat of dry air at constant pressure (1005 J kg^{-1} K^{-1})
d_0 = Zero plane displacement (m)
ET = Evapotranspiration (mm)
ET_p = Potential evapotranspiration (mm)
E_p = Potential evaporation (mm)
E = Mass flux by evaporation or condensation (kg m^{-2} s^{-1})
F = Stability function (dimensionless)
g = Acceleration of gravity ($\approx$ 9.80616 m s^{-1})
G = Surface conductive energy flux (W m^{-2})
H = Sensible energy flux (W m^{-2})
h_0 = Height of roughness obstacle (m)
k = Von Karmen's constant ($\cong$ 0.4)
L = Obukhov stability length (m)
L_v = Latent heat of vaporization or sublimation (J kg^{-1})
PM = Penman-Monteith model
PT = Priestley-Taylor model
Q = Snow cover energy flux (W m^{-2})
Δq = Near surface humidity gradient (mb)
q, q_s = Specific humidity of the air and surface (gm kg^{-1})
q_a = Vapor pressure of air (mb)
q_{sat} = Saturation vapor pressure of air (mb)
r_a = Aerodynamic resistance (s m^{-1})
r_c = Canopy resistance (s m^{-1})
R_{iB} = Bulk Richardson number for the surface layer
R_n = Net radiation (W m^{-2})
s = Slope of the saturation vapor pressure-temperature curve (mb)
T_s, T_a, T_{avg} = Surface, air and averaged profile air temperatures (K)
ΔT = Near surface temperature gradient (K)
TT = Turbulent transfer model

u^* = Friction velocity ($m\ s^{-1}$)

u = Horizontal wind velocity at height z ($m\ s^{-1}$)

z_u, z_t, z_q = Measurement heights for wind, temperature and humidity (m)

z_0 = Surface roughness (m)

z_m, z_h, z_v = Surface roughness for momentum, heat and water vapor (m)

z = Measurement height (m)

ρ = Air density ($kg\ m^{-3}$)

Ψ_{sm}, Ψ_{sh}, Ψ_{sv} = Dimentionless stability functions for momentum, heat and water vapor

γ = Psychrometric constant ($\cong 0.66\ mb\ K^{-1}$)

Θ_a ,Θ_s = Potential temperature of air and surface (K)

α = Priestley-Taylor parameter (Dimensionless)

4 THE EFFECTS OF DATA TEMPORAL SCALE ON SURFACE ENERGY EXCHANGE CALCULATIONS

4.1 Abstract

The purpose of this study was to evaluate the effect of temporally averaged data on estimates of sensible and latent energy exchange, potential evaporation and sublimation. Temperature, wind and humidity data were collected by integration over 20 minute time intervals over a stand of Alta fescue grass for 10 days and over an alpine snowcover for approximately 12 months. Hourly meteorological data were averaged over 3, 6, 12, and 24 hour time intervals. An aerodynamic turbulent transfer model was used to calculate sensible and latent energy fluxes, potential evaporation and sublimation from these data and the results were compared with model results derived from the hourly meteorological data. Estimated energy and mass fluxes over the alpine snowpack were relatively unaffected as temperature, humidity and wind speed data were averaged from 1 to 24 hours. The magnitudes of the fluxes were increasingly underestimated using coarser temporal resolution data over the grass surface. The proportions of sensible and latent energy fluxes in the net turbulent transfer over the grass surface were maintained at approximately 10 and 90 percent, respectively, up to a 6 hour time interval but were altered to 3 and 97 percent, respectively, at the 12 and 24 hour time intervals. Estimated energy fluxes over the grass cover were maintained within approximately 93% of hourly estimates up to the 6 hour time period but were reduced to less than 50% of hourly estimates at coarser temporal scales. The Standard

Error of the Estimate between estimated E_p and reference conditions was generally within 0.4 mm day^{-1} using 3 and 6 hour data but increased to more than 1.7 mm day^{-1} using 12 and 24 hour data. The results of this study illustrate the importance of the diurnal range of wind and humidity on energy and mass flux calculations and provide a framework for the application of temporally averaged data in hydrologic studies.

4.2 Introduction

Surface fluxes of momentum, heat and moisture are major surface-atmosphere interactions which strongly influence, both directly and indirectly, key hydrologic processes such as snow metamorphism, runoff and available moisture through the regulation of surface energy. A substantial amount of research has been devoted towards the development of accurate parameterizations of these fluxes (Monteith, 1965; Priestley and Taylor, 1972; Brutsaert, 1982; Sharma, 1985; Monteith and Unsworth, 1990). Numerous micrometeorological approaches have been developed for estimating surface energy and moisture conditions. Most of these methods utilize hydrologic, meteorologic and plant physiological concepts to varying degrees to derive estimates of sensible and latent energy and mass exchange. These methods range in complexity from simple empirical approaches to more detailed, process oriented models that require inputs of temperature, humidity, wind velocity at one or more levels and radiant energy. The choice of model is generally dependent on the accuracy desired, the availability of quality, hydrologic and meteorological data and the temporal and spatial scales involved.

Aerodynamic turbulent transfer methods have been shown to accurately parameterize sensible and latent energy over a variety of surface conditions when driven by high quality input data (Brutsaert, 1982; Stewart, 1982; Marks and Dozier, 1992). These data generally consist of temperature, humidity and wind speed measurements at 2 or more levels. The turbulent transfer methods have generally been developed for use with high temporal resolution data on the order of minutes to an hour. The meteorological data required to drive these models, however, are rarely available at less than daily time periods.

Latent energy exchange in the forms of evaporation, condensation and sublimation represents the linkage between surface-atmosphere hydrologic and energy exchange processes. The accurate parameterization of latent energy is therefore of major importance in hydrologic research. The latent energy exchange from a cold snow surface represents a complex process whereby ice moves directly to the gaseous phase and back again by the process of sublimation. Latent energy exchange between a snowpack and the atmosphere can also occur in the form of evaporation and condensation of liquid water but this process is generally considered minimal when the temperature of the surface layer of the snowpack is less than 0.0 °C (Male and Gray, 1981; Marks and Dozier, 1992). Over snow, internal resistances to sublimation are minimal and the rates of energy exchange and sublimation are controlled by the surface roughness and external factors such as wind speed and temperature and humidity gradients between the surface and atmosphere (Stewart, 1982; Marks, 1988; Marks et al., 1992).

Evapotranspiration (ET) represents the combined evaporation from the surface and transpiration from vegetation. Potential evaporation (E_p) represents the upper limit of the evapotranspiration rate for a sufficiently moist surface under prevailing meteorologic conditions (Sharma, 1985; Brutsaert, 1982). The evapotranspiration rate over a vegetated surface when water is limiting is generally constrained by soil and vegetation resistances and will be less than the potential rate (Brutsaert, 1982). When a vegetated surface is sufficiently moist ET can be considered approximately equal to E_p when the surface roughness is not large (McNaughton and Black, 1973; Brutsaert, 1982).

E_p is an important indicator of the upper limit of the evapotranspiration rate over most surfaces and is a widely used approximation of the actual evapotranspiration rate over moist surfaces (Priestley and Taylor, 1972; Dickinson, 1984; Sharma, 1984). The potential evaporation component in regional climate and general circulation models has been demonstrated to play a major role in determining the likelihood of droughts (Rind et al., 1990), regional vegetation types and distributions (Neilson, 1993), the increased vigor of the hydrologic cycle and the diurnal range of surface temperatures over deserts (Warrilow and Buckley, 1989).

The diurnal cycle of energy exchange over a water body is usually weak, but over a non-water surface, latent and sensible energy fluxes typically exhibit a pronounced diurnal cycle (Brutsaert, 1982; Monteith and Unsworth, 1990; Parlange and Katul, 1992). Jobsen (1972) demonstrated that for a semi-empirical mass transfer method, the error associated with computed evaporation rates over Lake Hefner increased by a factor of more than 6 as the averaging time interval for wind speed and humidity data

increased from 3 hours to 1 day. The sensitivity of the turbulent transfer approach to the data averaging period is not well understood for non-water surfaces (Brutsaert, 1982). Because of the larger diurnal cycles in temperature, humidity and wind generally associated with non-water surfaces, it is likely that the effects of the data averaging period on computed energy and evaporation rates may be much larger than over water surfaces.

Detailed micro-meteorological data are rarely available at less than daily time-scales due to enormous equipment and man-power costs and data processing and storage requirements. The temptation may exist to derive estimates of surface energy exchange from micro-meteorological methods using more readily available daily climate data. For these reasons it is important to understand the errors that can be expected for longer data-averaging periods. The purpose of this study is to evaluate the effect of temporally-averaged wind speed, temperature and humidity data on computed rates of sensible and latent energy exchange and mass fluxes. This investigation is intended to help provide a framework for the application of temporally-averaged data in hydrologic studies.

4.3 Model background

Sensible and latent energy and net radiation represent the major components of the energy balance over most surfaces. In any given system, evaporation represents the

connection between surface energy and hydrologic processes. The energy balance of most land surfaces can be defined as follows:

$$0 \cong R_n + L_vE + H + G + M \quad (1)$$

where R_n, H, G, and M are the net radiative, sensible, conductive and advective energy fluxes, respectively, and L_vE is the latent energy flux where L_v is the latent heat of vaporization, condensation or sublimation and E is the evaporation rate. In most terrestrial environments, G and M are relatively small while turbulent energy and mass fluxes represented by sensible and latent energy are second only to net radiant energy in importance in the surface energy balance of terrestrial ecosystems (Budyko, 1974; Baumgartner and Reichel, 1975; Korzun et al., 1978). The energy balance over a snowpack is similar to that described by Equation (1) except for an additional snowcover energy term, Q, which is a residual term equal to the sum of R_n, L_vE, H, G and M. In temperature equilibrium, Q is equal to zero. A negative energy balance will tend to cool the snowcover while a positive energy balance will warm the snowpack, redistributing energy by mass transfer to lower snow layers. A positive Q will continue to warm the snowcover until the entire snowpack is approximately isothermal at 0.0 °C and any additional transfer of energy to the snowpack will result in snowmelt.

Numerous micrometeorological approaches for obtaining indirect estimates of sensible and latent energy exchange have been well documented (Tanner, 1967; Fleagle and Businger, 1980; Male and Gray, 1981; Brutsaert, 1982). Most of these methods

utilize one or some combination of two approaches, namely, the parameterization of components of the energy balance to derive sensible or latent energy or an aerodynamic approach where H and L_vE are estimated from wind speed, temperature and humidity gradient information (Brutsaert, 1982). Micrometeorological methods have generally been developed for use over short time periods ranging from several minutes to an hour. Most of these methods are based on physical principles but nearly all possess some form of empiricism.

The turbulent transfer of momentum, heat and water vapor between the surface and atmosphere are complicated forms of energy exchange and are not easily measured in the natural environment due to high spatial and temporal variability in these parameters. The turbulent transfer method attempts to describe the aerodynamics of flow near a surface so that the processes that control the transport of momentum, water vapor, and heat can be understood. The magnitudes of these transfer processes are driven by the horizontal wind velocity, the steepness of the vertical humidity and temperature gradients and atmospheric stability. The method used for this experiment is an aerodynamic turbulent transfer model adapted from Brutsaert (1982) and later modified by Marks (1988). The turbulent transfer model requires inputs of air density, air and surface temperatures and specific humidities, horizontal wind speed and surface roughness.

The following equations are solved iteratively at each timestep to obtain estimates of sensible and latent energy fluxes at a point:

Obukhov stability length:

$$L = (u^{*3}\ p)/ [k\ g\ (H / (T_a\ C_p) + 0.61\ E)] \quad (2)$$

Friction velocity:

$$u^* = (u\ k) / \ln [((z_u - d_0) / z_0) - (\psi_{sm}\ (z_u / L))] \quad (3)$$

Sensible energy flux:

$$H = ((\Theta_a - \Theta_s)\ a_H\ k\ u^*\ p\ C_p) / \ln [\ ((z_T - d_0) / z_0) - (\psi_{sh}\ (z_T / L))] \quad (4)$$

Mass flux:

$$E = ((q - q_s)\ a_E\ k\ u^*\ p) / \ln [\ ((z_q - d_0) / z_0) - (\psi_{sv}\ (z_q / L))] \quad (5)$$

The latent energy flux is defined as L_vE, where L_v is the latent heat of vaporization ($\cong 2.5*10^6$ J kg^{-1}) or sublimation ($\cong 2.8*10^6$ J kg^{-1}) and E is the mass flux by evaporation or condensation (kg m^{-2} s^{-1}). The variables a_H and a_E are the ratios of eddy diffusivity and viscosity for heat and water vapor, respectively. While there is some uncertainty associated with the values of these ratios, Brutsaert (1982) suggests that for most natural surfaces, $a_H = a_E = 1.0$. d_0 is the zero-plane displacement height. Brutsaert (1982) suggests $d_0 = (2/3)7.35*z_m$ where z_m is the surface roughness length for momentum (Paeschke, 1937; Kondo, 1977). For this investigation, a_H, a_E, and d_0 were set to the constant values indicated. Measurement heights, z_u, z_T and z_q were set at a constant 1.4 m height above the surface at the grass site. At the snow site, measurement heights varied from 1 to 4 meters over the course of the snow season due to

snowpack accumulation and ablation. The station elevations, z, were 70 m and 3087 m for the grass and snow sites, respectively. The surface roughness values for momentum, heat and water vapor were assumed to be equal to z_0 which was set at 1 cm over the grass site (Brutsaert, 1982). This value was selected as a representative roughness for Alta fescue grass cover (Oke, 1978; Brutsaert, 1982; Dickinson, 1984) and was assumed constant for the duration of the study period. At the snow site, z_0 ranged from 3 cm to 0.05 cm between the summer and winter months, respectively (Brutsaert, 1982; Marks and Dozier, 1992). Air and surface temperatures, T_a, T_s, air and surface humidities, q, q_s and wind speed, u, were obtained from station measurement data. The friction velocity, u*, was solved iteratively in Equations (2-5) at an hourly time-step. The variables ψ_{sm}, ψ_{sv} and ψ_{sh} are the stability functions for mass, heat and water vapor, respectively, and are calculated at each time-step follows:

For stable conditions, $\zeta = (z/L) > 0$:

$$\psi_{sm}(\zeta) = \psi_{sv}(\zeta) = \psi_{sh}(\zeta) = -\beta_s,\ 0 < \zeta \leq 1,\ \beta_s = 5 \tag{6}$$

$$\psi_{sm}(\zeta) = \psi_{sv}(\zeta) = \psi_{sh}(\zeta) = -\beta_s,\ \zeta > 1,\ \beta_s = 5 \tag{7}$$

For unstable conditions, $\zeta = (z/L) < 0$:

$$X = (1 - \beta_u \zeta)^{1/4},\ \beta_u = 16 \tag{8}$$

$$\psi_{sm} = 2\ln[(1+X)/2] + \ln[(1+X^2)/2] - 2\arctan X + \pi/2 \tag{9}$$

$$\psi_{sh}(\zeta) = \psi_{sv}(\zeta) = 2\ln[(1+X^2)/2] \tag{10}$$

The three most critical terms in the turbulent transfer Equations (3)-(5) are wind speed and the temperature and humidity gradients between the air and surface. The latent energy flux is primarily controlled by the magnitude of wind speed and the humidity gradient while the sensible energy flux is controlled by the magnitude of wind speed and the temperature gradient. Air temperature is only marginally involved in the determination of latent energy through the calculation of the Obukhov stability length (i.e. Eqn. 2).

4.4 Experimental design

4.4.1 Site 1

The Oregon Evapotranspiration Investigation Plot (ETIP) was located at the Oregon State University Schmidt Farm, approximately 15 km north of Corvallis, OR. The ETIP site was 2.11 ha (136 m x 155 m) in area and was covered by a uniform, well established stand of Alta fescue (*Festuca elatior*) grass maintained to a height of 8-20 cm. The soils found at the site were classified as Amity and Woodburn silt loams. These soils are deep and moderately to well drained through most of the profile. The ETIP site had manual and automatic meteorological stations, Bowen ratio and radiation stations. The stations were located in the center of the field site to maximize wind fetch. Vapor pressure, air temperature and horizontal wind speed were measured at 1.4 m by a dewpoint hygrometer (DEW-10), chromel-constant thermocouple and a three cup anemometer-photochopper, respectively. Surface temperatures were measured by an

Everest Interscience temperature transducer with a 45° field-of-view and a resolution of 0.5 °C. Surface conditions were maintained near saturation (soil moisture >= 85% of field capacity). Wind velocities at the surface were assumed to be zero. All measurements were collected every 5 seconds and integrated over 20 minute time intervals. These data were then averaged over 1, 3, 6, 12 and 24 hour time periods and used to derive estimates of the sensible and latent energy exchange using the aerodynamic turbulent transfer approach. A total of 10 days were used in this study representing both clear (i.e. cloud cover <= 1% of a 90° overhead field-of-view) and cloudy sky conditions for 1992. The days selected were Julian days 141-150.

4.4.2 Site 2

The Emerald Lake watershed (EML) is a remote, high elevation, alpine cirque located in Sequoia National Park in the Southern Sierra Nevada mountains of California. The site is 125 ha in area and is composed of bare, granite rock and talus with scattered patches of thin organic soil and alpine vegetation. Detailed meteorologic measurements were collected over a period of approximately 334 days during the 1986 water year at 4 sites within the basin. The data selected for this investigation were obtained on an exposed ridge approximately 300 m above a small tarn lake. This site remained snow covered over the period of data collection.

Temperature, wind speed and humidity measurements were obtained every 30 seconds and integrated over 15 minute intervals. The 15-minute data were then averaged

over 1, 3, 6, 12 and 24 hour time periods. Data collection at the EML site was extremely problematic due to its remote location and extreme weather conditions. Instruments and recording systems failed on several occasions during the 1986 snow season. Four instrument sites were maintained so that multiple measurements of critical parameters could be made. Missing data were synthesized from a combination of the current diurnal pattern, nearby measurements of the same parameter and manual field measurements. A detailed description of the site characteristics, meteorological measurements and monitoring within the Emerald Lake watershed is presented by Marks, Dozier and Davis (1992) and Marks and Dozier (1992).

Horizontal wind speed was measured using a combination of a totalizing anemometer and wind sensor attached to a current generator. The totalizing anemometer was most accurate at wind velocities less than 27 m s^{-1}. This anemometer was adequate for characterizing wind speeds during the spring and summer months but was not able to accurately measure winds during the winter months when wind velocities routinely exceeded 27 m s^{-1}. During the midwinter period the totalizing anemometer was replaced with a wind sensor attached to a current generator which was more sensitive at higher wind velocities. Air temperatures were measured using a series of three types of thermistors and a thermograph which provided an effective range from -40 to 80 °C and a measurement accuracy of within 0.5 °C. Snow surface temperature is exceedingly difficult to monitor on a sustained basis at remote locations because methods such as physical thermometry and radiative temperature measurements utilize instrumentation that requires frequent maintenance (Davis et al., 1984; Marks et al., 1992).

Research at a similar site in the Sierra Nevada mountains showed that the near-surface snow temperature tends to track the air temperature (Davis et al., 1984). This phenomenon occurs due to the low thermal conductivity of snow ($\cong 0.01$ J m^{-1} K^{-1} s^{-1}) which allows the surface layer to come into temperature equilibrium with the air even though large temperature differences may occur between the surface and lower layers of the snowpack. Snow surface temperatures were thus approximated as a function of the difference between the current air temperature $T_{a(i)}$ and the surface temperature $T_{s(i-1)}$ which was measured or calculated at the preceding time step:

$$T_{s(i)} = T_{s(i-1)} + [T_{a(i)} - T_{s(i-1)}] * a_{Ts} \quad (11)$$

This method was shown to provide stable estimates of snow surface temperatures at the Emerald Lake site (Marks, 1988; Marks et al., 1992). A value of 0.1 was used for the snow surface temperature change factor a_{Ts} because this produced a best fit with measured values obtained from snow pits and radiant thermometers. Snow surface temperatures were constrained to be at or below 0.0 °C, and once air temperatures remained above this temperature for any length of time, the snow surface temperature was held constant. This method was generally found to produce estimated surface temperatures over the 1986 snow season that were consistent with frequent snow pit temperature measurements of the top few centimeters of the snow surface (Marks et al., 1992).

Humidity is an exceedingly difficult parameter to monitor by direct measurement in remote alpine environments due to large extremes in air temperature and unreliable instrumentation. Humidities were therefore obtained using a combination of direct measurement and indirect estimation approaches. Humidities were measured over the snow surface using a capacitance-type sensor which was generally sensitive to within 0.25 mb at air temperatures greater than -15 °C but unreliable at lower temperatures. A second method was used to estimate humidities indirectly from air temperature and thermal radiation measurements using an approach described by Brunt (1932) and Brutsaert (1975) and later applied by Marks and Dozier (1979) and Marks (1988). This method generally produced diurnal ranges and daily means which were consistent with measured data but was found to be less accurate during cloudy conditions, wind free periods and when temperatures were extremely cold. Overall, however, this approach was found to be the most reliable method for obtaining humidities at the Emerald Lake site (Marks et al., 1992).

4.4.3 Climate

One of the fundamental factors governing the use of aerodynamic and combination energy balance models is the availability of detailed meteorological data required for model inputs. Detailed temperature, humidity and wind data are rarely available from meteorological stations at more than a single measurement height. These limitations generally require some simplification of model inputs. Continuous records of humidity and horizontal wind speeds were obtained from measurement data at a single height.

Surface and air temperature data were also available for both sites. Additional model input requirements were derived from assumptions of surface conditions. A snow surface layer is generally composed of a mixture of ice, water and air and the air fraction can be considered to be approximately at saturation (Langham, 1981). Surface vapor pressures at the snow site were thus approximated as the saturation vapor pressures at the surface temperatures. At the grass site, the surface was maintained near saturated conditions and the saturation vapor pressure at the measured surface temperature was used as a surrogate for a surface vapor pressure measurement. Horizontal wind speeds at the surface were also assumed to be zero.

A summary of hourly, wind, temperature and humidity at the grass and alpine sites is presented in Table 4.1. Mean daily wind velocities over the snow site showed little month to month variation, averaging approximately 7 m s^{-1} (i.e. Std. Dev. = 4.2 m s^{-1}) over the entire 1986 water year. Daily winds were relatively high and steady exhibiting a large diurnal range of between 5 and 14 m s^{-1}. Daily wind velocities at the grass site were of a much lower magnitude than the snow site by an approximate factor of 4. These winds exhibited a diurnal range of approximately 3 m s^{-1} with average daily velocities of 1.8 m s^{-1} (i.e. Std. Dev. = 1.0 m s^{-1}) over the 10 day period. Wind data from both sites showed strong diurnal patterns which were fairly consistent from day to day and month to month. Daily winds at both sites generally attained maximum velocities during the early afternoon and decreased to minimum values in the early morning. Overall, the alpine site had a much higher mean, maximum, minimum and

Table 4.1. Summary of hourly wind speed, temperature and humidity at the snow (EML) and grass (ETIP) sites

EML FIELD SITE (sample size = 8015)

	Mean	Max.	Min.	Range	Coeff. of Var.
U (m/s)	7.02	13.6	2.16	11.40	0.60
Ta (C)	2.46	12.98	-6.18	19.16	1.72
Ts (C)	-1.56	0.00	-5.49	5.49	0.88
Ta-Ts (°C)	4.01	13.18	-2.09	15.27	15.91
qa (mb)	3.32	4.69	1.74	2.95	0.19
qs (mb)	5.45	6.07	4.04	2.03	0.10
qa-qs (mb)	-2.13	-3.58	-0.07	3.51	0.39

ETIP FIELD SITE (sample size = 240)

	Mean	Max.	Min.	Range	Coeff. of Var.
U (m/s)	1.84	3.40	0.53	2.87	0.54
Ta (°C)	16.94	24.60	8.86	15.74	0.31
Ts (°C)	17.11	30.94	6.25	24.69	0.48
Ta-Ts (°C)	-0.16	-8.69	6.60	15.29	7.94
qa (mb)	13.20	15.90	1.03	0.55	0.11
qs (mb)	22.10	45.00	0.96	3.53	0.52
qa-qs (mb)	-8.80	-31.60	2.56	34.16	1.27

diurnal range in wind velocities than the grass site due to its more exposed, high elevation location.

The Emerald Lake field site remained snow covered during the entire period of data collection. Surface temperatures at the site were thus constrained to a narrow range between approximately -5 °C and 0.0 °C throughout the entire study period. Air temperatures at the snow site showed a moderate diurnal variation throughout the year with

daily ranges from approximately 2 °C during the coldest month of December to a maximum of 14 °C in April during active snowmelt.

The temperature gradient between the sensor and surface at the snow site was generally positive over the year ranging from a maximum monthly mean of 10 °C in August to near neutral or slightly negative conditions during the coldest months from November to March. The positive temperature gradient indicates a net daily transfer of sensible heat energy from the air to the colder snowpack for most of the year except during the coldest months when there was virtually no surface-air temperature difference. Negative temperature gradients during the winter months were mainly the result of sublimation and radiant cooling of the snow surface. Because the surface temperature was constrained to be at or below 0.0 °C, the temperature gradient between the surface and the air was primarily controlled by the variation in air temperature. On a daily basis, the temperature gradient between the air and the surface ranged from a maximum difference of approximately 8 °C during early afternoon to near zero at night. On a monthly basis, the daily temperature gradient was greatest during June, July and August when active melting of the snowpack was occurring and at a minimum during the coldest months of November through March.

The grass site remained near field capacity soil moisture conditions throughout the study period. Air and surface temperatures at this site were much warmer than the snow site. Surface temperatures generally ranged from a maximum near 30 °C during the early afternoon to a minimum of approximately 6 °C at night. Air temperatures

ranged between 9 and 25 °C and followed a similar diurnal pattern though of a smaller magnitude than the surface.

Surface and air temperatures at the grass site exhibited a large diurnal amplitude with the surface temperature amplitude approximately 1.5 times the amplitude in air temperature. While the surface and air temperatures were much greater at the grass site, the magnitude of the mean temperature difference between the surface and the air was similar between the grass and snow sites over a 24 hour time period. This is attributed to the observation that the temperature gradient at the grass site, though strongly negative during the day, tended to reverse at night due to radiant cooling of the surface.

The grass site was generally characterized by much larger average estimated daily humidities than the snow site. These characteristics can be attributed to the greater surface and air temperatures and more humid conditions found over the grass site. Vapor pressures at both sites exhibited distinct diurnal patterns corresponding to daily temperature progressions. These daily patterns varied little over the entire period of measurement for both sites. The diurnal range of vapor pressures and the differences in humidity between the surface and air were much greater over the grass surface due to the warmer, more unstable conditions. The daily range of estimated surface humidity at the grass site was approximately 5 times greater than the humidity range of the overlying air due to more extreme heating and cooling of the grass surface. The estimated humidity gradient over the grass surface was therefore predominantly influenced by the estimated surface humidity. The mean daily range in snow surface humidity was

approximately 50% of the daily humidity range of the overlying air because surface temperatures were confined to a very narrow range. As a result, the steepness of the humidity gradient was predominantly controlled by the humidity of the overlying air. Humidity gradients were greatly reduced over the snow site in response to the very low surface and air temperatures and were predominantly negative (away from the surface) over daily and monthly temporal scales. Humidity gradients over the grass site were strongly negative during mid-day periods in response to much warmer surface temperatures relative to the air. The humidity gradients reversed at night becoming slightly positive in response to radiative cooling of the surface. Over a 24 hour period the mean humidity gradient was generally slightly negative.

4.5 Results and discussion

The most critical terms governing the sensible and latent energy exchange in Equations (3) - (5) are wind speed and the temperature and humidity gradients between the air and the surface. The latent energy flux is controlled by the magnitude of wind speed and the humidity gradient while the sensible energy flux is controlled by wind speed and the temperature gradient. The importance of wind, humidity and temperature in the determination of sensible and latent energy at the surface is dependent on the relative magnitudes of these parameters and can be expected to vary depending on temporal and site conditions.

4.5.1 Sensible and latent energy

The turbulent transfer approach was used to calculate sensible and latent energy fluxes using hourly temperature, humidity and wind data collected over both study sites. These results are summarized in Table 4.2. The magnitude and direction of sensible and latent energy exchange over the grass and alpine snow sites was predominantly controlled by the magnitude and sign of the temperature and humidity gradients and the wind velocity. At the EML site, latent energy represented the dominant turbulent energy exchange process during the winter and spring months but was exceeded by sensible energy exchange during the summer months. Over the 1986 snow season latent energy exchange represented a slightly larger component of the net turbulent transfer of energy. Large estimated snow surface humidities relative to the extremely dry alpine atmosphere resulted in a turbulent transfer of latent energy away from the surface over the entire snow season. Colder snow surface temperatures relative to the air resulted in an average sensible energy transfer toward the surface over most of the snow season except during the coldest month of December when the direction of sensible energy exchange was reversed.

At daily temporal scales the snow site was characterized by a relatively small diurnal range in sensible and latent energy exchange due to the small daily range in surface temperatures, air temperatures and humidities. The grass site was characterized by large sensible and latent energy fluxes away from the surface during the day with latent energy representing approximately 90 % of the net transfer of energy from the surface. The magnitudes of these fluxes were driven primarily by large temperature and

Table 4.2. Summary of the estimated turbulent transfer at the snow and grass sites. Fluxes are derived from hourly input data and presented as daily and monthly means

SNOW SITE (sample size = 8015)							
MONTH	H+LvE W/m^2	H W/m^2	Coeff. of Var. (H)	H / H+LvE	LvE W/m^2	Coeff.of Var. (LvE)	LvE / H+LvE
Nov.	-45.2	6.6	4.4	0.11	-51.8	0.71	0.89
Dec.	-28.5	-0.2	41.2	0.01	-28.3	1.03	0.99
Jan	-63.0	4.1	8.2	0.06	-67.1	0.65	0.94
Feb.	-46.5	8.5	4.3	0.13	-55.0	0.72	0.87
March	-56.8	9.4	4.0	0.12	-66.2	0.86	0.88
April	-58.7	26.5	2.9	0.24	-85.2	0.64	0.76
May	-10.3	56.3	1.3	0.46	-66.6	0.81	0.54
June	26.2	92.9	0.8	0.58	-66.7	0.78	0.42
July	34.5	93.2	0.8	0.61	-58.7	0.74	0.39
Aug.	37.2	111.6	0.9	0.60	-74.3	0.83	0.40
Sept.	-46.5	52.3	1.5	0.35	-98.8	0.74	0.65
Year	-23.1	42.0	6.4	0.39	-65.2	0.77	0.61
GRASS SITE (sample size = 240)							
DOY	H+LvE W/m^2	H W/m^2	Coeff. of Var. (H)	H / H+LvE	LvE W/m^2	Coeff. of Var. (LvE)	LvE / H+LvE
142	-144.8	-17.2	1.98	0.12	-127.6	1.48	0.88
143	-151.3	-14.3	2.16	0.09	-137.0	1.43	0.90
144	-136.9	-7.8	3.83	0.06	-129.1	1.42	0.94
145	-93.5	-5.1	3.96	0.05	-88.4	1.08	0.94
146	-116.7	-17.1	1.98	0.15	-99.7	1.35	0.85
147	-158.2	-28.7	1.54	0.18	-129.4	1.32	0.82
148	-99.9	-14.0	2.01	0.14	-85.9	1.44	0.86
149	-178.3	-23.1	1.93	0.13	-155.1	1.29	0.87
150	-181.9	-22.6	1.88	0.12	-159.2	1.37	0.87
151	-143.2	-14.7	2.39	0.10	-128.5	1.37	0.90
10 Day	-142.9	-14.9	2.35	0.10	-127.9	1.39	0.90

humidity gradients generated by very warm surface temperatures. At night radiant cooling of the surface resulted in a reversal in the direction of both sensible and latent energy exchange with sensible energy becoming the dominant form of energy transfer.

4.5.2 Temporal averaging experiment

Hourly wind speed, temperature and humidity data were integrated over 3, 6, 12 and 24 hour time intervals in order to evaluate the effects of temporally averaged data on estimated surface energy exchange. Coefficients of variation were computed from the averaged data and used in conjunction with mean and data range information as a measure of the relative variability and central tendencies in the data. The impact of the temporal averaging process on the data variability was markedly different between the grass and snow sites. Wind, temperature and humidity variability as defined by coefficients of variation over the snow site decreased by approximately 44, 6, and 9 percent, respectively, between the hourly and 24 hour time steps. The relatively moderate response in temperature and humidity variability is most likely due to the fairly stable conditions observed over the snow site which resulted in generally small daily ranges in temperatures and humidities over the entire snow season. The impact of the averaging process on temperature and humidity gradients was also minimal over the snow surface since the daily ranges in these gradients were also relatively small and of a constant direction. The snow site represented an exposed, alpine ridge. Wind velocities were routinely very large and exhibited a high variability over time ranging from approximately 2 to 14 m s^{-1}. Because of the larger degree of variability in this data

parameter, wind velocities were more impacted by the averaging process than the other variables.

The variability of the averaged data parameters at the grass site decreased from the hourly to 24 hour time intervals. Coefficients of variation show that the data variability was generally within 80 to 90 percent of hourly conditions for the 3 and 6 hour time periods but decreased to less than 50% at the 12 and 24 hour time steps. These results generally reflect a dampening of the magnitude of the diurnal range in the data through successive averaging periods which resulted in a decrease and increase in daily data maxima and minima, respectively. The parameters most impacted by the averaging process were those that exhibited the greatest daily range in magnitude, namely, estimated surface humidity and surface temperature. The grass site data were more heavily impacted at the 12 and 24 hour time intervals because daily maxima and minima were minimized to a greater extent at these courser time periods which resulted in a greater suppression of diurnal variability. Temperature and humidity gradients were also impacted to a greater degree at the 12 and 24 hour time steps due to the reversal in the directions of these gradients at night which resulted in an averaging of positive and negative values at these coarser time intervals.

4.5.3 Temporal averaging effects on energy flux estimates

The turbulent transfer approach was used to estimate sensible and latent energy fluxes from 3, 6, 12 and 24 hour wind, humidity and temperature data. These results

were then compared with fluxes estimated from hourly data and are summarized in Table 4.3. Estimated turbulent flux and mass flux results are also presented in Figures 4.1 and 4.2 for the snow and grass sites, respectively. Mean sensible and latent energy values and the proportions of these terms in the estimated net turbulent transfer of energy over the snow surface was generally maintained regardless of the temporal resolution of the input data. The variability in the estimated energy fluxes as indicated by coefficients of variation decreased by approximately 37% between the hourly to 24 hour time steps. Overall, however, the predicted fluxes were only slightly impacted by the averaged data for the entire period of record at the snow site.

The results obtained over the grass surface were generally comparable to those obtained over the snow surface for the 3 and 6 hour time intervals, but substantially different at coarser temporal resolutions. Average latent and sensible energy fluxes estimated from 3 and 6 hour data were within approximately 90% of estimates derived from hourly data. H and L_vE estimates decreased markedly to approximately 14 and 49 percent of hourly estimates, respectively, using 12 hour data intervals and 15 and 47 percent of hourly estimates at 24 hour data intervals. The relative proportions of sensible and latent energy in the net turbulent transfer of energy were generally maintained at approximately 10 and 90 percent, respectively, using both the 3 and 6 hour data. The proportion of the net turbulent transfer due to H decreased to approximately 3% while the proportion of H+LvE due to LvE increased to approximately 97 % at the 12 and 24 hour time-steps. Coefficients of determination indicate that mean daily energy fluxes derived from 3 and 6 hour data accounted for approximately 70% of the variation in

Table 4.3. Summary of the estimated turbulent transfer derived from temporally averaged data

SNOW SITE									
1 HOUR		3 HOUR		6 HOUR		12 HOUR		24 HOUR	
	Mean W/m^2	Mean W/m^2	3 hr./ 1 hr.	Mean W/m^2	6 hr./ 1 hr.	Mean W/m^2	12 hr. / 1 hr.	Mean W/m^2	24 hr. / 1 hr.
H	42.0	41.7	0.99	41.9	0.99	42.2	1.00	42.4	1.01
LvE	-65.2	-64.8	0.99	-64.7	0.99	-65.2	1.00	-65.8	1.01
H+LvE	-23.2	-23.1	0.99	-22.8	0.98	-23.0	1.00	-23.4	1.01
H / Net	0.39	0.39	1.00	0.39	1.00	0.39	1.00	0.39	1.00
LvE / Net	0.61	0.61	1.00	0.61	1.00	0.61	1.00	0.61	1.00
GRASS SITE									
1 HOUR		3 HOUR		6 HOUR		12 HOUR		24 HOUR	
	Mean W/m^2	Mean W/m^2	3 hr. / 1 hr.	Mean W/m^2	6 hr. / 1 hr.	Mean W/m^2	12 hr. / 1 hr.	Mean W/m^2	24 hr. / 1 hr.
H	-14.9	-15.2	1.02	-13.7	0.92	-2.0	0.14	-2.2	0.15
LvE	-127.9	-129.5	1.01	-118.4	0.93	-62.6	0.49	-60.2	0.47
H+LvE	-142.8	-144.7	1.01	-132.1	0.92	-64.6	0.45	-62.5	0.44
H / Net	0.10	0.10	1.00	0.10	1.00	0.03	0.29	0.03	0.35
LvE / Net	0.90	0.90	1.00	0.90	1.00	0.97	1.08	0.96	1.07

mean daily energy fluxes derived from the hourly data. Mean daily energy fluxes derived from the 12 and 24 hour data, however, accounted for only 15% of the variation in the energy fluxes derived from hourly data. Overall, estimates of sensible and latent energy exchange derived from 3 and 6 hour data were comparable to hourly estimates. These fluxes were underestimated by more than 50%, however, using 12 and 24 hour data.

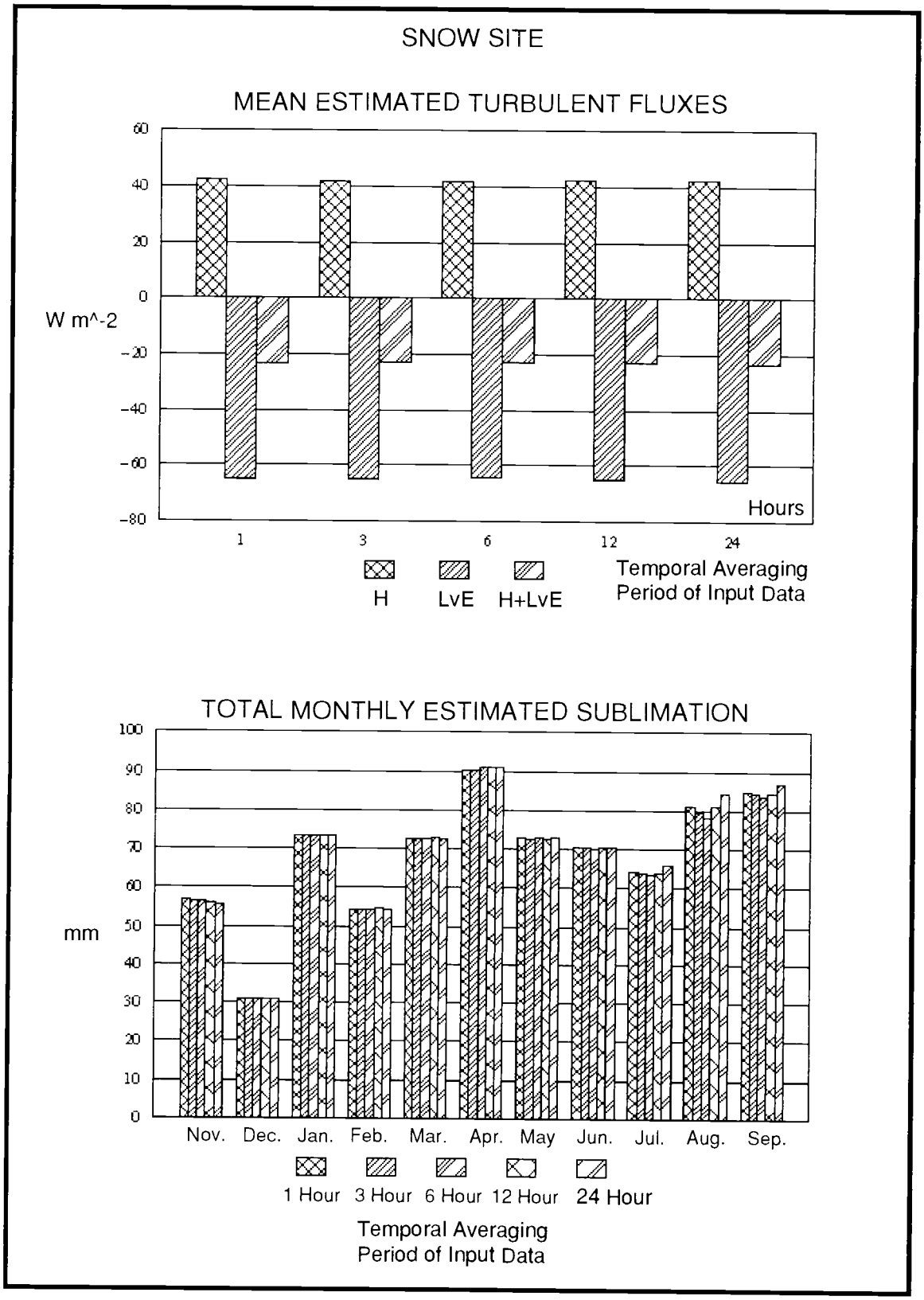

Figure 4.1. Summary of estimated turbulent transfer and sublimation at snow site

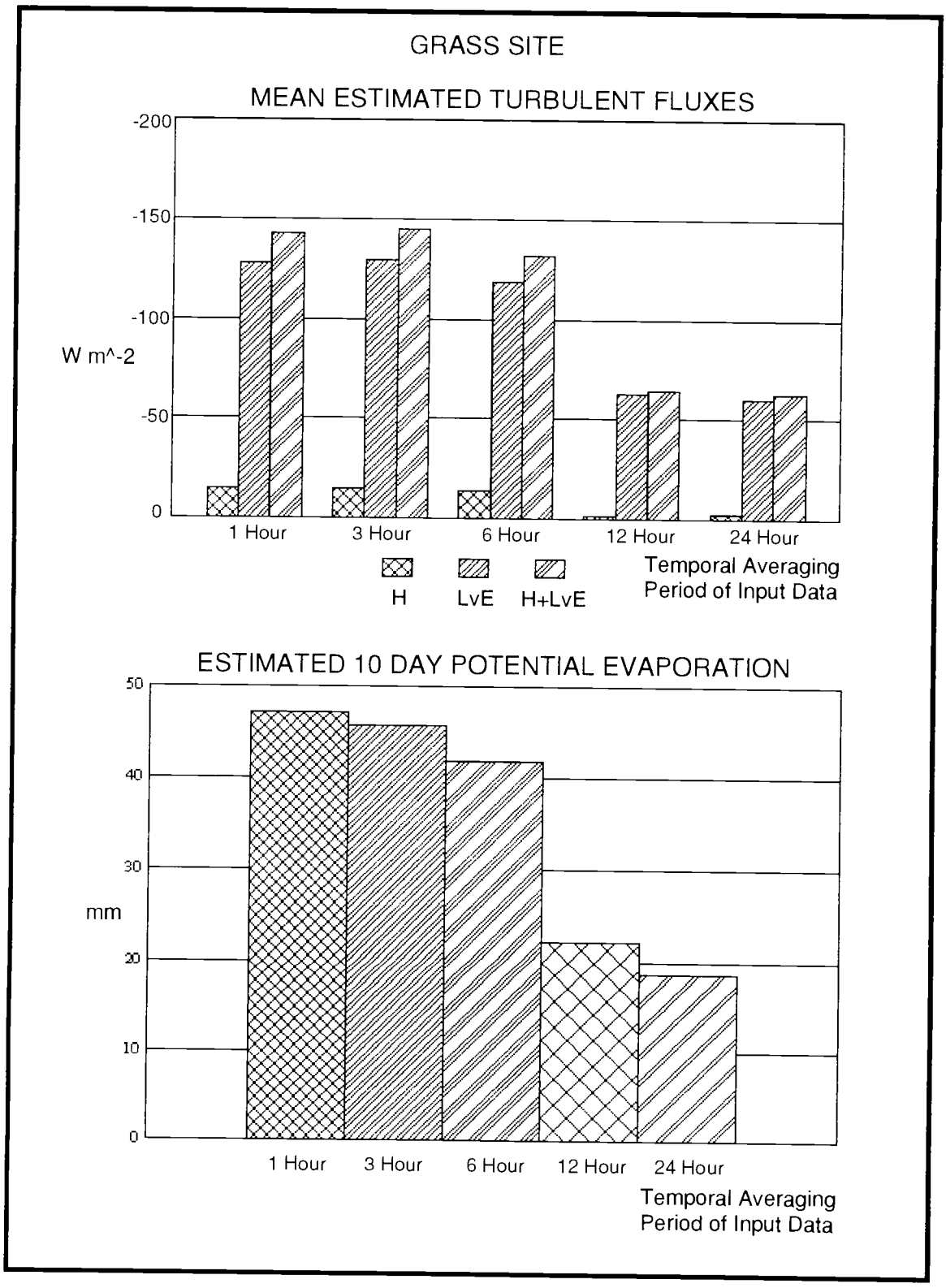

Figure 4.2. Summary of estimated turbulent transfer and potential evaporation at grass site

4.5.4 Mass flux estimates

Latent energy fluxes (W m^{-2}) derived from temporally averaged humidity, wind and temperature data were converted to mass fluxes (mm s^{-1}) and accumulated to represent total daily E_p, and sublimation (mm day^{-1}) over the grass and snow sites. Daily E_p and sublimation derived from hourly data were used as a reference upon which all other daily mass flux estimates were compared. The standard error of the estimate (SEE) provides a measure of the scatter of data around a reference point (Clark and Hosking, 1986). The SEE was used to determine the degree of difference between daily E_p and sublimation estimates derived from temporally averaged input data and hourly results. The coefficient of determination (R^2) was used to assess the degree of correlation between daily mass fluxes derived from temporally averaged and hourly input data. These results are summarized in Table 4.4.

Sublimation losses averaged approximately 2 mm day^{-1} at the snow site over the 1986 snow season. Total monthly sublimation losses averaged roughly 68 mm over the entire snow season, accounting for a total loss for the year of 751 mm. This figure represents the principal loss of water from the snowpack, accounting for approximately 80% of the total precipitation for the 1986 snow season (Kattelmann and Elder, 1991). Sublimation losses were generally greatest at the snow site during the spring and summer months when drier, windy conditions maximized temperature and humidity gradients. A comparison of sublimation estimates derived from hourly and temporally averaged input data show that sublimation derived from temporally averaged data were within 96% of hourly results for the entire snow season. Standard errors of estimated

daily mass fluxes increased from 0.06 to 0.12 mm day^{-1} using input data averaged from 3 to 24 hour time periods. This degree of error was not determined to be significant since these values were well within the estimation parameter uncertainty of approximately 0.5 mm day^{-1} (Marks and Dozier, 1992). Coefficients of determination computed between sublimation estimates derived from hourly input data and temporally averaged results showed that temporally averaged results accounted for approximately 99% of the variation in hourly results regardless of the time period examined. Overall, no significant differences were observed between temporally averaged and reference (i.e. derived from hourly input data) sublimation estimates over the entire snow season.

Estimated daily potential evaporative losses derived from hourly data over the grass site ranged from 3.2 to 6.2 mm day^{-1} with a total loss of 47 mm for the 10 day data collection period. Daily mass exchange rates were generally much greater over the grass site due to much larger temperature and estimated humidity gradients relative to the more stable snow surface. Daily E_p was generally underestimated using temporally averaged data for the entire 10 day period. The underestimation of E_p relative to hourly estimates ranged from approximately 3 and 12 percent using 3 and 6 hour data to 53 and 61 percent using 12 to 24 hour data, respectively. The differences between E_p estimates and hourly reference conditions were relatively small up to the 6 hour time interval with estimated E_p within approximately 88% of the reference state. This discrepancy increased markedly at the 12 and 24 hour time steps with estimated E_p decreasing to less than half of the reference state. The degree of error between

Table 4.4. Summary of monthly sublimation and daily potential evaporation derived from temporally averaged data

SNOW SITE (sample size = 334 days)									
	1 HOUR	3 HOUR		6 HOUR		12 HOUR		24 HOUR	
MONTH	Subl. (mm)	Subl. (mm)	3 hr. / 1 hr.	Subl. (mm)	6 hr. / 1 hr.	Subl. (mm)	12 hr. /1 hr.	Subl. (mm)	24 hr. /1 hr.
Nov.	-57	-57	1.00	-56	0.98	-56	0.98	-56	0.98
Dec.	-31	-31	1.00	-31	1.00	-31	1.00	-31	1.00
Jan.	-73	-73	1.00	-73	1.00	-73	1.00	-73	1.00
Feb.	-54	-54	1.00	-54	1.00	-55	1.00	-54	1.00
March	-72	-72	1.00	-73	1.00	-73	1.00	-73	1.00
April	-90	-90	1.00	-91	1.00	-91	1.00	-91	1.00
May	-73	-73	1.00	-73	1.00	-73	1.00	-73	1.00
June	-71	-70	0.99	-70	0.99	-70	0.99	-70	0.99
July	-64	-64	1.00	-64	1.00	-64	1.00	-66	1.00
Aug.	-81	-79	0.97	-78	0.96	-81	1.00	-84	1.00
Sept.	-85	-84	0.99	-83	0.98	-84	1.00	-87	1.00
Year	-751	-747	0.99	-746	0.99	-751	1.00	-759	1.00
SEE (mm/day)	-----	0.06	-----	0.09	-----	0.10	-----	0.12	-----
R^2	-----	0.99	-----	0.99	-----	0.99	-----	0.99	-----
GRASS SITE (sample size = 10 days)									
	1 HOUR	3 HOUR		6 HOUR		12 HOUR		24 HOUR	
	Ep (mm)	Ep (mm)	3 hr. / 1 hr.	Ep (mm)	6 hr. / 1 hr.	Ep (mm)	12 hr / 1 hr.	Ep (mm)	24 hr. / 1 hr.
10 Day	-47.2	-45.7	0.97	-41.8	0.88	-22.1	0.47	-18.4	0.39
SEE (mm/day)	-----	0.18	-----	0.64	-----	2.94	-----	3.0	-----
R^2	-----	0.99	-----	0.97	-----	0.40	-----	0.37	-----

estimated E_p and reference conditions as indicated by the SEE showed an average error of approximately 0.4 mm day^{-1} at the 3 and 6 hour time intervals. The amount of error increased markedly at the 12 and 24 hour time intervals to approximately 3 mm day^{-1}. These errors are within the acceptable limits dictated by the model estimation error of

approximately 0.5 mm day^{-1} at the 3 and 6 hour time intervals. Significant errors occur, however, when the 12 and 24 hour time interval data are used to estimate E_p. Coefficients of determination between estimated and reference daily E_p decreased as the time interval of the data increased from 3 to 24 hours. E_p estimated from 3 to 6 hour data correlated well with reference E_p with R^2 values above 0.95. The correlation between reference and estimated E_p decreased markedly using 12 and 24 hour data where the amount of variance in reference E_p accounted for by the averaged data dropped to approximately 38%. Overall, these results indicate that accurate estimation of evaporation over the grass site using a turbulent transfer approach requires a data temporal resolution of 6 hours or less. The use of coarser resolution data has the potential to underestimate E_p by more than 50%.

4.6 Summary and conclusions

Temporal averaging of temperature, humidity and wind data from 1 to 24 hours reduced the daily range and variability in the data. The variables most affected by the averaging process tended to exhibit the largest daily ranges while the impacts on data with small daily variations was minimal. The snow surface was fairly stable over 24 hour periods. As a result, the daily variations in temperature, humidity and wind speed were generally small and temperature and humidity gradients maintained a constant direction over a 24 hour period. Estimated energy and mass fluxes over the alpine snowpack were therefore relatively unaffected as temperature, humidity and wind speed data were averaged from 1 to 24 hours .

Temperatures, humidities and wind speeds over the grass surface exhibited very large daily ranges. These characteristics were most prevalent in surface temperatures and estimated surface humidities due to extreme day-night surface heating and cooling. Temperature and estimated humidity gradients at this site were also large and tended to reverse at night in response to radiant cooling of the surface. The averaging process strongly reduced the magnitudes and variability in these gradients particularly over 12 and 24 hour time periods. As a result, energy and mass fluxes were generally underestimated using averaged temperature, humidity and wind data, especially at the coarser time-scales. The proportions of sensible and latent energy in the estimated turbulent transfer of energy at the surface were generally maintained at 10 and 90 percent, respectively, up to a 6 hour time interval but were altered to approximately 3 and 97 percent at the 12 and 24 hour time intervals. The magnitudes of these fluxes were increasingly underestimated using coarser resolution data. Mean sensible and latent energy fluxes were maintained within approximately 97% of estimates derived from hourly input data up to the 6 hour time interval, but were reduced to less than half of hourly results at the 12 and 24 time periods. Errors associated with estimates of potential evaporation also increased with coarser temporal resolution data but were generally within 0.7 mm day^{-1} for 3 and 6 hour time periods. Potential evaporation derived from 12 and 24 hour data underestimated reference E_p by more than 2.9 mm day^{-1}.

Climate and hydrologic studies that use temporally averaged temperature, humidity and wind data to predict surface energy and mass exchange using turbulent transfer

methods must take into account the temporal resolution of the data and the physical conditions of the surfaces over which these models are applied. This study has demonstrated that while fairly coarse temporal resolution data can be used over a stable snowpack, these data can cause energy and mass fluxes to be underestimated by more than 50% when large diurnal variations in wind speeds and temperature and humidity gradients are present. These results relate the need to account for the diurnal variation in temperature, humidity and wind over surfaces where these variables exhibit a pronounced diurnal cycle and the applicability of coarse resolution data where the diurnal cycle of wind, temperature and humidity is weak.

4.6 Terms

A = Advective energy flux (W m^{-2})
a_H, a_E = Ratio of eddy diffusivity and viscosity for heat and water vapor ($a_H = a_E \cong 1.0$)
C_p = Specific heat of dry air at constant pressure ($\cong 1005$ J kg^{-1} K^{-1})
d_0 = Zero plane displacement (m)
E = Mass flux by evaporation or condensation (kg m^{-2} s^{-1})
ET = Evapotranspiration (mm)
ET_p = Potential evapotranspiration (mm)
E_p = Potential evaporation (mm)
G = Surface conductive energy flux (W m^{-2})
g = Acceleration of gravity (≈ 9.80616 m s^{-1})
H = Sensible energy flux (W m^{-2})
h_0 = Height of roughness obstacle (m)
k = Von Karmen's constant ($\cong 0.4$)
L = Obukhov stability length (m)
L_v = Latent heat of vaporization or sublimation (J kg^{-1})
Q = Snow cover energy flux (W m^{-2})
Δq = Near surface humidity gradient (mb)
q_a = Vapor pressure of air (mb)

q_{sat} = Saturation vapor pressure of air (mb)

q, q_s = Specific humidity of the air and surface (gm kg^{-1})

R_n = Net radiation (W m^{-2})

s = Slope of the saturation vapor pressure-temperature curve (mb)

ΔT = Near surface temperature gradient (K)

T_s, T_a, T_{avg} = Surface, air and averaged profile air temperatures (K)

u* = Friction velocity (m s^{-1})

u = Horizontal wind velocity at height z (m s^{-1})

z = Measurement height (m)

z_u, z_t, z_q = Measurement heights for wind, temperature and humidity (m)

z_0 = Surface roughness (m)

z_m, z_h, z_v = Surface roughness for momentum, heat and water vapor (m)

ρ = Air density (kg m^{-3})

Θ_a ,Θ_s = Potential temperature of air and surface (K)

γ = Psychrometric constant ($\cong$ 0.66 mb K^{-1})

Ψ_{sm}, Ψ_{sh}, Ψ_{sv} = Dimensionless stability functions for momentum, heat and water vapor

5 SENSITIVITY OF A SNOWPACK TO RAIN-ON-SNOW CONDITIONS

5.1 Abstract

Rain-on-snow events are a common occurrence on mountain slopes within the Pacific Northwest. In cleared areas, such as those resulting from clear-cut logging practices, advective energy from rainfall combined with increased turbulence is suspected to enhance snowmelt, increasing the risk of erosion and downstream flooding during rainfall events. The objective of this investigation was to evaluate the sensitivity of snowmelt processes to conditions which occur during rain-on-snow events in order to 1) determine why rain-on-snow floods occur and 2) evaluate whether clear-cut logging practices enhance snowmelt. An energy balance, snowmelt model was used to evaluate the energy and mass balance of a snowpack during spring melt conditions in a clear-cut. The snowpack was found to be thermodynamically active and under a continuous state of melt during rain-on-snow events. The snowcover became saturated with liquid water within 1-2 hours after the initiation of a rainfall event and rainfall was translated directly through the snowpack as runoff. Snowmelt was generally light during rainfall events, averaging less than 1.0 mm hr^{-1} under measured, calm wind conditions. The advective energy from rainfall had a minimal effect on estimated snowmelt except under extreme events. Net all-wave radiation controlled approximately 52% of estimated snowmelt under low wind conditions while sensible and latent energy exchange contributed approximately 34% of the total snowmelt. Air temperature and humidity had a moderate influence on snowmelt during rain-on-snow events through the regulation of incident thermal radiation. Wind velocity

had the greatest influence on snowmelt through the regulation of sensible and latent energy exchange. For moderate to windy conditions estimated rates of snowmelt increased markedly and sensible and latent energy exchange contributed between 65 to 91 percent of the total snowmelt. The results of this investigation demonstrate that snowmelt processes are more sensitive to increased humidity and winds that accompany a rainfall event than the magnitude and intensity of precipitation. The results also suggest that clear-cut logging practices are more likely to increase the risk of rain-on-snow induced flooding because 1) rainfall is generally translated directly to runoff due to snowpack saturation and 2) the enhanced turbulence in cleared areas results in increased rates of snowmelt.

5.2 Introduction

Rain-on-snow events are a common occurrence on mountain slopes within the snow transition zone of the Pacific Northwest. This zone extends from approximately 300 to 1000 meters in elevation throughout western Oregon and Washington, coastal British Columbia and California (Beaudry and Golding, 1983; Harr, 1986). The region is characterized by a maritime climate with moderate winter temperatures. Rainfall occurs frequently during the winter months from relatively warm, moist frontal systems that move in from the Pacific Ocean. Winter snowcover is generally shallow with temperatures at or slightly below 0.0 °C. Under these conditions little energy is needed to initiate melt. The snowcover within this region is dynamic and can experience successive periods of accumulation and ablation during the winter months. It is not uncommon for an entire snowpack to melt during a single rainfall event. During warm or rainy periods runoff is rapidly produced due

to a low capacity for storage of additional liquid water in either the snowpack or soil (Berris and Harr, 1987).

Harvesting of forests in the transitional snow zone is a common occurrence throughout the Pacific Northwest and in cleared or exposed areas, such as those resulting from clear-cut logging practices, advective energy from rainfall combined with increased turbulence is suspected to enhance snowmelt, increasing the risk of erosion and downstream flooding during rainfall events. The purpose of this investigation is to determine why rain-on-snow floods occur and to assess whether clear-cut logging practices are likely to enhance snowmelt during rainfall events. The specific objective is to evaluate the sensitivity of snowmelt processes to conditions which occur during rain-on-snow events. An energy balance, snowmelt model is used to determine the energy and mass balance of a snowcover in a cleared area in the western Cascade mountains of Oregon. Snowmelt processes are evaluated at an hourly time step using integrated hourly meteorological data collected during documented rain-on-snow events. These results are compared to our understanding of the physics of snowmelt and to estimates of snowmelt and runoff derived from snow lysimeter measurements. Snowmelt processes are then evaluated under more extreme, simulated climate conditions to determine wind, radiation, air temperature and precipitation effects on snowmelt.

5.3 Energy exchange at the snow surface

In a seasonal snowcover, newly fallen snow is thermodynamically unstable, undergoing continuous metamorphism until it melts and becomes runoff during spring (Colbeck, 1982). Snowmelt and snow metamorphic changes are driven by temperature and vapor density gradients within the snowcover, which are caused by energy exchange at the atmosphere-snow and snow-soil interfaces (Colbeck et al., 1979; Male and Granger, 1981). In general the energy balance of a snowcover is expressed as:

$$\Delta Q = R_n + H + L_vE + G + M \qquad (1)$$

where R_n, H, L_vE, G, and M are the net radiative, sensible, latent, conductive and advective energy fluxes, respectively. The sum of the energy transfer terms is referred to as an energy balance because at thermal equilibrium the net change in snowpack energy, ΔQ, is approximately zero. If the snowcover is not in thermal equilibrium, a negative ΔQ term denotes a net decrease in snowpack energy, indicating a cooling snowcover, while a positive ΔQ denotes a net energy transfer to the snowpack. If the snowpack is at a temperature less than 0.0 °C, a positive ΔQ will warm the snowcover until the entire snowpack is approximately isothermal at 0.0 °C. At this point any additional energy transferred to the snowcover must result in melt. Each component of the energy balance is presented below in the context of its overall contribution to snowmelt processes and its importance during rain-on-snow events.

5.3.1 Net radiation at the snow surface

In most mountainous regions, net radiation is the most important component of the snowcover energy balance. The radiant energy flux, or net all-wave radiation at a point is the incident spectral irradiance less spectral exitance integrated over all wavelengths:

$$R_n = I - E_x \tag{2}$$

where R_n, I and E_x are the net all-wave radiation, incident irradiance and radiant exitance ($W\ m^{-2}$), respectively. Net radiation at the Earth's surface can be separated into solar and thermal spectral bands. In forested areas thermal radiation is generally the dominant contributor to R_n, while in cleared areas solar radiation is the most important component of R_n. Solar radiation (effectively 0.3 to 3.0 um) is absorbed and scattered by terrestrial materials, but not emitted. For snow, absorption and scattering are functions of wavelength, incidence angle, and the optical properties of the surface (Bohren and Barkstrom, 1974; Warren, 1982).

The spectral features of the solar radiation component of R_n should be considered when describing the energy balance over snow. In general, however, only broad-band radiation data are available and albedos must be estimated from assumed site and snowcover conditions. The net solar radiation at a point can be defined as:

$$R_{n,sol} = I_{sol}\ (1.0 - \alpha) \tag{3}$$

where $R_{n,sol}$, I_{sol} and α are the net solar radiation (W m^{-2}), solar irradiance (W m^{-2}) and solar albedo, respectively. For this investigation the irradiances were derived from measured values, while the albedo was assigned a value of 0.7 using models developed by Marshall and Warren (1987) and Marks and Dozier (1992) to integrate the visible and near-infrared spectral effects for newly fallen, wet snow into a single, broad-band reflectance.

Thermal radiation (effectively 3.5 to 50 um) is absorbed and emitted without appreciable scattering (Paltridge and Platt, 1976). Because net thermal radiation is a function of the absolute temperature of its constituents, the assumption is made that spectral variations are minimal. This simplifies the measurement of thermal irradiance and the calculation of the net thermal radiation by eliminating spectral considerations and allowing the use of broad band emissivities for the snow surface and surrounding terrain. In a mountainous region the net thermal radiation at the surface is a function of the air and surface temperature and thermal properties, atmospheric conditions, and terrain effects (Marks and Dozier, 1979). If thermal irradiance is measured, net thermal radiation is:

$$R_{n,lw} = I_{lw} - (\varepsilon_s \sigma T_s^4) \tag{4}$$

where $R_{n,lw}$ is the net thermal radiation (W m^{-2}), I_{lw} is the thermal irradiance (W m^{-2}), σ is the Stefan-Boltzmann constant ($\cong 5.67 \times 10^{-8}$ W m^{-2} K^{-1}), and ε_s and T_s are the surface temperature (K) and emissivity ($\cong 0.99$), respectively.

Considerable effort has gone into modeling thermal irradiance from the atmosphere, with most of this work focused on estimating atmospheric emissivity (e.g., Idso and Jackson, 1969; Marks and Dozier, 1979; Satterlund, 1979; Idso, 1981; Kimball et al., 1982; Heitor et al., 1991). For this study, thermal irradiance was estimated using the approach described by Marks and Dozier (1979) and adjusted for cloud cover effects. Net all-wave radiation is then defined at the sum of the net solar and net thermal components:

$$R_n = R_{n,sol} + R_{n,lw} \tag{5}$$

$$R_n = I_{sol}\,(1.0 - \alpha) + I_{lw} - (\varepsilon_s \sigma T_s^4) \tag{6}$$

5.3.2 Turbulent transfer at the snow surface

In general, turbulent energy exchange at the snow surface is second only to net all-wave radiation in importance during the snowmelt season. The turbulent transfer of momentum, heat, and water vapor at the snow surface are the most complicated forms of energy exchange and are not easily measured in a natural environment. Turbulent exchange over snow is difficult to measure at a point because the data demands are fairly extensive, requiring sensitive measurements using costly instrumentation. In unforested, alpine regions, significant mass loss can occur by sublimation (Beaty, 1975; Stewart, 1982; Davis et al., 1984), while in forested regions within the snow transition zone, the magnitude of snowmelt during rain-on-snow events is tightly coupled to the magnitude of the turbulent fluxes. Therefore, to evaluate the impact of turbulent transfer on the snowcover energy

balance, the calculation of sensible and latent heat exchange at the snow surface should be done as carefully and accurately as possible.

Several approaches to calculating sensible and latent energy fluxes have been presented (Sellers, 1965; Businger, 1973; Fleagle and Businger, 1980; Brutsaert, 1982). Several of these approaches have been adapted for use over seasonal snowcover (Andreas et al., 1979, 1984; Stewart, 1982; Marks and Dozier, 1992). For the general case of bulk transfer near the snow surface, sensible, H, and latent, E, energy exchange can be defined as:

$$H = \rho\, C_p\, K_H\, (T_a - T_s) \tag{7}$$

$$L_v E = \rho\, K_W\, L_v\, (q - q_s) \tag{8}$$

where T_a and T_s are the air and snow surface temperatures (K), q and q_s are the air and snow surface humidities (Pa), ρ is the density of the air (kg m^{-3}), C_p is the specific heat of dry air at constant pressure (J kg^{-1} K^{-1}) and L_v is the latent heat of vaporization ($\geq 2.5 \times 10^6$ J kg^{-1}). The bulk transfer coefficients for heat and water vapor, K_H and K_W, are functions of surface-atmosphere temperature and humidity gradients, wind speed and surface roughness and may vary significantly in both time and space.

The three most critical parameters affecting turbulent energy exchange between the snow surface and atmosphere are wind speed and temperature and humidity gradients. If the wind speed decreases to zero, H and E also go to zero. If the air and surface temperatures are the same, H is zero, and if the air and surface humidities are equal, E is zero. Turbulent transfer of heat and mass is controlled first by the magnitude of the wind speed,

and then by the temperature and humidity gradients between the snow surface and the air (Stewart, 1982).

The magnitudes of sensible and latent energy fluxes are controlled by the wind speed and will therefore be generally smaller at forested sites than in more exposed, open locations. The direction (positive toward, negative away from the surface) of these fluxes is controlled by the signs of the surface-atmosphere temperature and humidity gradients. For both H and L_vE to be negative, the air must be both colder and less humid than the snow surface. This condition occurs occasionally during winter but does not persist as the snow surface either cools to the air temperature or the air temperature increases during at the beginning of a diurnal cycle. In the characteristic, warm, snow environment of the snow transition zone, above freezing air temperatures frequently occur during part of the day throughout the snow season.

For both H and L_vE to be positive, the air must be warmer and more humid than the snow surface. These conditions are most common during rain-on-snow events. A warm rain event accompanied by high winds would be an extreme case of combined, positive turbulent transfer at the snow surface.

5.3.3 Conduction and advected energy transfer to the snowcover

Both conductive and advective energy transfer tend to be small when compared to the seasonal energy balance of the snowcover. One dimensional, steady-state energy flow in a homogeneous layer can be defined as:

$$G = K\,(\partial T/\partial z) \tag{9}$$

where K is the thermal conductivity (J m^{-1} K^{-1} s^{-1}), T is the temperature (K) and z is the layer thickness (m). Because soil and snow temperatures near their interface are usually very similar, the calculation of energy transfer between them is based on the assumption that the two represent homogeneous layers in contact with each other. If the temperatures of the snow and soil layers, $T_{s,l}$ and T_g, are known, heat transfer between the layers can be approximated as:

$$G = |2K_{es,l}\,K_{eg}\,(T_g - T_{s,l})| \,/\, (K_{eg}\,z_{s,l} + K_{es,l}\,z_g) \tag{10}$$

where $z_{s,l}$ and z_g are the snow and soil layer thicknesses. The effective thermal conductivities of the lower snow layer, $K_{es,l}$, and soil, K_{eg}, determine the rates of conduction, G, between the soil and snow layers and are functions of density, temperature and air pressure. K_{eg}, is assumed essentially constant using a representative value for a moist, coarse textured soil (2.2 J m^{-1} K^{-1} s^{-1}; Davis, 1980; Oke, 1978). The thermal conductivity of a snowpack is generally very low even under saturated conditions (Male and Granger, 1981). There are a variety of empirical methods for estimating $K_{es,l}$ as a function of density (Yen, 1969; Langham, 1981). The method described by Yen (1965) was selected as the most appropriate method for the observed conditions, where $K_{es,l}$ is calculated as a function of snow density, ρ_s (kg m^{-3}):

$$K_{es,l} = 3.2238 \times 10^{-8} \rho_s^2 \quad (11)$$

Because the air fraction of the snowcover is always at saturation, and the air fraction of soil is usually at saturation, vapor diffusion is estimated as a function of snow and soil temperatures and air pressure. Both the snow and soil thermal conductivities are corrected for vapor diffusion by adding a value that is based on their specific humidities, $q_{s,l}$ and q_g, and the calculated vapor diffusion coefficient, D_e, for each. The effective diffusion coefficient for water vapor in snow or a saturated, inorganic soil at 0.0°C and sea level air pressure, $D_{e,0}$ was determined experimentally by Yen (1965) to be approximately 10^{-5} m^{-2} s^{-1}. Anderson (1976) developed a relationship for determining the diffusion coefficient at other temperatures and Marks and Dozier (1992) modified it so that pressure variation could be accounted for:

$$D_e = D_{e,0} (P_0/P_a) (T_{s,l}/T_{melt})^{nT} \quad (12)$$

where P_a and P_0 are the air and sea level air pressures (Pa), T_{melt} is the melting temperature of ice (273.15 K) and nT is the layer temperature exponent. The layer temperature exponent was empirically determined by Anderson to be approximately 14. Because the temperature for a snow or soil layer within the snow transition zone is generally near 273.15 K, and P_a is always equal to or less than the sea level value, precision of nT is not critical. The effective diffusion coefficient, D_e, is always small and relatively stable,

varying between 10^{-5} and $0.5x10^{-5}$ m^{-2} s^{-1} at an air pressure of 65 kPa and snow temperatures between 273.15 and 250.0 K.

Thermal conductivities are adjusted for vapor transport by an empirical correction based on D_e:

$$K_{es,l} = K_{s,l} + (L_v D_e q_{s,l}) \quad (13)$$

$$K_{eg} = K_g + (L_v D_e q_g) \quad (14)$$

where $K_{es,l}$ and K_{eg} are the effective thermal conductivities of the snow and soil layers (J m^{-1} K^{-1} s^{-1}) and $q_{s,l}$ and q_g are the specific humidities of the snow and soil layers (Pa), respectively. Though there is nearly a twenty-fold increase in the thermal conductivity of the snow when it is corrected for vapor diffusion, the conductivity still remains more than an order of magnitude lower than the uncorrected thermal conductivity of the soil (2.2 J m^{-1} K^{-1} s^{-1}). The effective thermal conductivity of the soil will also increase when adjusted for diffusion but this term generally remains very small.

In the snow transition zone, energy transfer between the soil and snowcover is almost always near zero. This is due to the percolation of 0.0°C liquid water into the soil which virtually eliminates any temperature gradient that might have existed. Davis (1980), utilizing a similar, but more detailed model of soil energy flux at several alpine sites found this to always be the case during melting conditions. As a result, the amount of energy transferred between the snow and soil by G is generally minimal compared to the other terms in the snowcover energy balance.

5.3.4 Advected energy transfer to the snowcover from rain or snow

Advected energy transfer, M, at the snow surface occurs when mass, in the form of precipitation (rain or snow) is added to the snowcover. If there is a temperature difference between the added precipitation and the snowcover, the energy transfer (J m^{-2}) is a function of the mass added, and the magnitude of the temperature difference:

$$M = [C_{p\text{-}p}\, \rho_{pp}\, z_{pp}\, (T_{pp} - T_{s,0})] \tag{15}$$

where z_{pp} and ρ_{pp} are the depth (m) and density (kg m^{-3}) of precipitation and $C_{p\text{-}p}$ is the specific heat of precipitation (J kg^{-1} K^{-1}). During rain-on-snow events, the difference between the snow surface and precipitation temperatures, $T_{s,0}$ and T_{pp} (K), is not likely to be large. The magnitude of the advected energy is therefore likely to depend primarily on the magnitude of the mass of precipitation ($\rho_{pp}\, z_{pp}$) deposited on the snow surface. Typically the dewpoint temperature during the precipitation event is assumed to be equivalent to the precipitation temperature. If precipitation is warmer than the snowcover, M will be positive.

The specific heat of a substance is the amount of energy required to change its temperature. The specific heat of both water and ice is a function of temperature. The specific heat of water at 273.15 K is approximately 4217 J kg^{-1} K^{-1}, and the specific heat of ice is approximately half the specific heat of water. The specific heats of ice, C_{p_ice}, and

water, C_{p_w}, can be approximated as a linear function of the absolute temperature in the region from -25 to 25°C as:

$$C_{p\_ice} = 104.369 + 7.369\ T_{ice} \tag{16}$$

$$C_{p\_w} = C_{p\_w,melt} - 2.55\ (T_w - 273.15) \tag{17}$$

where T_{ice} and T_w are the ice and water temperatures (K), and $C_{p\_w,melt}$ is the specific heat of water at 273.15 K (4217.7 J kg^{-1} K^{-1}). Advection will be relatively small unless both the temperature difference and the volume of precipitation are large. During rain-on-snow events, precipitation tends to be very close to the snow surface temperature and advection is minimal unless the volume of precipitation is extremely large. In contrast, condensation can potentially contribute much greater magnitudes of energy transfer to the snow surface during rain-on-snow events. For example, 10 cm of rain at 10°C on a 0.0°C snowcover would add 4.2×10^5 J m^{-2}, causing 1.26 mm of snowmelt. If 0.5 cm of condensation were to occur on the same snowcover, 14.2×10^6 Jm^{-2} would be added resulting in 42.5 mm of snowmelt.

5.4 A two-layer, energy balance snowmelt model

The snowmelt model used in this study was driven by independent inputs of net solar radiation, meteorological parameters, measurement heights, and snowcover properties to calculate the energy and mass balance of the snowcover during rain-on-snow conditions.

At each time-step, the model predicts melt in two snowcover layers, runoff from the base of the snowcover and adjusts snowcover mass, thermal properties, and measurement heights accordingly. The modeling approach is an adaptation of the model developed by Marks (1988), and Marks and Dozier (1992). The modeling approach is similar to that used by Anderson (1976), Morris (1982, 1986), and Tarboton, et al. (1994) but the data requirements are simpler and more general. A detailed description of the model and data requirements are given by Marks (1988) and Marks and Dozier (1992). An abbreviated description of the important components of the model relating to this investigation are given below.

Radiation, precipitation, air temperature and humidity, measurement heights and snowcover properties are used to calculate the energy and mass balance of a snowcover. At each time-step, snowmelt and runoff are calculated and snowcover mass, thermal properties and measurement heights are adjusted accordingly. The model subdivides the snowcover into 2 layers. The surface layer is considered the active layer and has a constant depth set to the approximate depth of significant solar radiation penetration. The lower layer makes up the rest of the snowpack. Each layer is considered to be homogeneous with a uniform temperature, density and liquid water content. All surface energy transfer occurs in the surface layer. Energy transfer between the surface and lower layer and between the lower layer and soil is assumed to occur by conduction and diffusion. If the calculated ΔQ is negative, the cold content of the snowcover is increased and the snow layer temperature decreases. If ΔQ is positive, the cold content of the snowcover is decreased until the snow layer temperature is isothermal at 0.0 °C. Once the layer is at 0.0 °C, additional inputs of energy

result in melt. If melt occurs it is assumed to displace air in the snowcover causing densification and increasing the liquid water content of the snowcover. Once the liquid water content attains a prescribed threshold, additional melt results in runoff. Though meltwater is usually generated in the surface layer, mass lost to runoff is removed from the lower layer. The thickness of the surface layer remains constant as long as there is a lower layer. Once the lower layer is completely melted the snowpack is treated as a single layer. The model does not account for hydraulic gradient or soil infiltration effects on runoff and assumes that all runoff generated by the snowcover is lost.

Precipitation depth, temperature and density information are used to adjust the thermal and mass balance of the snowpack. If precipitation occurs in the form of snow, the model increases the thickness of the lower layer according to the mass and density of precipitation and recalculates average layer densities, temperatures, liquid water contents and measurement heights. If rainfall occurs, advection is calculated from the temperature and mass of the precipitation input and new average layer densities, temperatures, measurement heights and liquid water contents are determined. Runoff occurs when the liquid water holding capacity of the snowcover is exceeded.

5.4.1 Energy and mass balance calculations

Radiation and meteorological data are used to determine net all-wave radiation and sensible and latent energy exchange between the atmosphere and snow surface layer, as well as conductive and diffusive energy exchange between the snowcover and soil. Net

all-wave radiation is calculated in Equation (6) from integrated hourly measurements of solar and thermal irradiance, solar albedo, and surface temperature and emissivity information. The initial surface temperature begins at the initial input value (0.0°C) and is then calculated and updated at the end of each time-step by the model. Surface emissivity, ε_s, is set at a constant value of 0.99 by the model.

Sensible and latent energy exchange at the snow surface are determined using an aerodynamic turbulent transfer approach adapted from Brutsaert (1982) and later modified by Marks and Dozier (1992). The following equations are solved iteratively to obtain estimates of latent and sensible energy exchange:

Obukhov stability length:

$$L = (u^{*3}\,\rho) / [k\,g\,(H / T_a\,C_p) + 0.61\,E] \tag{18}$$

Friction velocity:

$$u^{*} = (u\,k) / \ln [((z_u - d_0) / z_0) - (\psi_{sm}\,(z_u / L))] \tag{19}$$

Sensible energy flux:

$$H = ((T_a - T_{s,0})\,a_H\,k\,u^{*}\,\rho\,C_p) / \ln [((z_t - d_0) / z_H) - (\psi_{sh}\,(z_t / L))] \tag{20}$$

Latent energy flux:

$$L_v E = ((q - q_s)\,a_E\,k\,u^{*}\,\rho) / \ln [((z_q - d_0) / z_E) - (\psi_{sv}\,(z_q / L))] \tag{21}$$

The model requires inputs of air temperature, T_a (K), vapor pressure, q (Pa), and horizontal wind speed, u (m s^{-1}), in order to calculate sensible and latent energy exchange (W m^{-2}) at a point. The measurement heights (m) for air temperature, z_T, vapor pressure, z_q, and wind speed, z_u, are set as initial conditions and then updated by the model as the depth of the snowcover changes. The surface roughness lengths for momentum, heat and water vapor are defined as z_0, z_H, and z_E, respectively, and are assumed to be equal (Brutsaert, 1982). The snow surface temperature, $T_{s,0}$, is adjusted by the model at the end of each time-step. The snow surface vapor pressure, q_s, is calculated as the saturated value at the estimated surface temperature.

Energy exchange by conduction and diffusion will also occur between the soil and snowcover if a temperature or humidity gradient exists. The model approximates conductive energy exchange between the soil and snowcover at each time step from Equations (10) - (14). Energy transfer by conduction and diffusion between the snow surface layer and the lower snow layer is calculated in the same manner:

$$G_0 = [2K_{es,0}\, K_{es,1}\, (T_{s,1} - T_{s,0})] / (K_{es,1}\, z_{s,0} + K_{es,0}\, z_{s,1}) \qquad (22)$$

where $K_{es,0}$ is the effective thermal conductivity of snow surface layer (J m^{-1} K^{-1} s^{-1}). This calculation allows the transfer of energy from the surface layer to the rest of the snowcover.

Advected energy transfer to the surface layer is calculated only during time intervals when precipitation input has occurred according to:

$$M = [C_{p\text{-}p}\, \rho_{pp}\, z_{pp}\, (T_{pp} - T_{s,0})] / t_{step} \quad (23)$$

Advection is converted from a total (J m^{-2}), to an average flux (W m^{-2}) for the time-step, by dividing by the length of the time-step t_{step}(s). The density, depth and temperature of precipitation are model inputs. The temperature of the snow surface layer, $T_{s,0}$, is updated by the model at each time-step. The specific heat of precipitation C_{p_p}, is calculated as a function of precipitation temperature T_{pp} which is assumed to be the measured dewpoint temperature. If the precipitation temperature is greater than 273.16 K, the model assumes that rain has occurred and the specific heat of water is used in the calculation of M. Otherwise the model uses the specific heat of ice. The model estimates advection for either rain or snow and does not account for the simultaneous occurrence of both rain and snow. If a rain-snow mixture occurs, advection for each component must be estimated separately.

The surface energy exchange terms are summed to determine the net energy transfer to the snow surface layer:

$$\Delta Q_0 = R_n + H + L_vE + G_0 + M \quad (24)$$

and the total energy transfer to the snowcover:

$$\Delta Q = \Delta Q_0 + G \quad (25)$$

Equations (24) and (25) determine the energy available for melting or re-freezing in each layer of the snowpack. If the snow surface and lower layer energy contents, Q_0 and Q_l, are positive, melt is calculated, the liquid water content of the snowcover, w_S, is adjusted, and the layer cold contents, $cc_{s,0}$ or $cc_{s,l}$, are set to 0.0. If Q_0 or Q_l are negative, and liquid water is present, the energy required for re-freezing is calculated, the liquid water content is adjusted, or set to 0.0, and a new cold content is determined for each layer. Once layer cold contents are adjusted, new layer temperatures are calculated, and a new surface temperature is established for the next time-step.

If melt occurs during a time-step, the total thickness of the snowcover, z_s, and the thickness of the lower snow layer, $z_{s,l}$, will be reduced. Because no runoff has yet been predicted the specific mass of the entire snowcover has not changed. However, average snowcover density is increased and the specific masses of the snow surface and lower layers and the cold content of the entire snowcover is adjusted.

Mass lost or gained between the snow surface layer and the atmosphere through evaporation or condensation is derived from Equation (21). Evaporation or condensation between the lower snow layer and the soil is calculated for each time-step as:

$$E_l = \rho D_e [(q_g - q_{s,l}) / z_g] \tag{26}$$

where E_l is the evaporative flux between the soil and lower layer (kg m^{-2} s^{-1}), and q_g and $q_{s,l}$ are the specific humidities of the soil and lower snow layers, respectively. The specific mass of the snowcover is adjusted by the total mass of evaporative loss or gain. If liquid

water is present, it is preferentially evaporated in the model by the ratio of the latent heat of vaporization to sublimation (0.882). The snowcover liquid water content after adjustment for melt or re-freezing, is then adjusted for evaporation. The remaining evaporative loss, or all evaporation after liquid water has been depleted, is modeled as sublimated ice. This decreases total snowcover depth and causes adjustment of average snowcover density and the snow layer specific masses. Half of the ice lost is assumed to be decreased depth. The remaining sublimated ice and all evaporated liquid water decrease the density and mass of the snowcover.

The remaining liquid water content, after all snowcover depth, density, and mass adjustments for melt, refreezing, and evaporation or condensation, is checked to see if w_c is greater than the threshold retention proportion of the air fraction of the snowcover (generally less than 10%). If this threshold is exceeded, runoff is predicted and both the density of the snowcover and specific masses of the snow layers are appropriately reduced. If the cold content of the entire snowpack, cc_s, is equal to 0.0, the temperatures of both snow layers are set to 273.15 K. If not, each snow layer temperature is adjusted appropriately.

This model implements a full energy balance to predict snowcover melt and runoff. The data requirements of the model are simplified by separating all possible, non-coupled energy inputs from the model and parameterizing both the snowcover and soil in such a manner that reasonable estimates of their distribution over a watershed or region is possible. A test of the model over an alpine watershed showed that it predicted daily total runoff from the basin to within 5% of the measured volume of snowmelt (Marks, 1990; Marks and Kimball, 1991).

5.5 Methods

5.5.1 Site description

The study area was located within a 22 ha clear-cut at 900 m elevation on the McRae Creek drainage within the H.J. Andrews Experimental forest on the west slope of the Cascade range crest in Oregon. The site had been logged in 1981 and broadcast burned in 1982. The plot faced in a south-southwest direction towards the predominant direction of winter winds. An old-growth forest consisting of Douglas-fir and western hemlock trees ranging in height from 30-60 m was located approximately 40 m to the northwest of the plot. Instruments were located on nearly level ground but surrounding slope gradients approached 80%. Further description of site characteristics is presented by Berris (1984) and Berris and Harr (1987).

Annual precipitation at the site averages 2340 mm. Approximately 80% of annual precipitation falls during the winter months which are usually mild with air temperatures ranging between -12 °C and 12 °C during the coldest month of January. Precipitation is generally produced by moist, frontal systems from the Pacific Ocean delivered in the form of both rain and snow. The mild winter climate produces shallow snowpacks with internal temperatures that remain near 0.0 °C. The moderate climate and shallow snowcover of the snow zone within the lower to middle elevations of the western Cascades create conditions in which it is not uncommon for an entire snowpack to melt off within a matter of hours during a warm, moist frontal event.

5.5.2 Data collection

Model runs were based on meteorological and radiation data collected at the site over two, 120 hour study periods during February and March of 1984. A cursory overview of the data collection effort is presented here as it relates to the objectives of this paper. A detailed description of the site, data collection efforts and instrumentation is presented by Berris (1984) and Berris and Harr (1987).

Integrated, hourly solar irradiance was measured from a LI-COR pyranometer sensor calibrated for cloudy conditions. The solar albedo was estimated from a limited set of measured reflectances made at an alpine site in the Sierra Nevada Mountains under spring melt conditions (Marks, Dozier and Davis, 1992). An estimated solar albedo of 0.70 was derived from an integration of hourly measurements of visible and near-infrared reflectances obtained under cloudy conditions and held constant throughout the investigation period. The assumption of a constant albedo introduced a certain degree of error but was minimized because heavy cloud cover strongly suppressed both the magnitude and diurnal amplitude of measured hourly solar irradiance during rain-on-snow events and throughout most of the measurement period (Berris and Harr, 1987).

Thermal irradiance at the surface is composed of radiation emitted from ozone, carbon dioxide and water vapor at all levels within the atmosphere. The amount of thermal irradiance is a function of the emissivity of the atmosphere which is strongly dependent on surrounding terrain, cloud cover, air temperature, pressure, and humidity. Cloud cover and surrounding vegetation will cause marked increases in thermal irradiance at the snow surface and is not easily modeled. Thermal irradiance was estimated from temperature and

humidity information using an approach developed by Brutsaert (1975) and later modified by Marks and Dozier (1979) for use in alpine areas. This method accounts for variations in atmospheric emissivity with humidity, view factor and elevation and has been found to compare well with measured values during spring snowmelt conditions in the Sierra Nevada range of California (Marks and Dozier, 1979; Marks and Dozier, 1992). Cloud cover can significantly increase thermal irradiance over a snow surface due to the large absorption and emissivity of clouds in the thermal portion of the spectrum. Since the measurement plot was characterized by predominantly low cloud cover, estimated clear-sky thermal irradiance was increased by a factor of 1.34. This cloud correction factor represents the ratio of thermal irradiance under clear and cloudy conditions and was derived from thermal irradiance measurements at an alpine site in the Sierra Nevada mountains of California (Marks, Dozier and Davis, 1992).

Wind speed was measured at a height of 1.5 m above the ground with a Weathertronics, three-cup, low-threshold, anemometer. The anemometer's threshold of accuracy was approximately 0.9 m s^{-1} but was found to be most reliable at wind speeds from 3-10 m s^{-1}. Unfortunately, the anemometer was relatively insensitive to prevailing wind conditions at the site which rarely exceeded 2.0 m s^{-1}. The instrument frequently recorded hourly wind speeds of 0.0 m s^{-1} which was considered improbable even under calm conditions, since the site was located in a cleared area on an exposed mountain drainage. A factor of 0.9 m s^{-1} was added to measured wind speed data to adjust for instrument threshold error.

Air and dewpoint temperatures were measured at a height of 1.5 m above the ground with shielded thermistors and lithium chloride dew-point hygrometers, respectively. Pre-

cipitation was measured with a heated, tipping bucket rain gage and 4 storage rain gages. Snowpack runoff was measured from a network of eight flat, rectangular, fiberglassed, 0.25 m^2 wooden pans located throughout the measurement plot and connected by buried plastic pipe to a tipping bucket. A micrologger scanned all sensors at 10-second intervals and generated mean hourly radiation, temperatures and wind speeds, as well as hourly precipitation and snowcover runoff estimates.

5.5.3 Model assumptions and initial conditions

The energy balance snowmelt model requires initial estimates of several snowpack properties in order to effectively characterize snowmelt at a point. These parameters were derived from measured data when possible but most had to be estimated due to a lack of detailed measurements of snowpack conditions. Model initial conditions are summarized in Table 5.1.

The snowpack active-layer depth represents the maximum depth of radiation penetration and defines the mass of the snowcover involved in surface energy exchange. The depth of radiation penetration into snow is variable and depends on factors such as grain size and solar zenith angle. The depth of the active-layer has been found to range from 0.1 m to 0.2 m for deep snowpacks under spring melt conditions in the Sierra Nevada mountains of California (Marks, Dozier and Davis, 1992). For the purposes of this investigation the initial snowpack active layer depth was set at 0.1 m. Varying this parameter did not appear to influence model estimates of snowpack properties because measured solar radi-

ation at the site was low and the estimated snowpack profile remained at 0.0 °C and under active melt during rainfall events.

For comparison between lysimeter and model runoff and snowmelt results, the snowpack initial depth for the February 10 - 14 and February 27 - March 2 periods were based on measured depths of 0.242 m and 0.253 m, respectively. Initial snowpack depths of 0.5 m were used under more extreme, simulated meteorological conditions in order to ensure adequate snowcover throughout the model runs. Air temperature and snow depth measurements indicated that the snowpack was generally shallow (< 0.5 m), existing under average air temperatures of approximately 4 °C. Both the initial active and lower layer snowpack temperatures were therefore assumed to be isothermal at 0.0 °C and capable of producing melt.

The maximum free water content of the snowpack is defined as a proportion (between 0.0 and 1.0) of the air fraction of the snowcover following the convention set by Davis et al. (1985). Some controversy exists about the water retention capacity of a snowcover but the volume of liquid water held by a snowpack is probably relatively small (Colbeck, 1978). Maximum values during spring melt have generally been found to be on the order of 0.05 (5%) which corresponds to a liquid water retention threshold of approximately 23 kg m^{-3} (ρ_s = 500 kg m^{-3}).

The physical properties of a snowpack such as thermal conductivity, snow water equivalent and air permeability depend strongly on snow density. Snowpack densities have been found to range from 65 kg m^{-3} for new snow to upwards of 650 kg m^{-3} for a ripe snowpack under active snowmelt (Male and Granger, 1981; Marks et al., 1986). Snow densities were

Table 5.1. Summary of snowmelt model initial conditions

INITIAL CONDITIONS
1) Snow depth = 0.242 m (Feb. 10), 0.253 m (Feb. 27)
2) Maximum free water content = 5%
3) Initial free water content = 1.7%
4) Snowpack active layer depth = 0.10 m
5) Initial snowpack density = 500 kg m^{-3}
6) Initial active layer temperature = 0.0 °C
7) Initial lower layer temperature = 0.0 °C
8) Snow surface roughness = 0.003 m

initially calculated by weighing a known volume of snow. Although this method has been widely used, it is prone to error, especially when a snowpack is shallow or ice lenses are present. Snowpack densities derived from this method ranged from 149 - 265 kg m^{-3} and were substantially lower than expected for spring melt conditions. This method was therefore judged to be unreliable and abandoned. Instead, a density of 500 kg m^{-3} was used to represent initial snowpack conditions. Detailed snowpack profile density measurements conducted near the site during February, 1994 under similar snow and climate conditions

showed densities of approximately 490 kg m^{-3} which seemed to support the assumption of a higher density.

The snow surface roughness length (z_0) is used in the calculation of convective energy transfer. Over snow, which is fairly smooth, z_0 ranges from $1.0x10^{-4}$ to $5.0x10^{-3}$ m, though once vegetation and local terrain features have to be considered, the value can be much higher. z_0 was set to a constant 0.003 m for the model runs. Since the model runs were restricted to relatively short time periods with a complete snowcover, the assumption of a constant roughness value is considered valid.

Precipitation was measured by a heated tipping bucket rain gage and four storage rain gages. Precipitation type (rain or snow), temperature and density parameters were not measured and had to be estimated indirectly. Precipitation temperatures were assumed to be equal to measured dewpoint temperatures. Precipitation type and density, were estimated from dewpoint temperature data. Precipitation was classified as rain or snow based on a dewpoint temperature threshold of 0.0°C. Rainfall densities were assumed to be 1000 kg m^{-3}. Precipitation during periods with dewpoint temperatures between 0.0°C and -3.0°C was assumed to be a mixture of both rain and snow with an average density of 700 kg m^{-3}. When dewpoint temperatures were below -3.0°C, precipitation was assumed to be entirely composed of snowfall with a density of 350 kg m^{-3}. This investigation focuses on relatively short time periods with documented rain-on-snow events in order to minimize precipitation type and density estimation errors. It is likely that precipitation estimation errors are significant during snowfall events or when rain and snow precipitation is mixed.

Model accuracies are therefore likely to decrease over longer time periods without more detailed precipitation information.

5.5.4 Rain-on-snow events

Three rain-on-snow events were selected from the measured data representing a variety of climate and rainfall conditions. Each event exhibited distinct precipitation depths and intensities. The first rainfall event (A) occurred on February 28, 1984 over a 5 hour period. The measured precipitation depth for this event was 1.5 mm. The second event (B) began roughly 25 hours later on February 29 and continued over a 19 hour period. The measured precipitation depth for this event was larger at 15 mm. The third event (C) occurred on February 12, 1984 and represented the largest recorded rainfall event at the site. This event occurred over a 34 hour period and delivered 143.5 mm of rainfall.

Hourly climate, radiation and precipitation data for the two measurement periods are presented in Figures 5.1 and 5.2. A statistical summary of climate and radiation for the three rain-on-snow events is presented in Table 5.2. Rainfall events exhibited light to moderate intensities over durations of a few hours to two days. Rainfall intensities for event A averaged 0.3 mm hr^{-1} with peak intensities less than 1.0 mm hr^{-1}. Event B was of a more moderate rainfall intensity, averaging 0.8 mm hr^{-1} with a peak intensity of 1.5 mm hr^{-1}. Rainfall intensities for the largest event (C) peaked at 6.5 mm hr^{-1} and averaged approximately 4.1 mm hr^{-1}. Air temperatures during rain-on-snow events remained above freezing, averaging approximately 4.3 °C with relative humidities near 100%. Wind

Table 5.2. Summary of measured climate and radiation conditions during selected rain-on-snow events

EVENT A (5 hrs)

	Mean	Max.	Min.	Coeff. of Var. (%)
Net Solar (W/m^2)	48.5	83.3	11.4	54
Net Thermal (W/m^2)	14.1	25.0	2.3	52
Rn (W/m^2)	62.7	98.0	13.7	51
Ta (C)	5.0	6.2	3.3	22
U (m/s)	1.7	2.3	1.1	26
Ea (mb)	7.9	9.4	6.1	20
Rainfall (mm/hr)	0.3	1.0	0.0	123
Tdewpt (C)	3.3	6.2	0.0	71

EVENT B (19 hrs)

Net Solar (W/m^2)	4.7	28.0	0.0	203
Net Thermal (W/m^2)	5.6	11.0	2.2	43
Rn (W/m^2)	10.3	39.0	2.2	111
Ta (C)	3.2	4.1	2.6	13
U (m/s)	1.7	2.1	1.1	17
Ea (mb)	7.6	8.1	6.7	4
Rainfall (mm/hr)	0.8	1.5	0.0	50
Tdewpt (C)	3.1	4.0	1.3	18

EVENT C (34 hrs)

Net Solar (W/m^2)	1.7	13.4	0.0	216
Net Thermal (W/m^2)	12.2	28.2	-4.5	69
Rn (W/m^2)	13.8	37.9	-4.5	81
Ta (C)	4.6	7.0	0.7	1
U (m/s)	2.0	3.3	0.9	21
Ea (mb)	8.5	10.0	5.0	10
Rainfall (mm/hr)	4.1	6.5	0.0	44
Tdewpt (C)	2.7	5.2	0.7	48

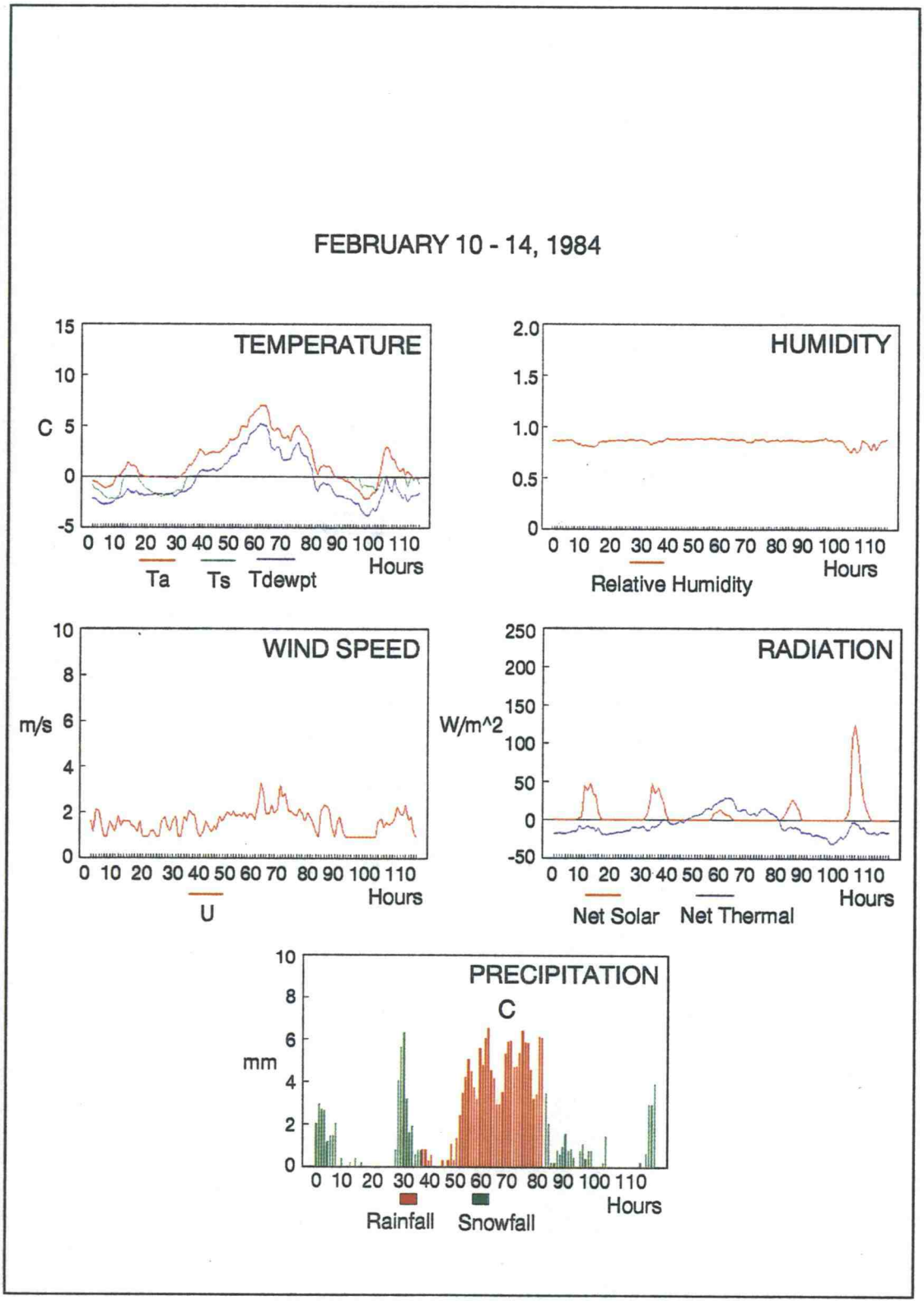

Figure 5.1. Measured climate and radiation for February 10-14, 1984

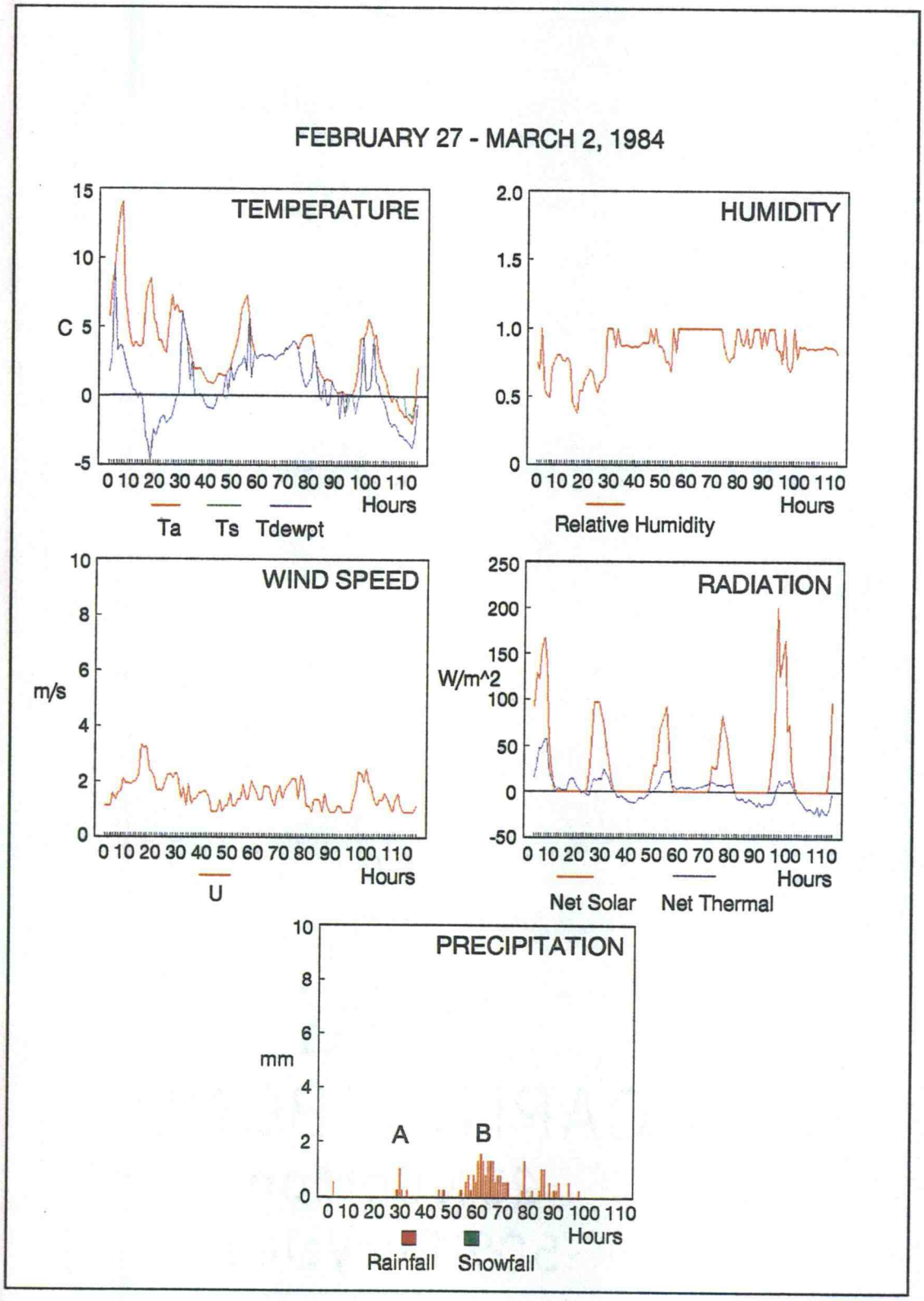

Figure 5.2. Measured climate and radiation for February 27-March 2, 1984

velocities during the three events were light averaging approximately 2 m s^{-1} with peak winds generally less than 3 m s^{-1}.

The site was overcast during the rain-on-snow events and over virtually the entire data collection period. Net all-wave radiation during rainfall periods was generally less than 90 W m^{-2} and averaged only 63, 10 and 14 W m^{-2} for events A, B, and C, respectively. R_n was small but positive during rain-on-snow events indicating a net transfer of energy to the snowpack. Net solar radiation during rainfall events was low, averaging only 18 W m^{-2} with peak values generally less than 80 W m^{-2}. The low magnitude of net solar radiation for events A and B was primarily due to the time of day in which these events occurred. The low net solar radiation for event C was probably due to a combination of low cloud cover and snow or other obstructions on the sensor.

Estimated thermal irradiance averaged approximately 324 W m^{-2} during rainfall events and exhibited little diurnal variation due to cloudy conditions, low temperatures and stable humidities. Thermal exitance from the snowpack was approximately 312 W m^{-2} and was constant during rainfall events since the snow temperature remained at 0.0 °C. These conditions resulted in low net thermal radiation values which averaged only 10.6 W m^{-2} yet composed approximately 37% of the net all-wave radiation.

5.5.5 Adjusted meteorological conditions

Snowpack conditions were evaluated under simulated drier, warmer, wetter, and windier meteorological conditions in order to evaluate the snowmelt response to air temperature,

rainfall, humidity, wind speed, thermal and solar radiation during rain-on-snow events. Net solar radiation has been shown to play a major role in controlling the rate of snowmelt under clear-sky conditions (Marks, 1988; Marks et al., 1992). The magnitude of net solar radiation during the heaviest rainfall event C was quite small, averaging less than 2.0 W m^{-2}. These characteristics have been observed during rainfall and snowfall events at other sites and were probably due to the combination of overcast conditions and snow or some other obstruction on the sensor. Hourly net radiation data from a subsequent cloudy day with no precipitation ranged from 0-126 W m^{-2} with a mean value of 13.8 W m^{-2} which was approximately 8 times larger than the net solar radiation data for event C. The model was run using the alternate radiation data combined with the meteorological data for event C in order to evaluate the snowpack response to increased radiation.

Temperature effects on snowmelt were evaluated by increasing measured hourly air and precipitation temperatures by 2.0 °C. The relative humidity of the air was held constant and thermal irradiance was recalculated at each time-step according to the adjusted air temperatures and specific humidities. Precipitation type and densities were also re-evaluated accordingly.

Wind speeds strongly effect snowmelt processes by regulating the amount of convection and condensation at the snow surface. Measured wind velocities were generally low at the measurement site, averaging less than 2.0 m s^{-1}. Hourly wind speeds were increased by factors of 4 and 6 and combined with measured data to evaluate snowmelt processes under light to moderately windy conditions. Measured rain-on-snow events represented very

light to heavy rainfall conditions. Measured rates of rainfall were doubled in order to assess the snowpack response to a greater range of rainfall events.

5.6 Results and discussion

5.6.1 Model results under measured meteorological conditions

The rate of snowmelt is dependent on the condition of the snowcover and the magnitude of energy transferred to the snow surface as defined by the energy balance equation (1). Although rainfall is capable of penetrating to considerable depths within a snowpack resulting in a mass transport of heat to lower snow-layers, active melt occurs predominantly at the snow surface (Male and Granger, 1981). Plots of calculated energy balance terms for the two measurement periods are presented in Figure 5.3. Results for the 3 rainfall events are summarized in Table 5.3. The snowpack during rain-on-snow events was thermodynamically active and approximately isothermal at 0.0 °C. Light winds, humid conditions and above freezing air temperatures resulted in a small net transfer of energy to the snowcover and small but fairly continuous rates of snowmelt. Snowmelt estimates for events A, B, and C were 4.1, 4.2 and 21.1 mm, respectively. The rate of snowmelt during rainfall events averaged approximately 0.55 mm hr^{-1} and was generally independent of the magnitude of the rainfall period and more a function of the net all-wave radiation and sensible and latent energy terms. The rate of snowmelt was generally low due to the small magnitude of energy transfer to the snowcover from net radiation and convection. Though of small magnitude, net radiation and convection were responsible for between 75 and 98

percent of snowmelt for the three rainfall events. The contribution of rainfall advection to the total snowmelt increased as the magnitude of the rainfall event increased accounting for 2.4, 13.9 and 25.3 percent of snowmelt for events A, B, and C, respectively. The amount of snowmelt from advection was generally moderate compared to radiation and convective processes under measured rainfall conditions. Energy transfer by conduction between the soil and snowcover did not contribute to snowmelt because of the low thermal conductivity of snow and low soil temperatures which remained at approximately 0.0 °C during rain-on-snow events.

Table 5.3. Factors controlling estimated snowmelt for the measurement period and selected rain-on-snow events

	TOTAL	A	B	C
Total Melt (mm)	80.4	4.1	4.2	21.1
	%Melt	% Melt	% Melt	% Melt
Net Solar	54.3	63.8	22.9	3.0
Net Thermal	-9.9	18.6	27.2	21.7
Rn	44.4	82.4	50.2	24.7
H	18.0	9.2	18.5	25.2
LvE	8.4	5.9	17.0	25.4
H+LvE	38.7	15.1	35.5	50.6
M	15.2	2.4	13.9	25.3
G	0.0	0.0	0.0	0.0

Rainfall did not freeze within the snowpack and resulted in a rapid runoff response because snow temperatures were at 0.0 °C and liquid water holding capacity was generally

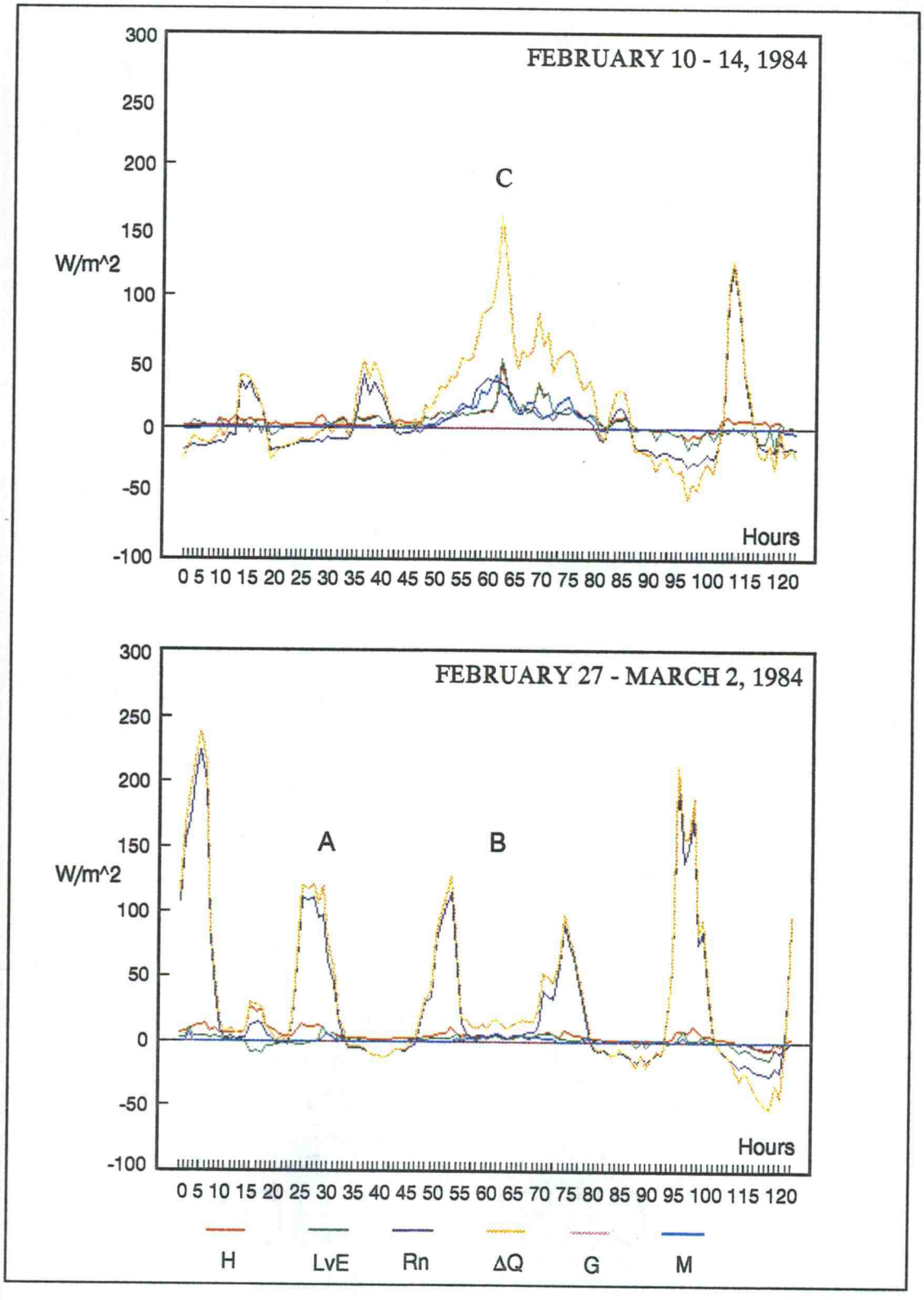

Figure 5.3. Estimated snowcover energy balance for measured conditions

attained within 1-2 hours following the initiation of rainfall. These results support conclusions reached under similar conditions using a matrix of thermistors to monitor rainfall infiltration into a maritime snowpack (Conway and Benedict, 1994). Rainfall represented a dominant 77 and 93 percent of estimated runoff for the largest events B and C, respectively, but represented only 26 percent of runoff for the smallest event A. Rainfall generally composed the majority of runoff because snowmelt was generally light during rainfall events and the rapid saturation of the snowcover at the onset of the larger rainfall events allowed liquid precipitation to be directly translated through the snowpack as runoff.

5.6.2 Model comparison to lysimeter outflow

Model and lysimeter results for the three rain-on-snow events are presented in Table 5.4. Plots of estimated hourly snowmelt and runoff for the two measurement periods are shown in Figure 5.4. Model and lysimeter estimates of hourly runoff and snowmelt compared moderately well, though results were more comparable for runoff than snowmelt. The lysimeter exhibited higher rates and total volumes of snowmelt and runoff than the model for the three rainfall events. Lysimeter results were generally 2.3 times larger than model estimates of snowmelt and 1.3 times larger than model estimated runoff. Model estimates of snowmelt for the entire measurement period were approximately 78% of lysimeter results while modeled runoff was 73% of lysimeter runoff. Precipitation generally represented a slightly lower 21, 49 and 78 percent of lysimeter runoff for events A, B, and C, respectively, due to the greater magnitude of lysimeter runoff.

Table 5.4. Snowmelt model and lysimeter results for the measurement period and selected rain-on-snow events

EVENT A (5 hrs)

	Model (mm)	Lysimeter (mm)	Model/Lysimeter
Melt	4.1	5.5	0.74
Runoff	5.8	7.0	0.83
Precipitation	1.5	1.5	------

EVENT B (19 hrs)

Melt	4.2	15.8	0.27
Runoff	19.4	30.8	0.63
Precipitation	15.0	15.0	------

EVENT C (34 hrs)

Melt	21.1	41.4	0.51
Runoff	154.1	183.2	0.84
Precipitation	143.5	143.5	------

TOTAL MEASUREMENT PERIOD (240 hrs)

Melt	80.4	103.6	0.78
Runoff	204.0	278.5	0.73
Precipitation	240.7	240.7	------

Model and lysimeter differences in estimated hourly snowmelt were likely due to a number of factors, including measurement error, model assumptions of meteorological conditions and parameterizations of snowpack properties. Lysimeter estimates of snowmelt were derived by subtracting hourly precipitation measurements from hourly lysimeter runoff values. As a result, lysimeter melt responded readily to fluctuations in precipitation intensities while model results responded more to radiation, air temperature,

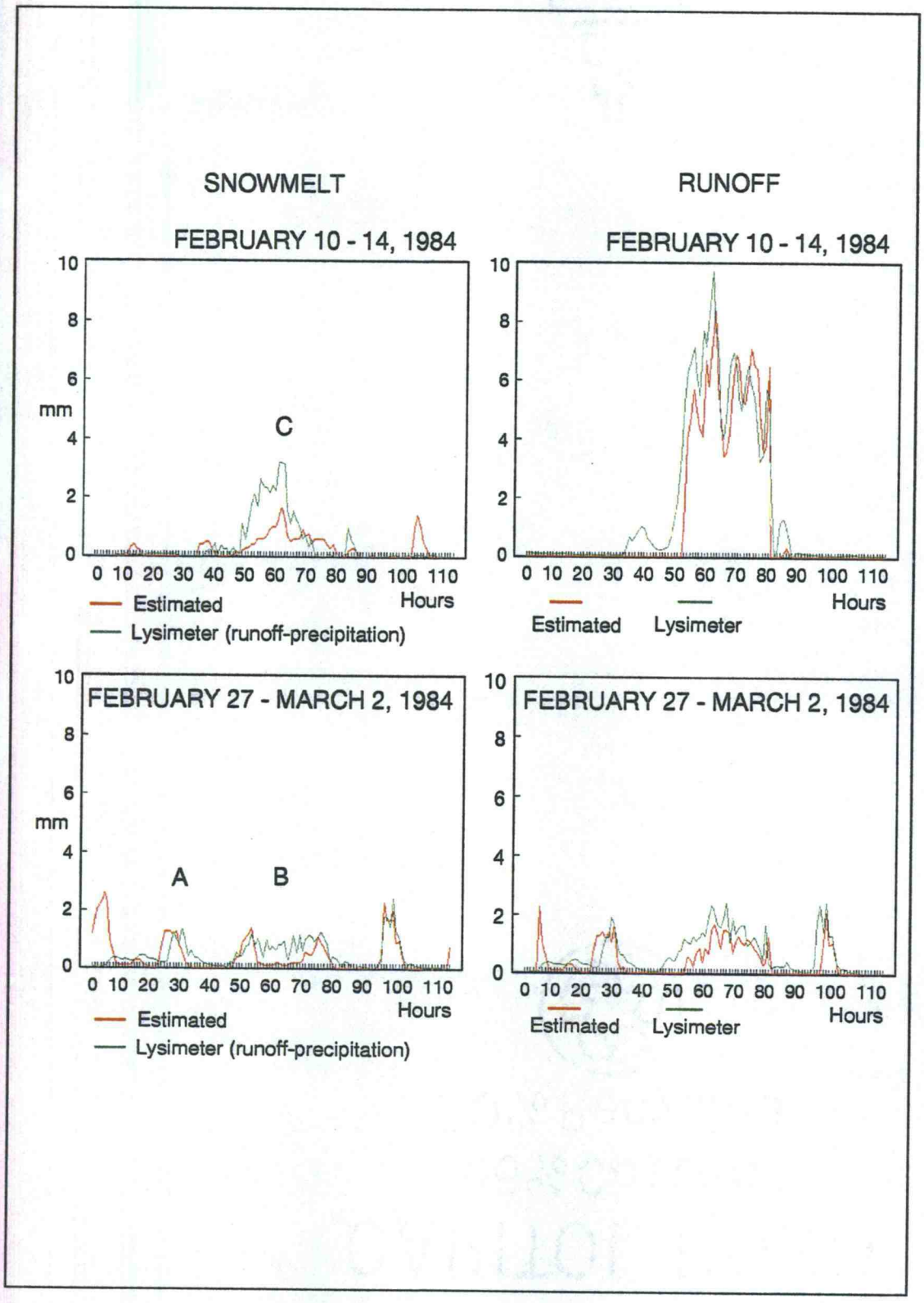

Figure 5.4. Comparison between model and lysimeter results

humidity and wind speed variations. It is difficult to attribute differences between model and lysimeter results to any single factor. Differences are most likely due to combinations of meteorological data and lysimeter runoff and snowmelt measurement errors as well as model assumption and input parameterization errors.

5.6.3 Potential measurement errors

Accurate monitoring of snowpack conditions using a physically-based energy balance approach is strongly dependent on the accuracy of the available data. It is likely that differences in estimated snowmelt and runoff between model and lysimeter results were due to combinations of several factors involving snowmelt, runoff, solar radiation, precipitation, temperature and wind measurement errors as well as incorrect parameterization of snowcover properties used to initialize the model. Potential sources of measurement error are reviewed below.

Runoff, climate, precipitation and snowpack properties are difficult to measure accurately in the field using unattended instruments. Solar radiation measurements are prone to error under rain-on-snow conditions due to the likelihood of sensor obstructions (Stanhill, 1992). Net solar radiation measurements were extremely low during rainfall events. During event C the peak mid-day value in $R_{n,sol}$ was only 13 W m^{-2}. Detailed $R_{n,sol}$ measurements under mid-day conditions with 100 % cloud cover over an alpine snowcover in the Sierra Nevada mountains of California showed typical values of $R_{n,sol}$ greater than 100 W m^{-2} (Marks, 1988). These results suggest that low $R_{n,sol}$ values obtained at the Cascade site

may be due to a sensor obstruction. Under-estimation of $R_{n,sol}$ would tend to reduce the model estimated snowmelt which might account for observed differences in model and lysimeter results during event C.

Thermal radiation is rarely measured in the field and is difficult to estimate due to cloud cover, humidity and terrain conditions which strongly influence atmospheric emissivities (Male and Granger, 1981; Marks, Dozier and Davis, 1992). Thermal irradiance was not measured at the Cascade site but was calculated from temperature and humidity measurements and estimates of atmospheric emissivity, cloud cover and surrounding terrain effects (Marks and Dozier, 1979). Errors associated with erroneous assumptions regarding the emissivities or relative contributions of the surrounding terrain and sky to thermal irradiance could account for differences between model estimated snowmelt and runoff and lysimeter results. A 10 percent increase in atmospheric emissivity, terrain view factor and cloud cover effects, for example, resulted in a 14 percent increase in the estimated thermal irradiance which approximately doubled the magnitude of the estimated snowmelt for the three rainfall events.

Accurate measurements of wind speed are possible to obtain in the field, but care must be taken in selecting the proper combination of instruments and recording devices that are sensitive enough to capture the characteristic range of wind speeds at the measurement site. The aerodynamic turbulent transfer method used to derive sensible and latent energy exchange in Equations (18) - (21) is highly sensitive to variations in wind speed (Stewart, 1982). Increases in hourly wind velocities by 1 and 2 m s^{-1}, for example, resulted in increases in the total depth of snowmelt for the three events by 81 and 159 percent,

respectively. It is thus likely that wind speed measurement errors contributed to observed differences between model and lysimeter results.

Snow density and liquid water holding capacity are important parameters for characterizing the thermal and mass properties of a snowpack yet these parameters are extremely difficult to measure without sensitive instrumentation (Colbeck, 1978). Under conditions of active snowmelt, however, these properties can be estimated with reasonable accuracy (Marks, 1988; Marks et al., 1992). The most difficult parameters to measure in a forested rain-on-snow zone next to radiation are precipitation and runoff. Precipitation falling as snow or a rain-snow mixture is easily displaced by winds due to high surface areas and low densities (McKay, 1970; McKay and Gray, 1981). These characteristics make it difficult to measure precipitation using rain gages even when sheltering devices are used (Allis et al., 1963; Goodison et al., 1981). The highly cohesive properties of snowfall under near zero air temperatures also increases the likelihood of rain gage bridging under moderate to heavy snowfall. Precipitation density information is needed to adjust snow depth and density as well as the liquid water content and mass balance of the snowpack. Under periods of rainfall, precipitation densities can be easily estimated. When snow or a rain-snow mixture occurs precipitation densities become exceedingly difficult to estimate without more detailed precipitation information (Goodison et al., 1981; Marks et al., 1992). It is likely that precipitation depth and density estimation errors contributed significantly to model snowmelt and runoff estimation errors with respect to actual conditions and also may have contributed to differences between lysimeter and model results.

Snowpack runoff measurements from small lysimeters are questionable and their usefulness is limited to providing general determinations of snowmelt and runoff. Point measurements of runoff are difficult to measure accurately using small lysimeters due to the spatial heterogeneity of precipitation and snowcover properties, the presence of ice lenses and the lateral movement of melt water within the snowpack, as well as altered snowcover properties and snow-soil interactions from the lysimeter (Kattelmann, 1993 Pers. Comm.; Conway and Benedict, 1994). The shallow, dense and highly heterogeneous nature of snowcover in the western Cascades make it especially difficult to monitor snowmelt and runoff with reasonable accuracy using small lysimeters. The usefulness of these devices is limited to determining the general onset, timing and duration of runoff rather than determining snowmelt or the magnitude of runoff from a snowpack. Based on the current understanding of the physics of snowmelt, the snowmelt model produced accurate results given the nature of the input data. In view of the limitations of snow lysimeters, the model and lysimeter results were generally comparable regarding the general onset and duration of snowmelt and runoff as well as the hourly variations in these parameters during rainfall events.

5.6.4 Model results under adjusted meteorological conditions

Hourly simulation results representing warmer, windier and wetter meteorological conditions are presented in Figures 5.5 - 5.8 and summarized in Table 5.5. Doubled precipitation rates generated total rainfall depths of 3, 30 and 287 mm for events A, B and C, respectively. The proportion of snowmelt due to advection increased from 3 to 15 percent

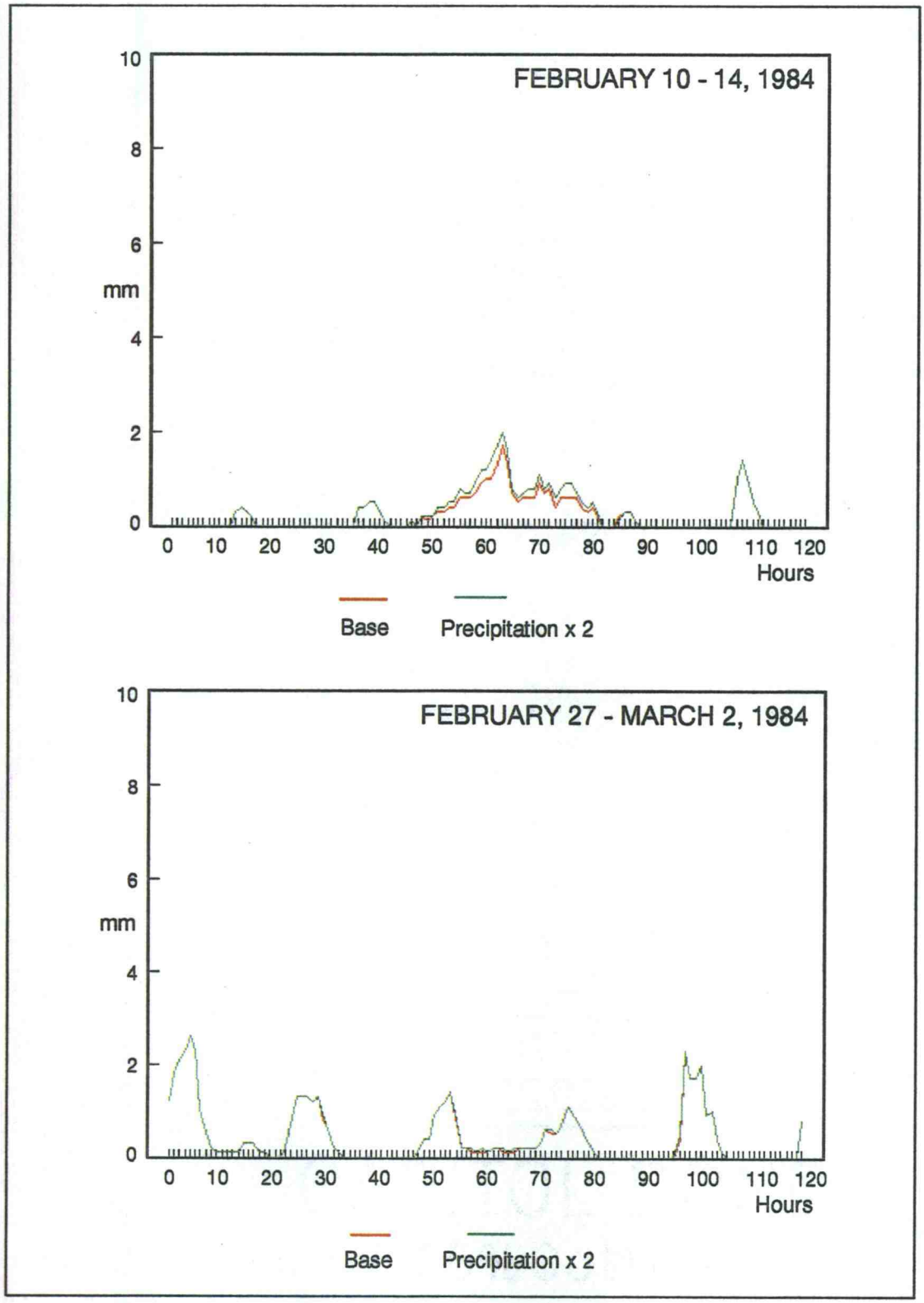

Figure 5.5. Advection effects on estimated snowmelt

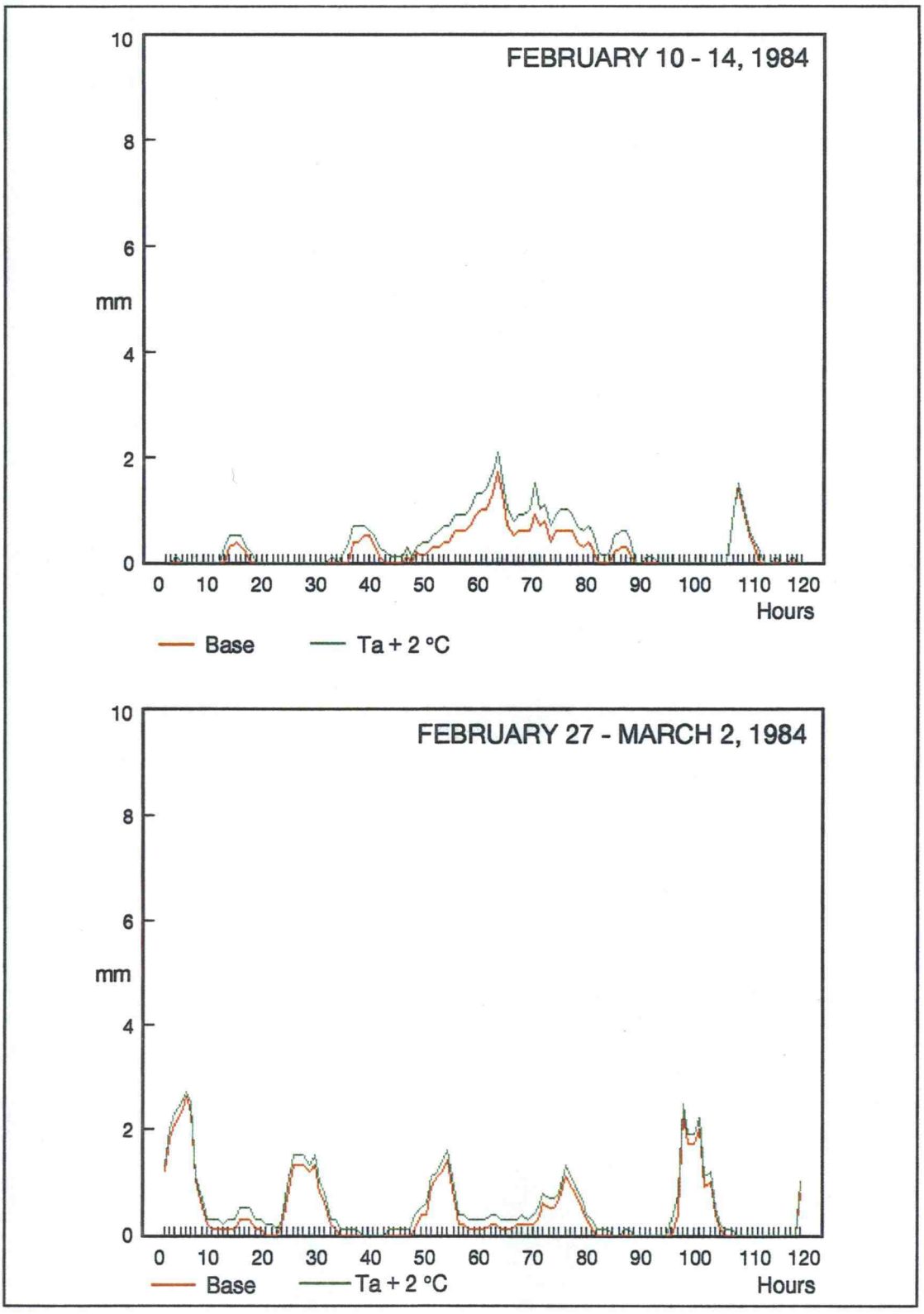

Figure 5.6. Temperature effects on estimated snowmelt

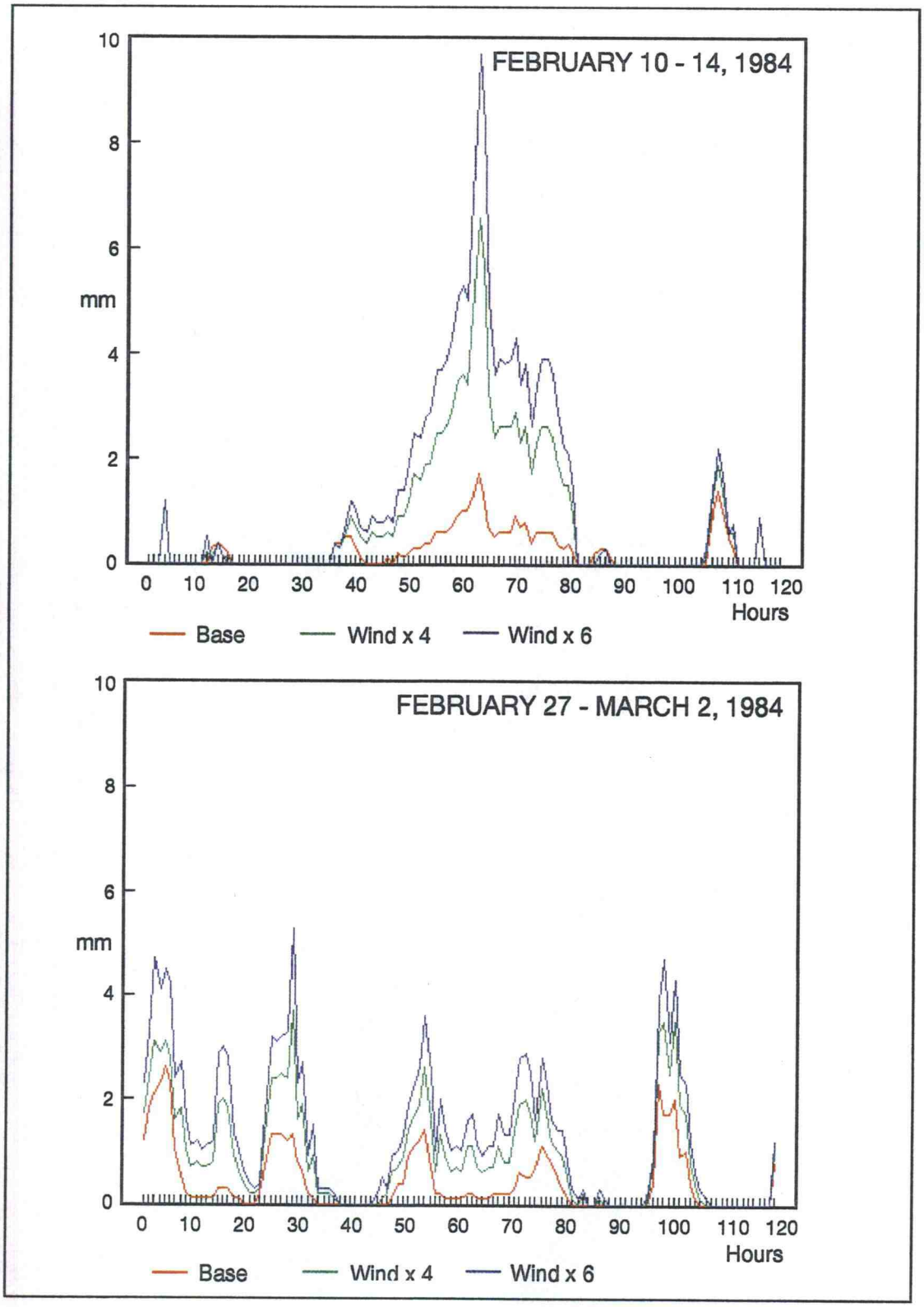

Figure 5.7. Wind effects on estimated snowmelt

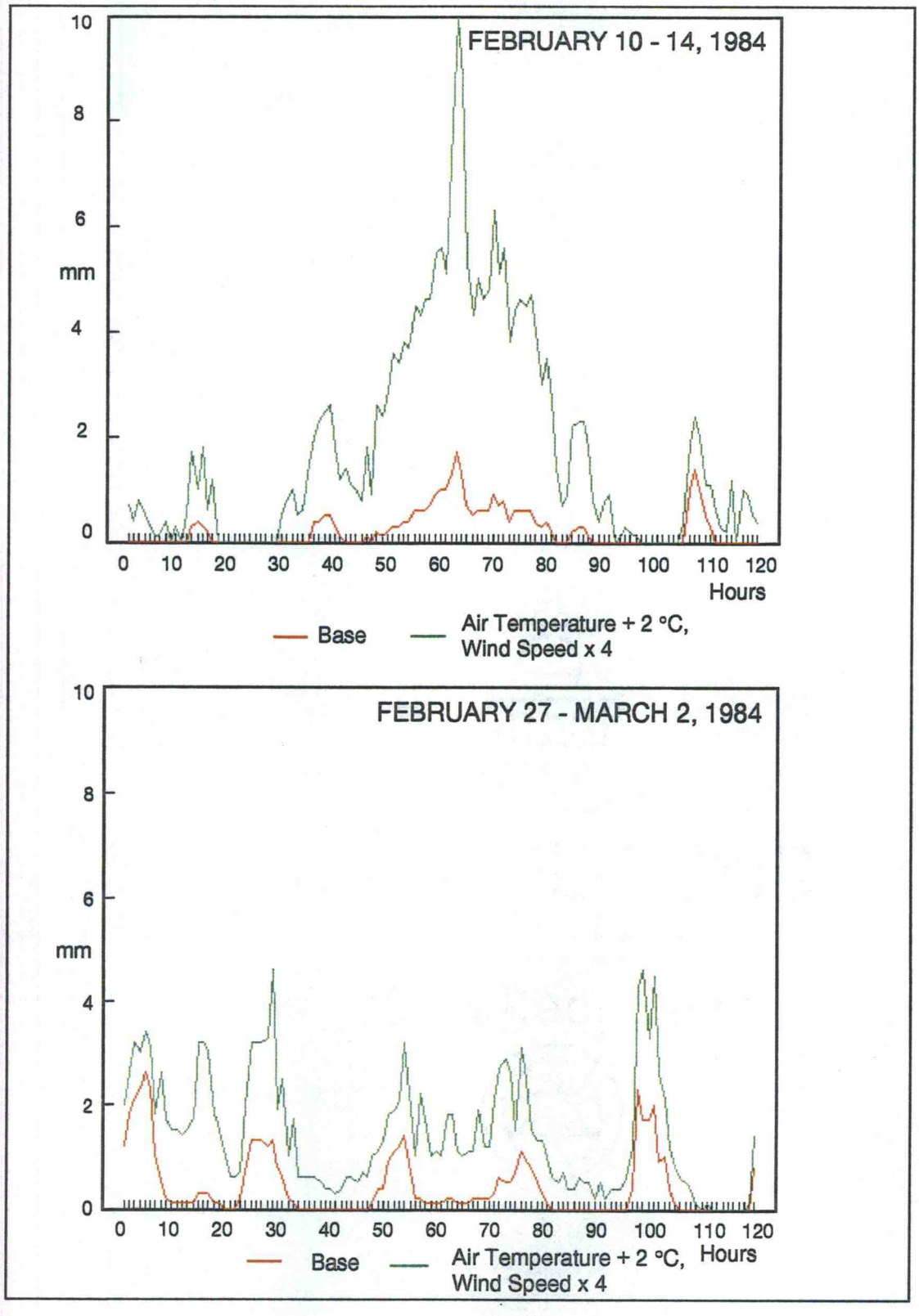

Figure 5.8. Air temperature and wind effects on estimated snowmelt

Table 5.5. Modeled snowmelt and snowpack energy balance for measured (base) and simulated conditions

EVENT A (5 hrs)								
	Melt (mm)	Net Solar (%melt)	Net Therm. (%melt)	Rn (%melt)	H (%melt)	LvE (%melt)	H+LvE (%melt)	M (%melt)
Base	4.1	64	19	82	9	6	15	2
Pcpx2	4.2	62	18	80	9	6	15	5
Ta+2	4.9	53	27	81	11	8	19	3
Ux4	10.2	26	7	33	40	25	65	1
Ux6	14.5	18	5	23	46	29	76	1
Ta+2, Ux4	13.3	20	10	30	40	30	70	1
EVENT B (19 hrs)								
Base	4.2	23	27	50	18	17	36	14
Pcpx2	4.7	20	24	45	17	15	32	25
Ta+2	7.8	12	42	55	16	16	32	12
Ux4	19.3	5	6	11	45	41	86	3
Ux6	29.6	3	4	7	47	44	91	2
Ta+2, Ux4	30.5	3	11	14	41	41	83	3
EVENT C (34 hrs)								
Base	21.1	3	22	25	25	25	51	25
Nsol,adj	25.8	20	18	38	21	21	41	21
Pcpx2	26.7	2	17	19	20	20	40	40
Ta+2	32.0	2	30	32	20	21	41	28
Ux4	87.8	1	5	6	56	32	88	6
Ux6	130.0	1	4	4	58	34	91	4
Ta+2, Ux4	161.0	1	6	6	42	45	88	5

over measured conditions for the three rainfall events. Average snowmelt rates did not increase significantly under greater rainfall, however, and total volumes of snowmelt increased only slightly above base conditions. The increase in total snowmelt over base conditions was minimal for the smaller events resulting in total increases of only 0.1 and 0.5 mm for events A and B, respectively. Net radiation and sensible and latent energy

exchange remained the primary factors controlling snowmelt during these events and were responsible for approximately 86% of total snowmelt for the two periods. The snowmelt response showed a somewhat larger 5.6 mm increase for the more extreme event, C, in which the proportion of melt due to advection increased from 25% under base conditions to 40% under doubled precipitation. Nevertheless, net radiation and convection-condensation ($H+L_vE$) remained the dominant processes controlling 59% of the total melt.

The amount of energy imparted to a snowpack by rainfall depends on the amount of precipitation and the temperature difference between the snowpack and precipitation as shown in Equation (15). In a transitional rain-on-snow zone, temperature differences between rainfall and the snowcover are small because the snowpack is approximately isothermal at 0.0 °C and precipitation temperatures are typically less than 5 °C. Advection therefore has a minimal impact on snowmelt under normal rainfall conditions and only becomes an important factor under extreme events.

The adjusted net solar radiation data for the largest event (C) increased the total volume of snowmelt by 22% over base conditions. The proportion of net solar radiation induced snowmelt increased by 719% over base conditions and accounted for 20% of the total snowmelt for the rainfall period. The snowmelt response to increased net solar radiation accounted for 95% of the total melt from advection but only represented 49% of the $H+L_vE$ contribution to the total melt.

The 2.0 °C increase in average hourly air temperatures resulted in a 44% increase in net radiation at the surface from approximately 27 W m^{-2} to 39 W m^{-2} due to increased thermal irradiance. The total amount of snowmelt increased from 20 to 86 percent over base con-

ditions resulting in total snowmelt ranging from 4.9 to 32.0 mm for the three rainfall periods. The increase in snowmelt was primarily due to enhanced thermal irradiance resulting in proportional increases in net thermal radiation induced snowmelt from 69 to 188 percent over base conditions. Warmer air temperatures and increased humidities enhanced average hourly sensible and latent energy fluxes to the surface for the three events from approximately 16 W m^{-2} (Std. Dev. = 8.8 W m^{-2}) to 21 W m^{-2} (Std. Dev. = 10.3 W m^{-2}) and resulted in proportional increases in $H+L_vE$ induced melt from 22 to 65 percent over base conditions. The effects of enhanced temperature and humidity gradients on sensible and latent energy exchange were strongly inhibited due to the general lack of appreciable wind at the site. The 2.0 °C increase in precipitation temperatures resulted in proportional increases in total snowmelt from 60 to 162 percent. Increased precipitation temperatures significantly enhanced the ability of rainfall to affect snowmelt, but the overall effect of advection was minimal compared to net radiation and convective processes for the smaller rainfall events and only became a major factor for the most extreme event (C).

Hourly wind speed increases by factors of 4 and 6 resulted in mean winds of 6.2 and 9.4 m s^{-1}, respectively. A four fold increase in wind speed resulted in a 275% increase in mean snowmelt rates over base conditions for the three events. Total snowmelt increased from 145 to 359 percent over base conditions for the three events. Enhanced snowmelt rates were produced by marked increases in surface convection and condensation in which the proportion of melt from $H+L_vE$ increased from 618 to 999 percent over base conditions to account for approximately 80% of the total snowmelt. A six fold increase in hourly wind speeds produced a 460% increase in snowmelt rates, and total snowmelt increased from

254 to 605 percent over base conditions for the three events. The proportion of snowmelt contributed by $H+L_vE$ increased from 168 to 1706 percent over base conditions, accounting for approximately 86% of the total snowmelt for the three events.

The combination of a 2.0 °C air temperature and 4 fold increase in hourly wind speeds resulted in an approximate increase of 287% in snowmelt rates over base conditions for the three rainfall events. The total amount of snowmelt for the three events increased from 224 to 663 percent over base conditions to 13.3 mm, 30.5 mm and 161.0 mm for events A, B and C, respectively. Snowmelt under these conditions accounted for approximately 5.3%, 12.2% and 64% of the total initial snowpack water equivalent for the three events. $H+L_vE$ was responsible for approximately 80% of the total snowmelt which represented proportional increases in $H+L_vE$ induced melt from 1450 to 1587 percent over base conditions for the three events.

5.7 Summary and conclusions

The objective of this investigation was to evaluate the sensitivity of snowmelt processes to conditions which occur during rain-on-snow events in order to 1) determine why rain-on-snow floods occur and 2) evaluate whether clear-cut logging practices enhance snowmelt and flooding. An energy balance snowmelt model was used to evaluate the energy and mass balance of a snowpack during rain-on-snow events under both measured and adjusted meteorological conditions. Based on the current understanding of the physics of snowmelt, the snowmelt model produced accurate results given the nature of the input data.

The snowpack was generally found to be thermodynamically active and under a continuous state of melt during rain-on-snow events. During rainfall periods the snowpack was approximately isothermal at 0.0 °C and the liquid water storage capacity of the snowpack was generally attained within 1-2 hours following the initiation of precipitation. Rainfall was therefore translated directly to runoff. Snowmelt rates under measured meteorological conditions were generally light during rainfall events. As a result, runoff during moderate to heavy rainfall periods was composed primarily of precipitation rather than snowmelt.

The snowpack was most sensitive to variations in wind speed which strongly controlled the amount of snowmelt from sensible and latent energy exchange. Snowmelt rates during measured rainfall events were generally small, averaging less than 1.0 mm hr^{-1} due to light winds and overcast conditions which dramatically reduced sensible and latent energy exchange and solar irradiance at the surface. Under moderately windy conditions, sensible and latent energy controlled between 65 and 91 percent of the total snowmelt while total volumes of snowmelt during rainfall events increased from 149 to 516 percent over base conditions. Snowmelt rates increased from less than 1.0 mm hr^{-1} under measured conditions to between 1.0 and 3.8 mm hr^{-1} under 4 and 6 fold wind increases.

Warmer air and precipitation temperatures enhanced both thermal irradiance and rainfall advection at the surface, resulting in moderate increases in snowmelt rates. Larger rainfall events were translated directly to increased runoff due to saturated snowcover conditions. The ability of rainfall advection to affect snowmelt processes was strongly dependent on the magnitude of the rainfall event. Advection generally accounted for only a small proportion of total snowmelt compared to radiation and convective processes, and did not

significantly affect snowmelt during light to moderate rainfall events. For the most extreme measured rainfall event, advection accounted for 25% of the total snowmelt volume of 21.1 mm. Doubling the precipitation volume resulted in only a moderate 22% increase in the total snowmelt volume. Overall, these results suggest that rainfall advection does not significantly enhance snowmelt under normal rainfall events and only exerts a moderate influence on snowmelt under more extreme events. The magnitude of advected energy to the snowpack from rainfall is limited in transitional rain-on-snow zones due to the generally low magnitudes of rainfall that occur over snow and the small differences between rainfall and snowcover temperatures.

Overall, these results indicate that snowmelt processes are much more sensitive to the increased wind velocities, air temperatures and humidities that frequently accompany rainfall events rather than the magnitude of the precipitation. In forested areas solar irradiance and wind speeds are generally reduced at the snow surface below the vegetation canopy which lead to reduced rates of snowmelt. Although thermal irradiance is increased below the vegetation canopy, low air and canopy temperatures, and high thermal emissivities of the snowcover generally limit the magnitude of net thermal radiation and the ability of this parameter to enhance snowmelt.

In cleared areas such as those resulting from clear-cut logging practices, increased solar irradiance combined with increased wind speeds at the snow surface are likely. These conditions have been shown to dramatically enhance snowmelt. The results of this investigation suggest that clear-cut logging practices increase the risk of rain-on-snow induced flooding within the snow transition zone of the Pacific Northwest because 1) rainfall is

generally translated directly to runoff and 2) the increased turbulence in cleared areas dramatically enhances snowmelt.

5.8 Terms

a_H, a_E = Dimensionless ratio of eddy diffusivity and viscosity for heat and water vapor; ($a_H = a_E \approx 1.0$)
CC_s, $CC_{s,0}$, $CC_{s,l}$ = Total snowcover, surface and lower layer cold contents (K)
C_p = Specific heat of dry air at constant pressure ($\approx$1005 J kg^{-1} K^{-1})
$C_{p\text{-}p}$, C_{p_ice}, C_{p_w} = Specific heat of precipitation, ice and water (J kg^{-1} K^{-1})
d_0 = Zero plane displacement height in meters (Brutsaert (1982) suggests $d_0 = 2/3 * 7.35\ z_0$)
D_e, $D_{e,0}$ = Calculated and standard effective diffusion coefficients for water vapor in saturated soil (m^{-2} s^{-1})
E_l = Evaporative flux between soil and lower snow layer (kg m^{-2} s^{-1})
E_x = Radiant exitance (W m^{-2})
G, G_0 = Conductive energy flux in surface layer and between snow layers (W m^{-2})
g = Acceleration of gravity ($\approx$9.80616 m s^{-2})
H = Sensible energy flux (W m^{-2})
I_{lw} ,I_{sol}, I = Thermal, solar and total irradiance (W m^{-2})
k = Von Karmen's constant ($\cong$ 0.40)
K_H, K_W = Bulk transfer coefficients for heat and water vapor
$K_{s,l}$, K_g = Thermal conductivity of snow and soil layers (J m^{-1} K^{-1} s^{-1})
$K_{es,0}$, $K_{es,l}$, K_{eg} = Effective thermal conductivities of the surface and lower snow layer, and soil (J m^{-1} K^{-1} s^{-1})
L = Obhukov stability length (m)
L_vE = Latent energy flux (W m^{-2}); L_v is the latent heat of vaporization or condensation ($\cong$2.5x10^6 J kg^{-1}) and E is the mass flux (kg m^{-2} s^{-1})
M = Advective energy flux from rainfall (W m^{-2})
nT = Dimensionless layer temperature exponent ($\cong$ 14)
P_a, P_0 = Estimated elevation corrected air and sea level air pressures (Pa)
$q_{s,l}$, q_g = Specific humidity of snow and soil layers (Pa)
q, q_s = Specific humidities of air and surface (Pa)
Q_0, Q_l, Q = Surface layer, lower layer and total snowpack energy (W m^{-2})
$R_{n,lw}$, $R_{n,sol}$, R_n = Net thermal, solar and all-wave radiation flux (W m^{-2})

T = Temperature (K)

T_a = Elevation corrected air temperature (K)

T_g, $T_{s,0}$, $T_{s,l}$ = Soil, surface and lower snow layer temperatures (K)

T_{ice}, T_w = Ice and water temperatures (K)

T_{pp}, $T_{s,0}$ = Precipitation and average temperature of the active snow layer (K)

T_{melt} = Melting temperature of ice ($\cong$ 273.15 K)

t_{step} = Model time step (s)

u^* = Friction velocity (m s^{-1})

u = Wind speed (m s^{-1})

w_s = liquid water content of the snowcover (kg m^{-3})

z_u, z_t, z_q = Measurement heights for wind, temperature and humidity (m)

z_0, z_H, z_E = Surface roughness lengths for momentum, heat and water vapor (m)

z_{pp} = Precipitation depth (m)

z_s, $z_{s,0}$, $z_{s,l}$ = Depth of total snowcover, surface and lower snow layers (m)

z_g = Soil measurement depth (m)

z = Layer thickness (z)

ψ_{sm}, ψ_{sv}, ψ_{sh} = Stability functions for momentum, water vapor and heat (Marks and Dozier, 1992)

ρ, ρ_{pp}, ρ_s = Air, precipitation and snow densities (kg m^{-3})

α = Albedo (Estimated as 0.70)

ε_s = Emissivity of the snow surface ($\cong$ 0.99)

σ = Stephan Boltzman Constant ($\cong$ 5.67 x 10^{-8} W m^{-2} K^{-4})

6 CONCLUSIONS

The purpose of this research was to examine the effect of cover type, climate and temporal scale on surface energy and mass exchange calculations. Penman-Monteith, Priestley-Taylor and aerodynamic turbulent transfer models were compared over a uniform, grass covered surface under near-saturated conditions and an alpine snowcover in the Sierra Nevada mountains of California. The turbulent transfer method responded primarily to wind speed and temperature and humidity gradients while the Penman-Monteith method responded to both radiation and turbulence. The Priestley-Taylor response was limited primarily to changes in radiation. At the grass site, wind velocities were light, averaging less than 2.0 m s^{-1}, and latent energy exchange was controlled primarily by net radiant energy. The three models compared favorably with with Bowen ratio estimates of hourly and total daily evaporation on cloudy days. On clear days the Penman-Monteith and Priestley-Taylor methods compared well with Bowen ratio results while the turbulent transfer model tended to over-predict during mid-day periods and under-predict during morning and evening periods. These differences were attributed to assumptions of surface saturation which resulted in large surface-atmosphere humidity gradients during warm, mid-day periods and an observed time lag between diurnal progressions of net radiation, which the Bowen ratio, Penman-Monteith and Priestley-Taylor methods were sensitive to and the surface-atmosphere humidity gradient, which the turbulent transfer method was sensitive to.

At the snow site turbulence dominated the evaporative process since wind velocities were large, often in excess of 15 m s^{-1}, and available radiant energy was near zero due to the high reflectance of the snow surface and the large energy storage capacity of the snowcover. The Penman-Monteith and turbulent transfer models produced similar results and compared favorably with estimates of snowpack sublimation losses from snowcover measurements. Differences in model results were attributed to differences in the magnitudes of the vapor pressure deficit and vapor pressure gradient terms used to drive the models. The Priestley-Taylor method performed relatively well at the grass site despite its relatively simplistic design but produced latent energy flux estimates that were significantly less than measured results at the alpine snow site. The Priestley-Taylor method appears to be limited to low wind conditions where the latent energy flux is controlled by net radiation.

The aerodynamic turbulent transfer method was found to be sensitive to the diurnal progression of meteorological data when evaluated using temporally averaged data. Turbulent transfer estimates of latent and sensible energy fluxes were generally within 90% of hourly results up to a 6 hour time interval but decreased markedly to less than 50% of hourly results at 12 and 24 hour time intervals. The turbulent transfer model was much less sensitive to temporally averaged input data when the diurnal ranges in temperature, humidity and wind were reduced such as over snow. Overall, these results relate the need to account for the diurnal variation in temperature, humidity and wind over surfaces where these variables exhibit a pronounced diurnal cycle and the applicability of coarse temporal resolution data where the diurnal ranges of wind, temperature and humidity are weak.

The aerodynamic turbulent transfer method, incorporated within an energy balance, snowmelt model, was used to evaluate the energy and mass balance of a snowcover during spring melt conditions in a clear-cut within western Cascade mountains of Oregon. Snowmelt rates were strongly influenced by surface winds which regulated the amount of convection-condensation melt from sensible and latent energy exchange. Snowmelt rates averaged less than 1.0 mm hr^{-1} under rainy, overcast, low wind conditions. Net solar and thermal radiation controlled approximately 52% of snowmelt under these conditions while sensible and latent energy exchange contributed approximately 34% of the total snowmelt. Under moderately windy conditions snowmelt rates increased markedly and sensible and latent energy exchange accounted for between 65 to 91 percent of the total snowmelt. The advective energy from rainfall had a minimal effect on snowmelt except under extreme events. Overall, the results of this investigation showed that snowmelt processes are more sensitive to increased humidity and winds that accompany a rainfall event than the advective energy from rainfall. The results also suggested that clear-cut logging practices may increase the risk of rain-on-snow induced flooding because 1) rainfall is generally translated directly to runoff due to rapid snowpack liquid water saturation and 2) the increased turbulence in cleared areas dramatically enhances snowmelt.

BIBLIOGRAPHY

Allis, J. A., B. Harris, and A. L. Sharp (1963) A comparison of performance of five rain-gage installations, *Journal of Geophysical Research* 21: 1649-1729.

Anderson, E. A. (1976) A point energy and mass balance model of a snowcover, Technical Report NWS 19, National Oceanic and Atmospheric Administration, Washington, DC, 150 pp.

Andreas, E. L., C. A. Paulson, R. M. Williams, R. W. Lindsay, and J. A. Businger (1979) The turbulent heat flux from Arctic leads, *Boundary-Layer Meteorology* 17: 57-91.

Andreas, E. L., W. B. Tucker III, and S. F. Ackley (1984) Atmospheric boundary-layer modification, drag coefficient, and surface heat flux in the Antarctic marginal ice zone, *Journal of Geophysical Research*, 89: 649-661.

Aylor, D. E., J. Y. Parlange and A. D. Krikorian (1973) Stomatal mechanics, *American Journal of Botany* 60: 163-171.

Bailey, W. G. and J. A. Davies (1981) Evaporation from soybeans, *Boundary-Layer Meteorology* 20: 417-428.

Baumgartner, A. and E. Reichel (1975) *The World Water Balance*, Elsevier Scientific Publications, Amsterdam, 179 pp.

Beaty, C. B. (1975) Sublimation or melting: observations from the White Mountains, California and Nevada, U.S.A., *Journal of Glaciology*, 14: 275-286.

Beaudry, P. G. and D. L. Golding (1983) Snowmelt during rain-on-snow in coastal British Columbia, *Proceedings of the 51st Western Snow Conference*. Colorado State University, Fort Collins. 55-56.

Berris, S. N. (1984) Comparative snow accumulation and melt during rainfall in forest and clearcut plots in western Oregon, *M.S. thesis*. Oregon State University, Corvallis. 152 pp.

Berris, S. N. and R. D. Harr (1987) Comparative snow accumulation and melt during rainfall in forested and clear-cut plots in the western Cascades of Oregon, *Water Resources Research* 23(1): 135-142.

Bohren, C. F. and B. R. Barkstrom (1974) Theory of the optical properties of snow, *Journal of Geophysical Research*, 79: 4527-4535.

Braun, L., and P. K. Zuidema (1982) Modeling snowmelt during advection-melt situations in a small basin (Rietholzbach), *Proceedings of the International Symposium on Hydrological Research Basins and Their Use in Water Resource Planning*. International Association of Hydrological Sciences, Bern. 3: 771-780.

Broecker, W. S. (1987) Unpleasant suprises in the greenhouse?, *Nature* 329: 123-126.

Brunt, D. (1932) Notes on radiation in the atmosphere, *J. R. Meteorol. Soc*. 58: 389-420.

Brutsaert, W. (1975) On a derivable formula for long-wave radiation from clear skies, *Water Resources Research* 11: 742-744.

Brutsaert, W. (1982) *Evaporation into the Atmosphere*. D. Reidel, Dordrecht. 299 pp.

Brutsaert, W. and S. L. Yu (1968) Mass transfer aspects of pan evaporation, *Journal of Applied Meteorology* 7: 563-566.

Budyko, M. I. (1974) *Climate and Life*. Academic Press, New York. 508 pp.

Businger, J. (1973) Turbulent transfer in the atmospheric surface layer, *Workshop on Micrometeorology*, edited by D. A. Haugen. American Meteorological Society, Boston. 67-100,

Clark W.A.V. and P.L. Hosking (1986) *Statistical Methods for Geographers*. John Wiley and Sons, New York. 518 pp.

Colbeck, S. C. (1978) The difficulties of measuring the water saturation and porosity of snow, *Journal of Glaciology* 20: 189-201.

Colbeck, S. C. (1982) An overview of seasonal snow metamorphism, *Reviews of Geophysics and Space Physics*, 20: 45-61.

Colbeck, S. C., E. A. Anderson, V. C. Bissel, A. G. Crook, D. H. Male, C. W. Slaughter, and D. R. Wiesnet (1979) Snow accumulation, distribution, melt, and runoff, *Eos; Transactions of the American Geophysical Union*, 60: 465-474.

Cowan, I. R. (1977) Stomatal behavior and environment, *Advances in Botanical Research* 4: 117-227..

Davies, J. A., and C. D. Allen (1973) Equilibrium, potential and actual evaporation from cropped surfaces in southern Ontario, *Journal of Applied Meteorology* 12: 649-657.

Davis, R. E. (1980) Simulation of an alpine soil thermal regime beneath a snowpack, M.A. Thesis, Department of Geography, University of California, Santa Barbara, 60 pp.

Davis, R.E., J. Dozier, E. R. LaChapelle and R. Perla (1985) Field and latoratory measurements of snow liquid water by dilution, *Water Resources Research* 21(9): 1415-1420.

Davis, R.E., J. Dozier, and D. Marks (1984) Micrometeorological measurements and instrumentation in support of remote sensing observations of an alpine snow cover, *Proceedings of the Western Snow Conference* 52: 161-164.

Dickinson, R.E. (1984) Modeling evapotranspiration for three-dimensional global climate models, in *Climate Processes and Climate Sensitivity, Geophysical Monographs* 29, edited by J. E. Hansen and T. Takahashi, American Geophysical Union, Washington DC. 29: 58-72.

Dickinson, R. E. (1985) Climate sensitivity, in *Issues in Atmospheric and Oceanic Modeling, Part A, Climate Dynamics. Advances in Geophysics*, edited by S. Manabe, Academic Press. 28: 99-129.

Dickinson, R. E. and R. J. Cicerone (1986) Future global warming from atmospheric trace gasses. *Nature* 319(6049): 109-115.

Dickinson, R. E., A. Henderson-Sellers, P. J. Kennedy, and M. F. Wilson (1986) Biosphere-atmosphere transfer scheme (BATS) for the NCAR Community Climate Model, *Technical Note*/TN-275+STR, National Center for Atmospheric Research, Boulder, CO.

Fleagle, R.G. and J.A. Businger (1980) *An Introduction to Atmospheric Physics*, 2nd ed., Academic Press, New York. 432 pp.

Flint, A. L., and S. W. Childs (1991) Use of the Priestley-Taylor evaporation equation for soil water limited conditions in a small forest clearcut, *Agricultural and Forest Meteorology* 56: 247-260.

Goodison B. E., H. L. Ferguson and G. A. McKay (1981) Measurement and data analysis, *Handbook of Snow*, edited by D. M. Gray and D. H. Male. Pergamon Press, New York. 191-274.

Gurney, R. J. and P. J. Camillo (1984) Modelling daily evapotranspiration using remotely sensed data, *Journal of Hydrology* 69: 305-324.

Hall, A. E. and E. D. Schulze (1980) Stomatal response to environment and a possible interrelation between stomatal effects on transpiration and CO_2 assimilation, *Plant Cells and Environment* 3: 467-474.

Hansen, J., I. Fund, A. Lacis, D. Rind, S. Lebedeff, R. Ruedy and G. Russel (1988) Global climate changes as forecast by Goddard Institute for Space Studies three-dimensional model, *Journal of Geophysical Research* 93(D8): 9341-9364.

Harr, R. D. (1981) Some characteristics and consequences of snowmelt during rainfall in western Oregon, *Journal of Hydrology* 53: 277-304.

Harr, R. D., (1986) Effects of clearcut logging on rain-on-snow runoff in western Oregon: new look at old studies, *Water Resources Research* 22(7): 1095-1100.

Idso, S. B. (1981) A set of equations for full spectrum and 8 to 14 um and 10.5 to 12.5 um thermal radiation from cloudless skies, *Water Resources Research*, 17: 295-304.

Idso, S. B. and R. D. Jackson (1969) Thermal radiation from the atmosphere, *Journal of Geophysical Research*, 74: 5397-5403.

Jackson, R. D. (1985) Evaluating evapotranspiration at local and regional scales. *Proceedings of the IEEE* 73 (6): 1086-1096.

Jackson, R. D., J. L. Hatfield, R. J. Reginato, S. B. Idso and P. J. Pinter, Jr. (1983) Estimation of daily evapotranspiration from one time-of-day measurements, *Agricultural Water Management* 7: 351-362.

Jarvis, P. G. and T. A. Mansfield (1981) *Stomatal Physiology*, Cambridge University Press, Cambridge, England.

Jensen, M. E., R. D. Burman, and R. G. Allen (1990) *Evapotranspiration and Irrigation Water Requirements*, ASCE Manuals and Reports on Engineering Practice (70), Irrig. and Drain. Div., ASCE, New York.

Jobson, H.E. (1972) Effect of Using Averaged Data on the Computed Evaporation. *Water Resources Research* 8(2): 513.

Jury, W. A. and C. B. Tanner (1975) Advection modification of the Priestley and Taylor evapotranspiration formula, *Agronomy Journal* 67: 840-842.

Kanemasu E. T. (1989) Techniques for Calculating Energy and Mass Fluxes, 156-179.

Kanemasu E. T., L. R. Stone and W. L. Pokiers (1976) Evapotranspiration model tested for soybean and sorghum, *Agronomy Journal* 68: 569-572.

Kattelmann, R. (1993) Convergent flow in snow cover, in *Abstracts of the American Geophysical Union* H41D-10.

Kattelmann, R. and K. Elder (1991) Hydrologic characteristics and water balance of an alpine basin in the Sierra Nevada, *Water Resources Research* 27(7): 1553.

Katul G.G., R.H. Cuenca, P. Grebet, J.L. Wright and W.O. Pruitt (1991) Analysis of Evaporative Flux Data for Various Climates (*In Review*). 29 pp.

Keeling, C. D. (1973) The industrial production of carbon dioxide from fossil fuels and limestone, *Tellus* 25: 174-198.

Kimball, B. A. and S. B. Idso (1982) A model of thermal radiation from partly cloudy and overcast skies, *Water Resources Research*, 18: 931-936.

Kondo, J. (1971) Relationship between the roughness coefficient and other aerodynamic parameters. *Journal of the Meteorological Society of Japan* 49: 121-124.

Korzun, V.I. (1978) *World Water Balance and Water Resources of the Earth*, USSR National Committee for the International Decade, UNESCO Press, Paris. 663 pp.

Kuusisto, E. (1986) The mass balance of snow cover in the accumulation and ablation periods, in *Cold Regions Hydrology Symposium*, American Water Resources Association. 397-402.

Langham, E. J. (1981) Physics and properties of snowcover, in *Handbook of Snow*, edited by D. M. Gray and D. H. Male. 275-337.

Mahrt, L. and M. Ek (1984) The influence of atmospheric stability on potential evaporation, *Journal of Climate and Applied Meteorology* 23: 222-234.

Male, D. H. and R. J. Granger (1981) Snow surface energy exchange, *Water Resources Research* 17(3): 609-627.

Male, D. H. and D. M. Gray (1981) Snowcover ablation and runoff, in *Handbook of Snow*, edited by D. M. Gray and D. H. Male. Pergamon Press, New York. 360-436.

Marks, D. (1988) Climate, energy exchange and snowmelt in Emerald Lake watershed, Sierra Nevada, *Ph.D. Dissertation*, Departments of Geography and Mechanical Engineering, University of California, Santa Barbara. 158 pp.

Marks, D. (1990) Simulating the snow surface energy balance and snowmelt over an alpine watershed, *Eos, Transactions of the American Geophysical Union*, 71: 1335.

Marks D. (1993) A continental-scale simulation of potential evapotranspiration for historical and projected doubled-CO_2 climate conditions, *Climate Change*.

Marks, D. and J. Dozier (1979) A clear-sky longwave radiation model for remote alpine areas, *Arch. Meteorol. Geophys. Bioclimatol.* 27(B): 159-187.

Marks, D., and J. Dozier (1992) Climate and energy exchange at the snow surface in the alpine region of the Sierra Nevada, 2, snow cover and energy balance, *Water Resources Research* 28(11) 3043.

Marks, D., J. Dozier and R.E. Davis (1992) Climate and energy exchange at the snow surface in the alpine region of the Sierra Nevada, 1, meteorological measurements and monitoring, *Water Resources Research* 28(11): 3029.

Marks, D., R. Kattelmann, J. Dozier and E. Davis (1986) Monitoring snowcover properties and processes in a small alpine watershed. *Proceedings of the Sixth International Northern Research Basins Symposium/Workshop*, Michigan Technological University, edited by Houghton and H. S. Santeford. 259-275.

Marks, D., and J. Kimball (1991) Simulating the effect of topographic structure on energy flux and snowmelt, *Eos, Transactions of the American Geophysical Union*, 72: 191.

Marshall, S. E. and S. G. Warren (1987) Parameterization of snow albedo for climate models, in *Large Scale Effects of Seasonal Snow Cover*, edited by B. E. Goodison, R. G. Barry, and J. Dozier, IAHS-AIHS Publication, 166 pp.

McKay, D. C. (1979) An energy budget of a snow cover, in *Proceedings on Modeling of Snow Cover Runoff*, edited by S. C. Colbeck and M. Ray, U.S. Army Cold Region Research Engineering Laboratory, Hanover, N. H. 125-134.

McKay, G. A. (1970) Precipitation, *Handbook on the Principles of Hydrology*, D.M. Gray (editor), The Secretariat, Can. Nat. Comm. Int. Hydrol., Decade, Ottawa: 2.1-2.111.

McKay, G. A. and D. M. Gray (1981) The distribution of snowcover, in *Handbook of Snow*, edited by D. M. Gray and D. H. Male. Pergamon Press, New York. 153-190.

McKenney, M. S. and N. J. Rosenberg (1991) Simulating the impacts of climate change on potential evapotranspiration: a comparison of the climate sensitivity of selected methods, *Resources for the Future*, U. S. Dept. of Energy Report ENR91-17. 38 pp.

McNaughton, K. G. and T. A. Black (1973) A study of evapotranspiration from Douglas fir forest using the energy balance approach, *Water Resources Research* 9: 1579-1590.

McNaughton, K. G. and P. G. Jarvis (1984) Using the Penman-Monteith Equation Predictively, *Agricultural Water Management* 8: 263-278.

Monteith, J. L. (1965) Evaporation and environment, in *The State and Movement of Water in Living Organisms*, edited by G. E. Fogg. Sympos. Soc. Exper. Biol., Academic, San Diego, CA. 19: 205-234,

Monteith J. L. and M. H. Unsworth (1990) *Principles of Environmental Physics*, 2nd ed. Edward Arnold. 291 pp.

Moore, R. D., and I. F. Owens (1984) Controls on advective snowmelt in a maritime alpine basin, *Journal of Climatology and Applied Meteorology* 23: 135-142.

Morris, E. M. (1982) Sensitivity of the European Hydrological System snow models, *Hydrological Aspects of Alpine and High-Mountain Areas*. J. W. Glen (editor), IAHS-AIHS Publication 138, Wallingford, UK: 221-231.

Morris, E. M. (1986) Modelling of a seasonal snowcover, *Snow Watch '85*, G. Kukla, R. G. Barry, A. Hecht, and D. Wiesnet (editors), Glaciological Data Report GD-18, World Data Center for Glaciology, Boulder, CO: 225-240.

Neilson R. P. (1993) A mapped atmosphere-plant-soil system (MAPSS) for predicting contintental scale vegetation distribution, (*In review*).

Oke, T.R. (1978) *Boundary Layer Climates*. Halsted Press, New York. 372 pp.

Paeschke, W. (1937) Experimentelle Untersuchungen zum Rauhigkeits- und Stabilitatsproblem in der bodennahen Luftschicht. *Beitrage z. Phys. D. freien Atmos.* 24: 163-189.

Paltridge, G. W. and C. M. R. Platt (1976) *Radiative Processes in Meteorology and Climatology*, Elsevier, Amsterdam, 488 pp.

Parlange, M. B. and G. G. Katul (1992) Estimation of the diurnal variation of potential evaporation from a wet bare soil surface, *Journal of Hydrology* 132: 71-89.

Penman, H. L. (1948) Natural evaporation from open water, bare soil and grass, *Proc. R. Soc. London,* 193(A): 120-146.

Pereira, A. R. and N. A. V. Nova (1992) Analysis of the Priestley-Taylor parameter, *Agricultural and Forest Meteorology* 61: 1-9.

Philip, J. R. (1957) Evaporation and moisture and heat fields in the soil, *Journal of meteorology* 14: 354-366.

Price, J. C. (1982) On the use of satellite data to infer surface fluxes at meteorological scales, *Journal of Applied Meteorology* 20: 1111-1122.

Priestley, C. H. B. and R. J. Taylor (1972) On the assessment of surface heat flux and evaporation using large-scale parameters, *Monthly Weather Review* 100(2): 81-92.

Prowse, T. D. and I. F. Owens (1982) Energy balance over melting snow, Craigieburn range, New Zealand, *Journal of Hydrology* (N.Z.) 21(2): 137-147.

Ramanathan, V. R., R. J. Cicerone, H. B. Singh and J. T. Kiehl (1985) Trace gas trends and their potential role in climate change, *Journal of Geophysical Research* 90: 5547-5566.

Raupach, M.R. and B.J. Legg (1984) The uses and limitations of flux-gradient relationships in micrometeorology, *Agricultural Water Management* 8: 119-131.

Rind, D., R. Goldberg, J. Hansen, C. Rosenzweig, and R. Ruedy (1990) Potential evapotranspiration and the likelihood of future drought, *Journal of Geophysical Research* 95: 9983-10005.

Running, S. W., J. C. Coughlan (1988) A general model of forest ecosystem processes for regional applications. I. hydrologic balance, canopy gas exchange and primary production processes, *Ecological Modelling* 41: 125-154.

Running S.W., R. R. Nemani, D. L. Peterson, L. E. Band, D. F. Potts, L. L. Pierce, and M. A. Spanner (1989) Mapping regional forest evapotranspiration and photosynthesis by coupling satellite data with ecosystem simulation. *Ecology* 70: 1090-1101.

Sato, N., P. J. Sellers, D. A. Randall, E. K. Schneider, J. Shukla, J. L. Kinter III, Y-T. Hou and E. Albertazzi (1989) Effects of implementing the simple biosphere model in a general circulation model. *Journal of the Atmospheric Sciences* 46(18): 2757-2781.

Satterlund, D. R. (1979) An improved equation for estimating long-wave radiation from the atmosphere, *Water Resources Research*, 15: 1649-1650.

Sellers, P. J., Y. Mintz, Y. C. Sud, and A. Dalcher (1986) A simple biosphere model (SiB) for use within general circulation models, *Journal of the Atmospheric Sciences* 43: 505-531.

Sellers, W. D. (1965) *Physical Climatology*, University of Chicago Press, Chicago, 272 pp.

Sharma, M. L. (1985) Estimating evapotranspiration, *Advances in Irrigation* 3: 213-281.

Shuttleworth, W. J. and J. S. Wallace (1985) Evaporation from sparse crops - An energy combination theory, *Q. J. R. Meteorol. Soc.* 111: 839-855.

Stanhill, G. (1992) Accuracy of global radiation measurements at unattended, automatic weather stations, *Agricultural and Forest Meteorology* 61: 151-156.

Stannard, D. I. (1993) Comparison of Penman-Monteith, Shuttleworth-Wallace, and modified Priestley-Taylor evapotranspiration models for wildland vegetation in semiarid rangeland, *Water Resources Research* 29(5): 1379-1392.

Stewart, J. B. (1982) Sensitivity and significance of turbulent energy exchange over an alpine snow surface, *M.A. Thesis*. Department of Geography, University of California, Santa Barbara.

Stewart, J. B. (1984) Measurement and prediction of evaporation from forested and agricultural catchments, *Agricultural Water Management* 8: 1-28.

Warrilow, D. A. and E. Buckeley (1989) The impact of land surface processes on the moisture budget of a climate model, *Annales Geophysicae* 7: 439-450.

Wiscombe, W. J. and S. G. Warren (1980) A model for the spectral albedo of snow, *Journal of the Atmospheric Sciences* 37(12): 2712-2733.

Yen, Y. C. (1965) Heat transfer characteristics of naturally compacted snow, Technical Report 166, Cold Regions Research and Engineering Laboratory, Hanover, N. H., 9 pp.

Yen, Y. C. (1969) Recent studies on snow properties, in Advances in Hydroscience, edited by V. T. Chow, Academic Press, New York, 5: 173-214.